Image Segmentation Using Superpixel Ensembles

Xianbin Gu

a thesis submitted for the degree of

Doctor of Philosophy

at the University of Otago, Dunedin,

New Zealand.

June 29, 2017

Abstract

Recently there has been an increasing interest in image segmentation due to the needs of locating objects with high segmentation accuracy as required by many computer vision and image processing tasks. While image segmentation remains a research challenge, 'superpixel' as the perceptual meaningful grouping of pixels has become a popular concept and a number of superpixel-based image segmentation algorithms have been proposed. The goal of this thesis is to examine the state-of-the-art superpixel algorithms and introduce new methods for achieving better image segmentation outcome.

To improve the accuracy of superpixel-based segmentation, we propose a colour covariance matrix-based segmentation algorithm (CCM). This algorithm employs a novel colour covariance descriptor and a corresponding similarity measure method. Moreover, based on the CCM algorithm, we propose a multi-layer bipartite graph model (MBG-CCM) and a low-rank representation technique based algorithm (LRR-CCM). In MBG-CCM, different superpixel descriptors are fused by a multi-layer bipartite graph, and in LRR-CCM, the similarities of the covariance descriptors of the superpixel are measured by the subspace structure. Besides, we develop a new over-segmentation, called superpixel association, and propose a novel segmentation algorithm (SHST) which is able to generate hierarchical segmentation from superpixel associations.

In addition to those unsupervised segmentation algorithms, we also explore the algorithms for supervised segmentation. We propose a model for semantic segmentation, named 'generalized puzzle game', by which the segmentation information contained in the superpixels can be integrated into the supervised segmentation.

Acknowledgements

The Ph.D. process has been an intellectually stimulating and emotionally draining journey to me, but I am privileged to have received the support from many people. First of all, I'd like to thank my supervisors. To my primary supervisor Jeremiah D. Deng, thank you for your patient guidance and constant encouragement which helped me to go through the many ups and downs over the years. To my co-supervisor Martin K. Purvis, thank you for your academic advice and constructive comments which inspired me greatly in the research. And, I am also grateful to Dr. Brendon J. Woodford who gave me lots of advice and tips that are helpful in research.

I would like to thank the former and current postgraduate members in our Intelligent Computing and Networking (ICoN) lab, especially, Ahmad Shahi, Feng Zhou, Hanhe Lin, Joyce Zhang, Juan Zhang, Sean Lee, and Sepideh Zareei. The professional discussions and feedback from you undoubtedly contributed to my research. I also appreciate the staff in the Department of Information Science, University of Otago. To Associate Professor Peter Whigham, thank you for the feedback in the progress report meetings. To Gail Mercer, Heather Cooper and Stephen Hall-Jones, thank you for the liberal assistance. To the Technical Support Group (TSG), thanks for the efficient IT support.

Finally, I want to thank my parents and Jing Lu for their support and understanding during my whole Ph.D. study period. To my beloved wife, thank you most of all.

Contents

List of Tables

List of Figures

Chapter 1

Introduction

1.1 Image segmentation

Image segmentation is the process of partitioning an image into several independent regions that are supposed to be meaningful and semantically related (Wang *et al.*, 2013). For a human being, it is more like an inherent skill: the light comes into the eyes and the brain instantly perceives objects, such as people, buildings, cars, or other things that make up our real world. But in computer vision, things are completely different: the lights go through the camera and what the computer "perceives" are some dots of colour, namely, pixels. Unfortunately, such difference leads to a "semantic gap" (Liu *et al.*, 2007; Wu *et al.*, 2012) between the human and computer visual experiences, which has long frustrated the field of computer vision. Figure 1.1 is an example of semantic gap in image processing. Converting the pixels into meaningful objects is still a great challenge for researchers in this domain.

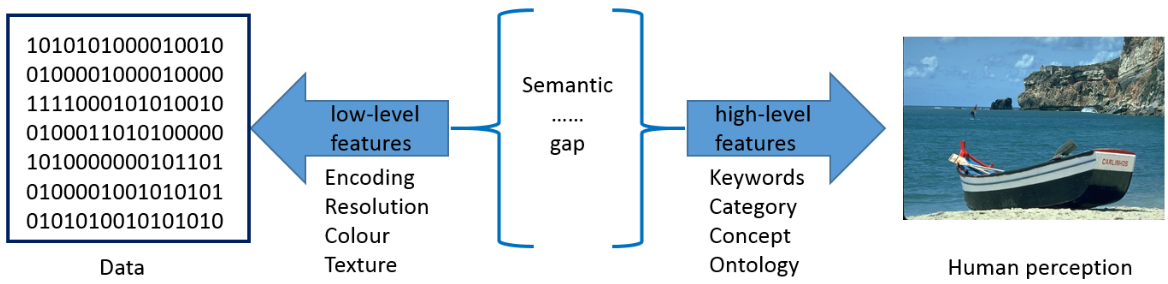

Figure 1.1: The semantic gap in computer vision.

Since the Gestalt movement in psychology (Wertheimer, 1938) pointed out that perceptual grouping plays a critical role in human visual perception, researchers have turned to mathematical models that simulate this perceptual grouping behaviour. Accordingly, the digital representations of an image, such as colour and texture, are regarded as low-level features since they are similar to the machine language, which is designed for describing elementary and reproducible operations. And those semantic image representations, such as contents in the image, or object-ontology (Liu *et al.*, 2007), are considered to be high-level features because they are more abstract and close to the natural language. To that extent, the image segmentation is actually a clustering problem in the view of data mining, which tends to group the points represented by low-level features into a set of clusters that are associated with the high-level features.

Many segmentation techniques have been developed (Zhu *et al.*, 2016). They are usually divided into two categories: supervised segmentation and unsupervised segmentation, based on the difference in their modeling approaches. For supervised segmentation, the algorithm is designed in a top-down manner, which means, when given a number of labelled images, the algorithm is able to learn the object descriptors from the pixels belonging to the same object (Kontschieder *et al.*, 2015). For the unsupervised segmentation, the algorithm is designed under a bottom-up style, by which the pixels are considered as one object if they are locally coherent (Ren and Malik, 2003). However, these two kinds of image segmentation methods are not mutually exclusive. A few works show that the unsupervised segmentation is able to improve the performance of supervised segmentation (Malisiewicz and Efros, Malisiewicz and Efros; Kohli *et al.*, 2009), because image cues contained in the unsupervised segmentations are informative. And, the unsupervised segmentations can also get merits from the supervised segmentations (Borenstein and Ullman, 2008; Fidler *et al.*, 2013), because the supervised segmentations provide the prior knowledge about the objects in the image.

1.2 Superpixel

The concept of superpixel was first proposed by Ren and Malik (2003) as a preprocessing stage for a two-class classification segmentation model. Essentially, superpixel is a group of pixels in which the pixels are close to each other in some given feature space. Usually, the superpixels can be obtained from the bottom-up segmentation algorithms which are regarded as superpixel algorithms in some literatures. And, the output of a superpixel algorithm is called superpixel segmentation, or superpixel representation. A number of works have shown that superpixel segmentation is an effective and efficient representation of the image (Ding and Yilmaz, 2008; Wang *et al.*, 2013; Fulkerson *et al.*, 2009; Li *et al.*, 2012; Gould *et al.*, 2014; Huang *et al.*, 2016).

There are a few reasons for using superpixels instead of pixels in computer vision applications. Firstly, even for an image at moderate resolution, the number of pixels is tremendous, which makes the pixel-level operation intractable. But if the image is represented by superpixels, the computational cost can drop down without too much loss of image information because they are local and inherent, preserving the structure needed for further segmentation.

Secondly, the pixels are not natural entities of an image but a consequence of the discrete representation of an image. So, in the view of the perceptual grouping theory, partitioning the image on a superpixel-level should be more likely to happen in real human vision than directly using pixels.

Thirdly, from the pixel grouping principles (Wertheimer, 1938; Palmer, 1999), it has been pointed out that proximity, similarity and continuation are critical for generating proper segments. However, those properties are always enveloped by different low-level features. For example, the similarity can be extracted from the colour space, while the continuation are always inferred from texture features. So, a feature that contains multiple low-level segmentation cues is preferred. Apparently, a superpixel is a richer source than a single pixel when extracting such combined features.

Generally, the superpixel representation of an image is obtained via an unsupervised segmentation, and as a pre-processing step in many real practice, the superpixel representation is always set to over segment the image. Figure 1.2 demonstrates an example of superpixel segmentations.

1.3 Challenges

The research in image segmentation has been carried out for years, and the researchers have indeed gone a long way towards achieving robust, high-quality segmentations. However, there are still several challenges facing the state of the art in this field.

The first challenge is to effectively link the semantic gap between low-level features and high-level semantic. Hundreds of segmentation algorithms have been proposed to implement pixel clustering and classification, which contains supervised and unsupervised models, but it remains difficult to ensure the segmentation result with meaningful partitions, especially for those unsupervised segmentation algorithms. Because even with small variations in brightness, lighting and view, the low-level appearance of an

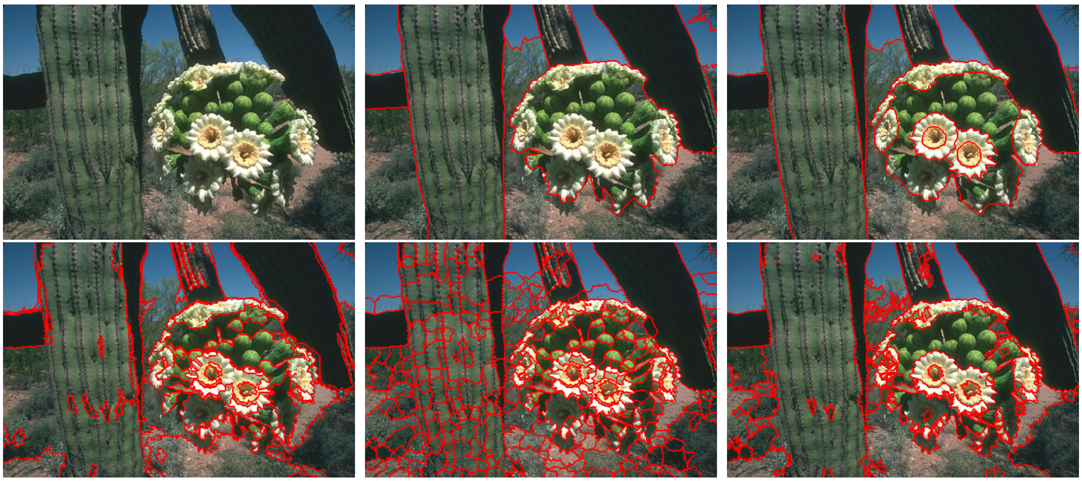

Figure 1.2: An example of superpixel segmentations: the upper row is the original image and two human-annotated ground-truth segmentations, the lower row is the example of suerpixel segmentations.

object will change drastically in different images. Although many descriptors have been developed for extracting robust features, such as SIFT (Ng and Henikoff, 2003) or HoG (Dalal and Triggs, 2005), there is still a long way to go for reducing the semantic gap.

The second challenge is to produce accurate segmentation for images. As an application-oriented task, accurate segmentation results may not be necessary in some cases. But the demand for accurate segmentation is rising. For example, those image/video processing applications that can automatically recognize the objects in photos are greatly required due to the popularity of mobile devices nowadays. Moreover, a robust and accurate segmentation will also improve many traditional applications such as object detection or content-based video coding (Liu *et al.*, 2007; Huang *et al.*, 2011). The research in deep learning has pushed the accurate segmentation a large step forward (LeCun *et al.*, 2010), but to obtain a well-trained convolutional neural network needs tremendous training samples, which may not be applicable in some cases. And for unsupervised segmentation, researchers employed ensemble techniques to generate robust and accurate segmentations (Li *et al.*, 2012). Although many of them are able to improve the accuracy of segmentations, we still lack knowledge about what kind of feature is necessary for ensemble and how to effectively combine the features from different feature spaces.

Finally, computational efficiency is another matter of concern. In the process of segmentation, it is quite common to process large affinity matrices. A segmentation procedure can become intractable because of the requirement for extremely large amounts of memory or loops. This may impose a limitation on the size of images that can be processed by the segmentation algorithms. Although the limitations may be solved gradually by the persistent increase in computation power and storage capacity of modern computers, the demand for efficient segmentation algorithms remains high. For instance, in most mobile devices, the computational ability of the processors is still limited.

1.4 Research objective

The research objective of the thesis is to develop superpixel-based techniques for image segmentation that are able to cope with the challenges mentioned above. More specifically, the goals are to study relevant issues and propose new methods for integrating the superpixel segmentations into image segmentation process. The research mainly focuses on the following questions:

- Can we develop an efficient descriptor for superpixels which is able to improve the existing segmentation algorithms?
- Can we find some methods for combining the superpixel descriptors extracted from different feature spaces?
- Is there any method that can improve the performance of the handcrafted superpixel descriptors?
- Is there a new method that can generate image segmentation with superpixels more effectively than the state of the art?
- Can we make use of the image cues in superpixel segmentations to improve the supervised segmentation?

1.5 Contributions

The main contributions of this dissertation include the following:

- Improving a state-of-the-art superpixel-based image segmentation algorithm by
  - proposing a novel descriptor for superpixel that provides a strong texture representation for the superpixels, and

  - finding a proper method for similarity measuring among the superpixels.

- Proposing a multi-layer bipartite graph model for combining superpixel descriptors extracted from different feature spaces. This includes

  - developing a multi-layer bipartite graph model, and
  - proposing a algorithm for partitioning the multi-layer bipartite graph.

- Proposing a low-rank representation method for the covariance descriptors of superpixel, which can improve the robustness of the algorithms that run with covariance descriptors.

- Proposing a new superpixel-based image segmentation method by first proposing a new type of primitive for image processing, namely, superpixel association, and then developing a segmentation algorithm based on superpixel association.

- Developing a framework for integrating unsupervised segmentation into supervised segmentation, which is considered as a concept study but provides a very promising direction for future research.

1.6 Organization of the thesis

The rest of the thesis is organized as follows:

- **Chapter 2 The Fundamentals**

  This chapter introduces the fundamentals of superpixel-based image segmentation. Details of algorithms for superpixel generation and ensemble segmentation are discussed. And, the methods and data sets for evaluation are also elaborated here. Furthermore, a general framework of our research is given.

- **Chapter 3 Superpixel-based Segmentation with Covariance Matrix**

  In this chapter, we propose a novel covariance descriptor for superpixel and develop an superpixel-based segmentation algorithm named CCM by integrating the covariance descriptor into an ensemble segmentation method. Some parts in this chapter have been published in Gu *et al.* (2014a).

- **Chapter 4 Improving the Colour Covariance Matrix-based Segmentation with Subspace Representation**

In this chapter, we proposed a method for improving the performance of the CCM algorithm, named MBG-CCM. In the MBG-CCM, we employ a multi-layer bipartite graph to model the superpixel descriptors from different feature spaces, and then a novel method is proposed for merging different features. Parts of this chapter have been published in Gu *et al.* (2014b).

- **Chapter 5 Low-rank Representation for Covariance Descriptor**

  In this chapter, we proposed a algorithm, called LRR-CCM. In LRR-CCM, a low-rank representation method is developed for the covariance descriptors of superpixel, which is able to remove the noises in the covariance descriptor set and improve the robustness of the segmentation. Parts of this chapter have been published in Gu and Purvis (2016).

- **Chapter 6 Superpixel Association**

  In this chapter we proposed a new concept of over-segmentation, named superpixel association. Some properties of superpixel association are discussed and we demonstrate that the superpixel association is more suitable to be the primitive for further image processing. Besides, a segmentation algorithm based on the superpixel associations is also proposed, which is able to produce hierarchical segmentations in a tree structure. Parts of this chapter have been published in Gu *et al.* (2016).

- **Chapter 7 Semantic Segmentation with Unsupervised Segmentation**

  In this chapter, we propose a semantic segmentation framework, called generalized puzzle game, by which the unsupervised segmentations can be integrated into the labelling process.

- **Chapter 8 Conclusion and Future work**

  This chapter contains the conclusion drawn for the research carried out in this dissertation, and some possible research directions for future work are also included.

Chapter 2

The Fundamentals

Image segmentation involves a wide range of disciplines in a broad sense, including mathematics, psychology, computer science, and machine learning, etc., some of which are far beyond the scope of this thesis. In this chapter, we concentrate on the fundamental techniques for this thesis, especially the algorithms for superpixel generation and methods of ensemble clustering.

The chapter is organized as follows. Section 2.1, Section 2.2, and Section 2.3 are the reviews of the image segmentation, superpixel algorithms, and ensemble segmentation respectively. Section 2.4 and Section 2.5 are the introductions to the data sets and the evaluation methods used in this thesis. In Section 2.6, we present our research framework, and Section 2.7 is a summary of this chapter.

2.1 Basic approaches for image segmentation

The research about the working mechanisms of the perceptual grouping ability in human vision has been carried out for about eighty years. The study began with the work by the scientists in cognitive science (Wertheimer, 1938), and the computer scientists joined them in the late 1960s (Boden, 2006). Researchers are interested in simulating the perceptual grouping ability by computers and keen on developing applications with it, which makes image segmentation a classical topic in the field of computer vision. As one of the basic operations in computer vision, image segmentation is considered to be a process that partitions a natural image into some independent, meaningful regions, for example, some particular objects or parts. However, the definition of the 'meaningful object' is ambiguous; it can be the things, such as a person or a car, or, sky or sea. More interestingly, even a combination of 'objects', sometimes, is also considered as one ‘object’. Figure 2.1 demonstrates an example. In the example, it is easy to notice that the ways for partitioning mountain and sky are obviously different between the human subjects, which means the perception of different people is not same. Thus, a ‘correct’ segmentation is hard to define, which makes the image segmentation not a well-defined problem. Another difficulty in image segmentation is the methods for rep-

Figure 2.1: An example of blurring definitions of ‘object’. The upper left is the original image, and the rest are human-annotated ground-truth segmentations.

resenting ‘object’. In human vision, the ‘objects’ are perceived by the brain as words, but in computers, they are a few sets of low-level features. To bridge this semantic gap is still a challenge nowadays.

Fortunately, some pathways for developing segmentation algorithms can be found from the research in human perception. The Gestalt theory and studies in cognition (Wertheimer, 1938; Hoffman and Singh, 1997) proposed a few principles of human perception. For example, in human vision, elements similar in colour, shape, or spatial position tend to be grouped together. Much research has been launched in the field of image segmentation. The existing methods can be categorized into two major categories: unsupervised methods and supervised methods. And for those supervised methods, they can again be divided into semisupervised and fully supervised methods based on how much supervision is involved.

For unsupervised segmentation, the pixels are grouped into non-overlapped regions by their similarity over the low-level features (e.g., colours, textures) without any prior knowledge about the image that is, there are no training examples. Therefore, they carry out image segmentation by clustering the pixels with mixture models, mode shifting, or graph partitioning. We divide the conventional unsupervised methods into two categories: the graph-based methods and the clustering-based methods (Zhu *et al.*, 2016).

The graph-based methods formulate an image as a graph $G(V, E)$, where V is set to be the pixels (or regions), E is the set of edges linking the vertices. Each edge is associated with a weight, which reflects the similarities between the pixels (or regions). The image is partitioned according to the optimization function defined on the graph. There are a few graph-based methods that are commonly used in unsupervised segmentation, which include the F-H method (Felzenszwalb and Huttenlocher, 2004), Normalize Cut (Shi and Malik, 2000), and Watershed (Vincent and Soille, 1991; Couprie *et al.*, 2009).

The clustering-based segmentation methods are developed on real analysis techniques in data mining. Generally, they encode the pixels into a feature vector space, and then run clustering in that space. These methods tend to partition image into small regions because most low-level features are actually local statistics. There are some popular clustering-based segmentation algorithms, which include K-means, Mixture of Gaussian (Rao *et al.*, 2009) and Mean Shift (Comaniciu and Meer, 2002; Vedaldi and Soatto, 2008).

It is worth noting that most of the superpixel algorithms come from unsupervised segmentation methods. In most cases, the superpixels can be generated directly by tuning the parameters in the unsupervised algorithms, for example, adjusting the cluster number in Normalized Cut. But there are also a few unsupervised algorithms partitclarly proposed for superpixel generation, such as TurboPixel (Levinshtein *et al.*, 2009), Superpixel lattices (Moore *et al.*, 2008) and SLIC (Achanta *et al.*, 2012).

For supervised segmentation, the algorithms are designed for incorporating high-level information as prior knowledge so that the ill-posed segmentation problem can get a better definition.

In semisupervised methods, the prior knowledge is obtained under a framework of interaction between human and machine, in which a few pixels in the given image are labelled manually and then the algorithms adopt a self-training procedure to learn the model parameters and conduct segmentation. The popular methods of semisupervised segmentation include GrabCut (Rother *et al.*, 2004) and OneCut (Tang *et al.*, 2013).

In fully supervised methods, the algorithms train a segmentation model by extracting knowledge about the objects from the given training samples, which generally are well labelled, that is, all pixels are assigned to some object class labels. Based on different applications, there are two major tasks in fully supervised segmentation: 'object proposals' and 'semantic segmentation' (Zhu *et al.*, 2016).

The first one seeks to locate the objects with regions that have high probabilities to cover the objects. And, the algorithms generally often employ a few bounding box detectors for generating the region candidates and select the optimal by some trained classifiers, such as SVM (Tsai *et al.*, 2015; Felzenszwalb *et al.*, 2010). Moreover, salient object detection methods are adopted to replace the bounding box detectors for region pooling in some works (Hosang *et al.*, 2014; Zhu *et al.*, 2015; Borji *et al.*, 2014).

For semantic segmentation, the goal is to develop the algorithms that can partition an image into independent regions and associate them with some object classes predefined, for example, people, cat, and sheep. Since the task of semantic segmentation is not simply producing the possible regions that objects may locate in but parsing the whole image into different 'things' and 'stuff', Markov random field (MRF) and conditional random field (CRF) are often employed for modelling the neighbourhood relations displayed in the training samples (Zheng *et al.*, 2015; Ladický *et al.*, 2010; Shotton *et al.*, 2006; Gould *et al.*, 2008).

Figure 2.2 shows a categorization of the image segmentation methods.

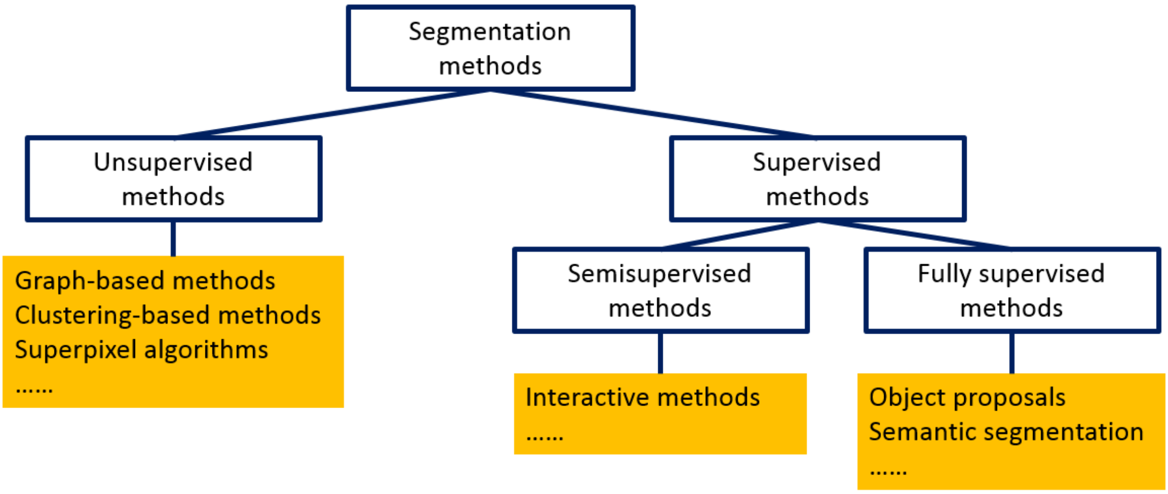

Figure 2.2: A categorization of existing image segmentation methods.

Image segmentation is one basic process of many computer vision applications, and the purpose of a segmentation algorithm varies depending on the applications it belongs to. Thus, there are various ideas for designing a new segmentation algorithm. But among them, there is a notable trend in developing superpixel-based algorithms. The motivations are obvious: for unsupervised segmentation, superpixel provides a format for extracting more complex and discriminative features; for supervised segmentation, using superpixel can reduce the time for training and inference. However, the superpixel is not a perfect replacement of pixel. For example, superpixel wrecks the regular grid structure of pixels which may bring problems to the definition of neighbourhood. And, the inappropriate parameters in superpixel algorithms will introduce structure errors into superpixel representation. All these problems are worthy of further investigation.

2.2 Algorithms for superpixel generation

2.2.1 Overview

Since superpixels are in fact perceptual groupings of pixels, naturally, most of the unsupervised segmentation algorithms can be used for superpixel generation. But in practice, because superpixels always serve as primitives for further computation, the algorithms for superpixel generation are supposed to have a few distinctive properties, including boundary coherency, computational efficiency, hierarchy, and topology preserving (Wei *et al.*, 2016; Achanta *et al.*, 2012). In the past few years, there have been considerable achievements in superpixel segmentation, and most of the state-of-the-art methods possess one or more of the properties mentioned. Liu *et al.* (2011) proposed a graph-based method which is able to produce segmentation with good accuracy. Van den Bergh *et al.* (2012) proposed the SEEDS algorithm that achieves a compromise between accuracy and efficiency for superpixel generation. In Moore *et al.* (2008, 2010), the proposed algorithms are able to generate superpixels that conform to a grid topology, which can be integrating into many vision algorithms conveniently. And, some superpixel algorithms (Felzenszwalb and Huttenlocher, 2004; Mei *et al.*, 2013) use a tree structure of regions to represent the image, which can characterize the hierarchical structure of the image with a relatively low computational complexity. In addition, a few unsupervised clustering algorithms are also widely used for generating superpixels, such as Normalized Cut (Shi and Malik, 2000) and Mean Shift (Comaniciu and Meer, 2002; Vedaldi and Soatto, 2008).

Frankly speaking, all superpixel generation approaches have their own advantages and drawbacks that may be better kindly to a particular application. Some emperical research shows that clustering-based superpixel algorithms are more efficient than graph-based ones (Wang *et al.*, 2017). Stutz *et al.* (2017) presented an overall ranking of superpixel algorithms, which enables researchers to select appropriate superpixel algorithms accordingly.

In this thesis, the superpixel generation task is done by two popular superpixel algorithms: the efficient graph-based F-H method (Felzenszwalb and Huttenlocher, 2004) and Mean Shift (Comaniciu and Meer, 2002). This choice is based on two facts.

First, these two algorithms are based on the data-driven models by which the intrinsic structure of the data can be easily investigated with a scale parameter. For example, the F-H method merges the pixels into superpixels according to a predefined minimum difference controlled by a threshold, and the Mean Shift is a nonparametric clustering-based method that seeks the modes along the surface of the data distribution with a given step length. So, different superpixel segmentations can be obtained by simply adjusting the threshold or step length.

Second, these two superpixel algorithms are complementary and practically efficient (Li *et al.*, 2012). The graph-based and clustering-based methods are motivated by different goal functions, which means the pixel data structure can be explored by different clustering procedures. In the view of ensemble clustering, this may contribute to the robustness of the final clustering (Zhou, 2012; Zhou *et al.*, 2015). Actually, in the existing works on superpixel-based image segmentation, this combination is widely used (Li *et al.*, 2012; Wang *et al.*, 2013, 2015). However, we have to mention that the algorithms we proposed in this thesis are also feasible with other choices on superpixel algorithms.

For completeness, we elaborate the F-H method and Mean Shift in the following.

2.2.2 The efficient graph-based image segmentation

The F-H method is proposed by Felzenszwalb and Huttenlocher (2004). Let $G(V, E)$ be an undirected graph, where vertices $v_i \in V$ represent the set of elements to be segmented, and edges $e(v_i, v_j) \in E$ correspond to pairs of neighbouring vertices. Moreover, each edge $e(v_i, v_j) \in E$ has a weight $w(v_i, v_j)$, which is a non-negative value measured by the dissimilarity between v_i and v_j. And, a segmentation $S = \{C_i\}$ is a partition of V, and, $\forall i, j \in \{1, 2, ..., n\}$, we have $C_i \cap C_j = \emptyset$ and $C_i \in S$.

For a given image I, the pixels are set to be the elements in V and the weight on an edge is some measure of the dissimilarity between two pixels connected by the edge, which could be the difference in intensity, colour, or some other attributes.

The basic idea of the F-H method is that the weights on the edges connecting vertices in the same component should be relatively smaller while those on the edges connecting vertices in different components should be larger. Thus, three indices are defined for describing this idea. The first is the *internal difference* of a component C, which is defined as,

$$\mathrm{Int}(C) = \max_{e \in \mathrm{MST}(C,E)} w(e), \tag{2.1}$$

where $w(e)$ is the weight on the edge e, and $\mathrm{MST}(C, E)$ represents the edges in the minimum spanning tree of the component C. The second is the *minimum internal difference*,

$$\mathrm{MInt}(C_i, C_j) = \min(\mathrm{Int}(C_i) + \tau(C_j), \mathrm{Int}(C_i) + \tau(C_j)), \tag{2.2}$$

where $\tau(C) = k/|C|$ is a threshold function controlling the degree of difference between two components. The third is the *difference* between two components C_i and C_j,

$$\mathrm{Dif}(C_i, C_j) = \min_{v_m \in C_i, v_n \in C_j, (v_m, v_n) \in E} w(v_m, v_n), \tag{2.3}$$

Then, the *pairwise comparison predicate* is defined as,

$$D(C_i, C_j) = \begin{cases} \text{true} & \text{if } \mathrm{Dif}(C_i, C_j) > \mathrm{MInt}(C_i, C_j), \\ \text{false} & \text{otherwise.} \end{cases} \tag{2.4}$$

If $D(C_i, C_J) = $ true, then C_i and C_j will be merged. The details of F-H method are as shown in Algorithm 2.1.

The computational complexity is $O(m \log m)$, where m is the number of edges in the graph (Felzenszwalb and Huttenlocher, 2004).

2.2.3 Mean Shift segmentation

The mean shift algorithm is proposed by Fukunaga and Hostetler (1975) and Cheng (1995); Comaniciu and Meer (2002) introduced Mean Shift into image segmenation. The algorithm is essentially a mode-seeking procedure, which is based on the density estimation.

Let $X = \{\mathbf{x}_1, \cdots, \mathbf{x}_n\} \subset R^d$ be a dataset , where $\mathbf{x}_i$ is a point in a d-dimension space and predefined kernel $K(\mathbf{x})$, and the diagonal $H = h^2 I$ be the bandwidth matrix, where h is a fixed bandwidth for all dimensions. Then, a multivariate kernel density estimator is defined as

$$\hat{f}(\mathbf{x}) = \frac{1}{nh^d} \sum_{i=1}^{n} K\left(\frac{\mathbf{x} - \mathbf{x}_i}{h}\right), \tag{2.5}$$

where $K_H(\mathbf{x})$ is defined as

$$K_H(\mathbf{x}) = |H|^{-\frac{1}{2}} K(H^{-\frac{1}{2}} \mathbf{x}). \tag{2.6}$$

Algorithm 2.1 F-H method

Input: A graph $G = (V, E)$

Output: A segmentation $S = (C_1, ..., C_r)$ of V

Sort E into $\pi = (e_1, ..., e_m)$, where $\forall i < j$, $w(e_i) \leq w(e_j)$;
Initializing S by setting $S^0 = V$
for $q = 1, \cdots, m$ **do**
    Let v_i, v_j be the vertices connected by e_q, and, C_i^{q-1} and C_j^{q-1} be the components of S^{q-1} containing v_i and v_j respectively,
    if $C_i^{q-1} \neq C_j^{q-1}$ and $w(e_q) \leq \mathrm{MInt}(C_i^{q-1}, C_j^{q-1})$ **then**
        merging C_i^{q-1} and C_j^{q-1} to get S^q
    else
        $S^q = S^{q-1}$
    end if
end for
$S = S^m$

Let $k(||\mathbf{x}||^2)$ be the *profile* of the kernel $K(\mathbf{x})$, which satisfies $K(\mathbf{x}) = c_{k,d}k(||\mathbf{x}||^2)$, where $c_{k,d} > 0$ is the normalization constant that makes $K(\mathbf{x})$ integrate to 1. Then, Eq. 2.5 can be rewritten as

$$\hat{f}(\mathbf{x}) = \frac{c_{k,d}}{nh^d} \sum_{i=1}^{n} k(||\frac{\mathbf{x} - \mathbf{x}_i}{h}||^2). \tag{2.7}$$

Since the modes are located in the place where the gradient $\bigtriangledown f(\mathbf{x}) = 0$, a mean shift procedure is designed to locate the zeros without estimating the density. From Eq. 2.7, we have

$$\hat{\bigtriangledown} f_{h,K}(\mathbf{x}) = \frac{2c_{k,d}}{nh^{d+2}} \sum_{i=1}^{n} (\mathbf{x} - \mathbf{x}_i) k'(||\frac{\mathbf{x} - \mathbf{x}_i}{h}||^2). \tag{2.8}$$

Let $g(x) = -k'(x)$, and introduce it into Eq. 2.8, which yields

$$\begin{aligned} \hat{\bigtriangledown} f_{h,K}(\mathbf{x}) &= \frac{2c_{k,d}}{nh^{d+2}} \sum_{i=1}^{n} (\mathbf{x}_i - \mathbf{x}) g(||\frac{\mathbf{x} - \mathbf{x}_i}{h}||^2) \\ &= \frac{2c_{k,d}}{nh^{d+2}} \left[\sum_{i=1}^{n} g\left(||\frac{\mathbf{x} - \mathbf{x}_i}{h}||^2 \right) \right] \left[\frac{\sum_{i=1}^{n} \mathbf{x}_i g\left(||\frac{\mathbf{x}-\mathbf{x}_i}{h}||^2 \right)}{\sum_{i=1}^{n} g\left(||\frac{\mathbf{x}-\mathbf{x}_i}{h}||^2 \right)} - \mathbf{x} \right]. \end{aligned} \tag{2.9}$$

The second term is defined as the *mean shift*, i.e.

$$\mathbf{m}_{h,G}(\mathbf{x}) = \frac{\sum_{i=1}^{n} \mathbf{x}_i g\left(||\frac{\mathbf{x}-\mathbf{x}_i}{h}||^2 \right)}{\sum_{i=1}^{n} g\left(||\frac{\mathbf{x}-\mathbf{x}_i}{h}||^2 \right)} - \mathbf{x}. \tag{2.10}$$

Let

$$\mathbf{y}_{j+1} = \frac{\sum_{i=1}^{n} \mathbf{x}_i g\left(||\frac{\mathbf{y}_i - \mathbf{x}_i}{h}||^2\right)}{\sum_{i=1}^{n} g\left(||\frac{\mathbf{y}_i - \mathbf{x}_i}{h}||^2\right)}, \tag{2.11}$$

it has been proved that $\{\mathbf{y}_j\}_{j=,1,2,...}$ will converge if the kernel $K(\mathbf{x})$ has a convex and monotonically decreasing profile (Cheng, 1995). So, the modes can be found by the mean shift procedure, i.e., updating $\{\mathbf{y}_j\}$ by $\mathbf{y}_{j+1} = \mathbf{m}_{h,G}(\mathbf{y}_j) + \mathbf{y}_j$ until it converges.

In image segmentation, every pixel is associated to a mode via a mean shift procedure, and those pixels connected to the same mode are grouped as a cluster. The computational complexity of the Mean Shift is $O(n^2)$ (Vedaldi and Soatto, 2008), and Algorithm 2.2 shows its details.

2.3 Ensemble clustering in image segmentation

2.3.1 Overview

The ensemble clustering technique aims to combine the results of different clustering methods into a more robust and better clustering (Huang *et al.*, 2016), and it is also called consensus clustering. In the past few years, a number of ensemble segmentation approaches have been developed by employing a variety of ensemble clustering techniques into image segmentation. The early research concentrates on developing the frameworks. Franek *et al.* (2010) proposed a framework for adapting ensemble clustering methods into image segmentation. In their algorithm, the superpixels are used as primitive objects and the general ensemble clustering methods are applied on the superpixel level. The weakness of their framework is the lack of ability to use the multiple image cues, such as colour, and lightness. Mignotte (2008) developed a relabelling-based ensemble segmentation method, in which the local histogram of class labels is used to control the fusing of different segmentations. But this method assumes that every input over segmentation should be partitioned into a fixed number of clusters, which is not applicable in some cases. Kim *et al.* (2014) proposed an algorithm which generates the final segmentation by using the hierarchical segmentations. In some works, the ensemble segmentation is formulated into an optimization problem, by which the final segmentation is obtained by maximizing some predefined similarities between the segmentations (Vega-Pons *et al.*, 2011; Alush and Goldberger, 2012; Mignotte, 2014; Wang *et al.*, 2014). Besides, Wang *et al.* (2013) and Ding and Yilmaz (2008) introduced the hypergrah into ensemble segmentation; their models also take single superpixel segmentation as primitives and use multiple features for clustering.

Algorithm 2.2 Mean Shift

Input: An image $I = \{p_1, ..., p_n\}$, bandwidth h, stop-threshold τ, merge-threshold ϵ

Output: A segmentation $S = (C_1, ..., C_k)$

/* mean shift procedure */
$M = \{m_1, \cdots, m_n\}$
for $i = 1, \cdots, n$ **do**
    $y_0 = p_i$, $j = 0$, $m_i = 0$
    Compute y_1 by Eq. 2.11
    while $||y_{j+1} - y_j|| > \epsilon$ **do**
        $j = j + 1$
        $y_j = y_{j-1}$
        Compute y_{j+1} by Eq. 2.11
    end while
    $m_i = y_{j+1}$
end for
/* segmentation */
$k = 1$, $C_k = \emptyset$
while $M \neq \emptyset$ **do**
    $m_i = M\{1\}$
    $M = M - m_i$
    $C_k = C_k \cup p_i$
    for $m_j \in M$ **do**
        if $||m_i - m_j|| < \tau$ **then**
            $C_k = C_k \cup p_j$
            $M = M - m_j$
        end if
    end for
    $k = k + 1$
end while

However, the quality of their final segmentations may be affected by the superpixel segmentations they used.

Unfortunately, the image data is generally made up of a tremendous number of pixels, which results in high computational cost for measuring the pixel-wise similarity globally. So, most of the existing ensemble segmentation algorithms are proposed to approach segmentation at the superpixel level, and the robustness of the output is inevitably affected by the quality of the superpixel segmentation they adopted. Alternatively, Li *et al.* (2012) proposed an ensemble segmentation algorithm, which takes multiple superpixel segmentations as segmentation cues and can generate robust final segmentation. This algorithm employs a bipartite graph to represent the pixel-superpixel relations from the input superpixel segmentations and obtains the final segmentation by a modified normalized-cut algorithm. Wang *et al.* (2013, 2015) improved this method by proposing a novel method for measuring the similarity between the superpixels in the bipartite graph construction.

The bipartite graph model employed in Li *et al.* (2012) and Wang *et al.* (2013, 2015) is first proposed by Fern and Brodley (2004), and named Hybrid Bipartite Graph Formulation (HBGF). In this thesis, we also use this model for superpixel-based segmentation.

2.3.2 The HBGF algorithm

The HBGF (Fern and Brodley, 2004) is a graph-based ensemble clustering method. This algorithm contains two parts: the first one is the construction of the bipartite graph which integrates the clustering information, and the second one is spectral clustering by which the final clustering is obtained.

Given a data set $X = \{x_1, \cdots, x_m\}$, let $C^i = \{c_1^i, \cdots, c_{K_i}^i\}$ be a clustering which partitions X into K_i disjoint clusters, and let $\mathcal{C} = \{C^1, \cdots, C^N\}$ be a collection of clusterings of X, where N is the number of clusterings, and $K = \{K_1, \cdots, K_N\}$ represents the set of cluster numbers of each clustering.

For a bipartite graph $G(V, E)$, the vertex set V can be divided into two parts, i.e., $V = V^I \cup V^C$, and for each edge $e \in E$, it connects a vertex in V^C to one in V^I, i.e., $\forall e_{ic} \in E$, $e_{ic} = (v_i, v_c)$, where $v_i \in V^I$ and $v_c \in V^C$. And, let each edge be associated to a weight w, we have $w(e_{ic}) = w_{ic}$. The bipartite graph can be rewritten as $G(V^I, V^C, W)$, when it needs to emphasize that G is weighted.

In HBGF, the bipartite graph G is constructed by setting the elements in X as the vertices in V^I, i.e., $V^I = \{x_1, \cdots, x_m\}$, and all the entries in $\mathcal{C}$ as the vertices in V^C, i.e., $V^C = \cup_{i=1}^N C^i = \{c_1^1, \cdots, c_{K_1}^1, \cdots, c_1^N, \cdots, c_{K_N}^N\}$; and for the weights on the edges, we set

$$w_{ic} = \begin{cases} 1 \text{ (or, other positive number)}, & \text{if } v_i \in v_c, \\ 0, & \text{otherwise}, \end{cases} \tag{2.12}$$

where $v_i \in v_c$ holds if a data point x_i (denoted by v_i) belongs to a cluster $c_{K_j}^j$ (denoted by v_c).

Let $n = \sum_{i=1}^N K_i$, then, $W = [w_{ic}]$ is a $m \times n$ matrix, which is called cross-adjacency matrix (Liu *et al.*, 2010). Algorithm 2.3 shows the details of the graph construction of HBGF.

Algorithm 2.3 Graph construction of HBGF

Input: A data set $X = \{x_1, \cdots, x_m\}$, a collection of base clusterings $\mathcal{C} = \{C^1, \cdots, C^N\}$, the cluster number k of the final clustering

Output: Final clustering $C = (c_1, ..., c_k)$

```
1: Set V^I = X, V^C = ∪_{i=1}^N C^i, n = Σ_{i=1}^N K_i;
2: W = ∅;
3: for i = 1, ··· , m do
4:     for c = 1, ··· , n do
5:         W = W ∪ w_ic
6:     end for
7: end for
```

The spectral clustering on G can be done by directly extending $W_{m\times n}$ into $W^{ext} = \begin{bmatrix} 0 & W \\ W^T & 0 \end{bmatrix}$, where W^{ext} is a $(m+n) \times (m+n)$ symmetric matrix. However, Dhillon (2001) proved that the normalized cut algorithm on a bipartite graph can be realized via SVD (i.e. singular value decomposition) on the cross-adjacency matrix W, and the clustering information of X is contained in the right singular vectors.

Li *et al.* (2012) proposed a more efficient algorithm for computing the singular vectors, which is called *T-cut*. This algorithm is proposed based on the truth that W can be converted into the probability of a two-step transition on the vertices of bipartite graph G. And, the *T-cut* algorithm makes use of the equivalence in the two-step transition and delivers the clustering of V^X from the clustering of V^Y without loss. The details of *T-cut* algorithm are given in Algorithm 2.4.

Algorithm 2.4 *T-cut*

Input: A cross-adjacency matrix W, the cluster number k of the final clustering

Output: Final clustering $S = (s_1, ..., s_k)$

1: Compute $D_X(i,i) = \sum_i w_{ij}$, $D_Y(j,j) = \sum_j w_{ij}$;
2: Compute $W_Y = W^T D_X^{-1} W$;
3: Compute $L_Y = D_Y - W_Y$;
4: Compute the bottom k eigenpairs $\{(\lambda_i, \mathbf{v_i})\}_{\mathbf{i=1}}^{\mathbf{k}}$ of $L_Y\mathbf{v}= \lambda D_Y \mathbf{v}$;
5: **for** $i = 1, \cdots, k$ **do**
6: Compute γ_i such that $0 \leq \gamma_i < 1$ and $\gamma_i(2 - \gamma_i) = \lambda_i$;
7: Compute $\mathbf{u_i}= \frac{1}{1-\gamma_i} D_X^{-1} W \mathbf{v_i}$;
8: **end for**
9: Cluster $\mathbf{u}$ into k clusters via k-means algorithm and obtain S.

2.4 Data sets

For evaluation of the performance of the proposed approaches, there are three data sets used throughout this thesis; these include the Berkeley Segmentation Data Set 300 ("BSDS300") (Martin *et al.*, 2001), the Berkeley Segmentation Data Set 500 ("BSDS500") (Arbelaez *et al.*, 2011), and the Microsoft Research Cambridge 21-Class Data Set ("MSRC21") (Shotton *et al.*, 2008).

BSDS300 is a public image segmentation database which is widely used in evaluating the performance of unsupervised image segmentation. This data set contains 300 natural images of diverse scene categories, and each image has a number of ground truth segmentations, which are manually segmented by different human subjects. There are at least four human annotations for each image, and all images are in the size of 481×321. BSDS500 is an update of BSDS300, which contains some more 200 images. The same as BSDS300, every image has a few human-annotated ground truth segmentations, and the image size is set to be 481×321.

Compared with other data sets, for example, VOC2012 (Everingham and Winn, 2011), and VOC2007 (Everingham and Winn, 2007), BSDS300 and its extension have a few unique advantages for evaluating the unsupervised segmentation algorithms. Firstly, it provides highly accurate human-annotated ground truth, and each object in the image has a precise boundary, which is critical for evaluating the unsupervised segmentation. Secondly, most of the images in the two data sets are natural images that always contain a variety of visual patterns, and they are able to examine the algorithm with different patterns. Thirdly, the data sets provide multiple ground truths for every image, which is very similar to the real case. Therefore, we use BSDS300 and BSDS500 to evaluate the algorithms, which are the same as Li *et al.* (2012), Arbelaez *et al.* (2011), Wang *et al.* (2015), among others. Figure 2.3 shows a few examples in the BSDS 300 and BSDS500 data sets.

MSRC21 is a classic data set for semantic segmentation. This data set consists of 591 images which are labelled with 21 classes: building, grass, tree, cow, sheep, sky, aeroplane, water, face, car, bicycle, flower, sign, bird, book, chair, road, cat, dog, body, boat. Normally, the data set is split into 276 training samples, 256 test samples, and the rest for validation, which is the same as Shotton *et al.* (2008). One difficulty for experiments on this data set is that the ground-truth labelling is approximate and many of the pixels on the object boundaries have void labels, which make the training difficult. Figure 2.4 demonstrates some images from MSRC21.

2.5 Evaluation

Evaluating the quality of segmentation is commonly referred to as cluster validity analysis (Zhou, 2012). For comparison purposes, we employ the evaluation methods that are widely used in the image segmentation society.

2.5.1 Evaluations for unsupervised segmentation

Evaluation of an unsupervised segmentation algorithm is in fact largely subjective, mainly because there is no unique ground-truth segmentation of an image against which the outputs may be compared. However, there are four popular segmentation evaluation methods that are widely used in qualifying the segmentation result; they include the Probabilistic Rand Index (PRI) (Unnikrishnan *et al.*, 2007), the Variation of Information (VoI) (Meilă, 2005), the Global Consistency Error (GCE) (Martin *et al.*, 2001), and the Boundary Displacement Error (BDE) (Freixenet *et al.*, 2002).

PRI is a generalization to the rand index, which measures the probability of an arbitrary pair of samples being labelled consistently in the two segmentations. In image segmentation, it can compare the segmentation result with a set of ground truths. Let S_t be the segmentation result and $\{S_g\}$ be a set of ground truths, the PRI is defined as follows,

$$\mathrm{PRI}(S_t, \{S_g\}) = \frac{1}{\binom{N}{2}} \sum_{i<j} [c_{ij} p_{ij} + (1 - c_{ij})(1 - p_{ij})], \tag{2.13}$$

where N is the number of pixels in the image, $c_{ij} \in [0, 1]$ is the event that pixel i and

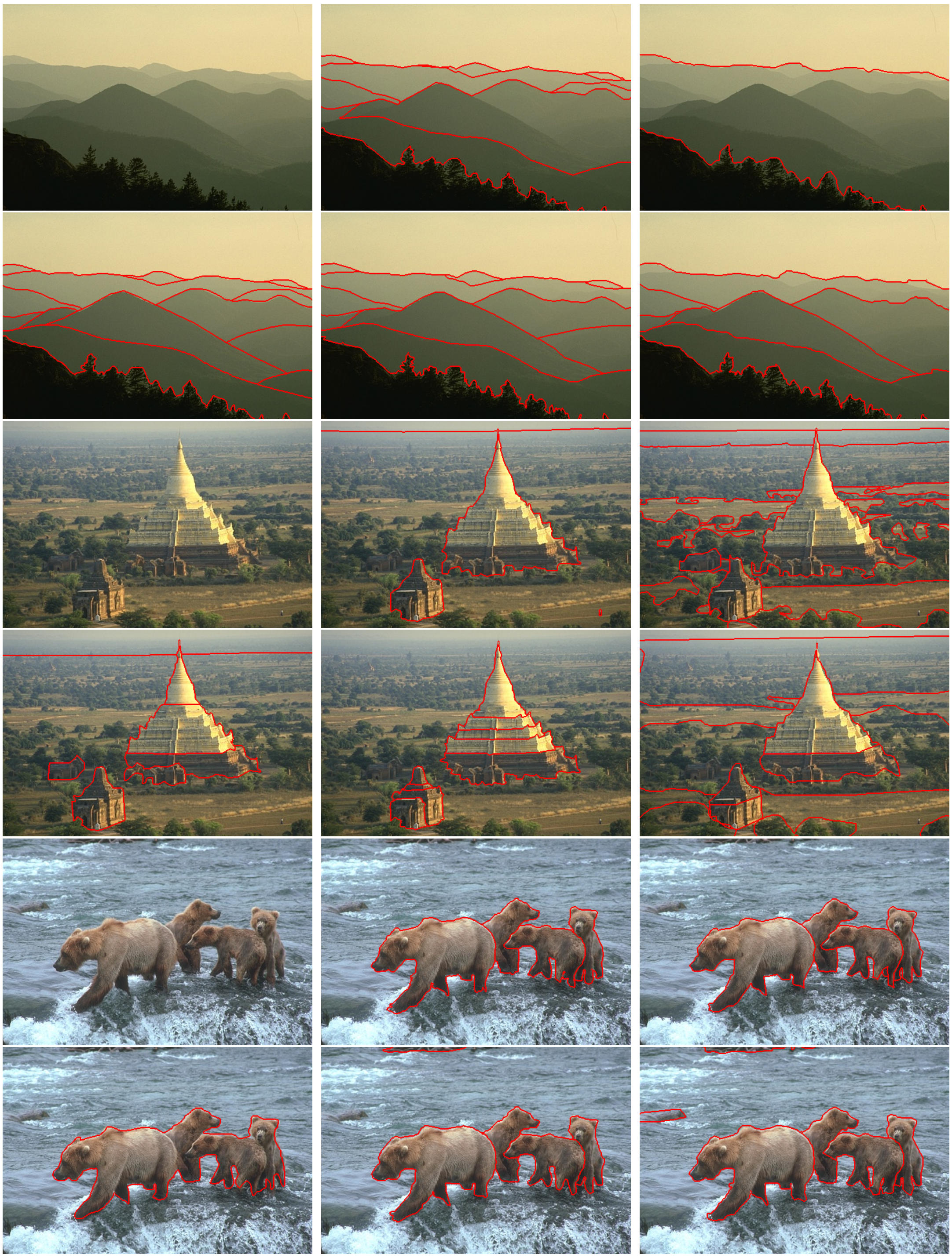

Figure 2.3: A few images and their ground-truth segmentations from BSDS300 and BSDS500 data sets. In every two rows: the upper left is the original image and the other five are the ground-truth segmentations made by different human subjects.

Figure 2.4: A few images and their ground-truth segmentations from MSRC21 data set. The original images are shown in odd columns, and the respective ground-truth segmentations are listed in the even columns with class labels shown in colour (the void label is in black).

pixel j have the same label in S_t, and p_{ij} is the corresponding probability estimated with the sample mean. A higher PRI value means a better segmentation.

The VoI is a metric that relates to the conditional entropies between the class label distribution. It measures the sum of information loss and information gain between the two partitions, and it is defined as

$$\mathrm{VoI}(S_g, S_t) = H(S_g) + H(S_t) - 2I(S_g, S_t), \tag{2.14}$$

where H and I are the respective entropies of the mutual information between two clusterings. A lower VoI value indicates better segmentation result.

The GCE measures the difference between two regions that contain the same pixel in different segmentations. Particularly, this metric compensates for the difference in granularity. Let $R(S, p_i)$ be the set of pixels within the regions in segmentation S that contains pixel p_i, and $'-'$ denote the set difference. The GCE is defined as

$$\mathrm{GCE}(S_t, S_g) = \frac{1}{N} \min \sum_i E(S_t, S_g, p_i), \sum_i E(S_g, S_t, p_i), \tag{2.15}$$

where $E(S_t, S_g, p_i) = \frac{|R(S_t,p_i) - R(S_g,p_i)|}{|R(S_t,p_i)|}$ is the local refinement error. Obviously, for the GCE values, being close to 0 implies a good segmentation.

The BDE measures the average displacement error of boundary pixels between two segmentations. The error of one boundary pixel is defined as the distance between the pixel and the closest pixel in the other boundary image.

For $p_i \in B_1$, we define $d(p_i, B_2) = \min_{p \in B_2} ||p_i - p||$ as the distance of a boundary point $p_i \in B_1$ to the boundary set B_2; let N_{B_1} and N_{B_2} denote the number of pixels in B_1 and B_2. The BDE is defined as

$$\mathrm{BDE}(B_1, B_2) = \frac{\sum_i^{N_{B_1}} \frac{d(p_i,B_2)}{N_{B_1}} + \sum_i^{N_{B_2}} \frac{d(p_i,B_1)}{N_{B_2}}}{2}. \tag{2.16}$$

A lower BDE value means less deviation between the segmentation and ground truth.

Since the performance of the algorithm is represented by a few indices, we use the average rank to represent the overall performance of the algorithm. Let $R = r_1, \cdots, r_n$ be the set of ranks on n evaluation indices of an algorithm. The average rank is defined as

$$\mathrm{Avg.R} = \frac{\sum_{i=1}^{n} r_i}{n}. \tag{2.17}$$

2.5.2 Evaluations for semantic segmentation

The performance of supervised segmentation is always evaluated based on the recall and precision criteria. Many researchers evaluated their algorithm via both the category average accuracy and the global accuracy (Shotton *et al.*, 2008; Gould *et al.*, 2014; Yao *et al.*, 2012). We follow their modus and use '*Global*' to refer the percentage of all pixels that were correctly classified and '*Avg(Class)*' for the average recall over all classes. Specifically, the recall of each class is computed by

$$Recall(Class_i) = \frac{\text{True Positive}}{\text{True Positive} + \text{False Negative}}, \tag{2.18}$$

and *Avg(Class)* is defined as

$$Avg(Class) = \frac{1}{N} \sum_{i=1}^{N} Recall(Class_i), \tag{2.19}$$

where N is the number of classes. *Global* is computed by

$$Global = \frac{\sum_{i=1}^{N} \text{True Positive}(Class_i)}{\sum_{i=1}^{N} \text{True Positive}(Class_i) + \text{False Negative}(Class_i)}. \tag{2.20}$$

2.6 General framework

The research in image segmentation is often connected with some particular applications. So, the frameworks may vary across different applications. However, our research concentrates on developing image segmentation approaches based on superpixels; consequently, we have a general framework which dominates our research.

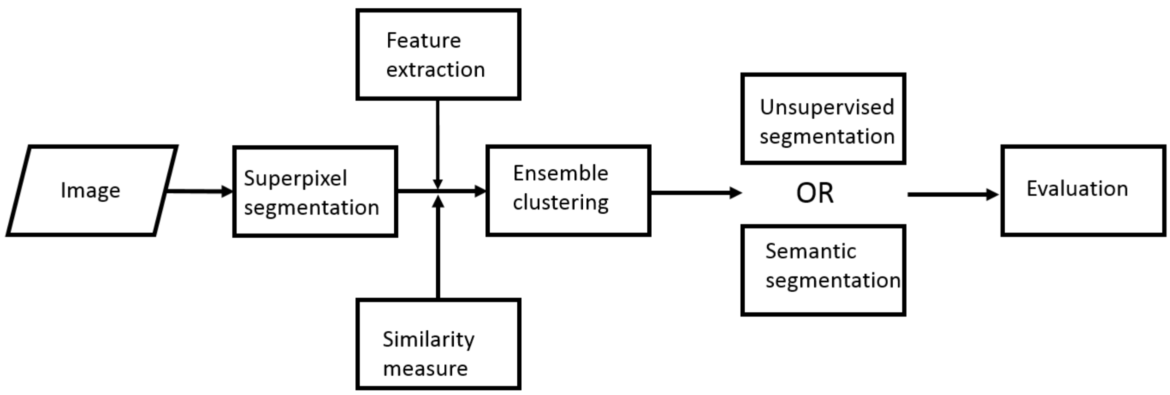

Figure 2.5: The flowchart of the research framework.

Generally, the work begins with generating superpixel segmentations and is followed by a model construction procedure, where different feature extraction and similarity measure methods are proposed. And then, image segmentation is carried out, which could be unsupervised or supervised. We have to mention that the supervised segmentation carried out in this thesis (i.e., semantic segmentation), actually involves both unsupervised and supervised methods. Finally, there is an evaluation procedure. Those unsupervised segmentation algorithms are evaluated by PRI, VoI, GCE and BDE on BSDS300 and BSDS500. For the supervised algorithms, the experiments are conducted on MSRC21 and evaluated by *Avg(Class)* and *Global*. Figure 2.5 demonstrates the flowchart of the research framework.

2.7 Summary

This chapter elaborates the fundamentals of our research that includes methods for generating superpixels, models for ensemble segmentation and a few popular segmentation evaluation methods. However, one thing that still needs to be addressed is the necessity of ensemble segmentation.

Figure 2.6: Segmentations from different superpixel algorithms. From left to right: the original image, Normalized Cut, F-H method, Mean Shift, and SLIC.

The superpixel algorithms are actually bottom-up segmentation algorithms, and most of them are proposed based on the perceptual grouping theory. But in real practice, there are no such algorithms that can produce segmentation as good as human vision does. Figure 2.6 shows a few segmentations made by some popular superpixel algorithms. It is easy to notice that they all tend to oversegment the objects. One possible reason for this phenomenon is that the perceptual grouping in human vision occurs by composing multiple features but most of the existing bottom-up segmentation algorithms lack the ability to group pixels in multiple feature spaces. Therefore, the ensemble techniques in image segmentation are worthy of investigation.

Chapter 3

Superpixel-based Segmentation with Colour Covariance Matrix

3.1 Introduction

A number of clustering algorithms can be used to segment an image, for example, the clustering-based algorithms such as Mean Shift (Comaniciu and Meer, 2002) and SLIC (Achanta *et al.*, 2012), and graph-based methods such as Ncut (Shi and Malik, 2000), F-H algorithm (Felzenszwalb and Huttenlocher, 2004) and Power Watersheds (Couprie *et al.*, 2009). Unfortunately, most of them have limited performance in practice because the visual patterns in the real-world images are broadly diverse and ambiguous while the algorithms are developed under some particular motivations. Actually, as is shown in Chapter 2, it is much easier for those algorithms to generate oversegmentations, that is, superpixels. However, in order to get a good image segmentation, some further treatment is required for the superpixels to be formed as the segmentation outcome (Panagiotakis *et al.*, 2013).

Notably, there is a growing trend in treating superpixels as cues to be merged through the clustering ensemble techniques. In Kim *et al.* (2010), a superpixel-based segmentation algorithm is proposed, in which the superpixel segmentations are fused by a graph model; Li *et al.* (2012) developed an efficient graph partition method, named *T-cut*, which can effectively reduce the computation complexity of bipartite-graph-based image segmentation. More recently, Wang *et al.* (2013) applied a sparse coding method to represent the superpixels in a ℓ_0 space, and achieved some impressive results by using a modified cross-adjacency matrix with the *T-Cut* algorithm.

In a wider context, it is found that the fusion of multiple cues can lead to better segmentation, for example, by combining colour histograms, local binary patterns feature, and Bag of Words (Cheng *et al.*, 2011). Apparently, a suitable representation of superpixels may improve the quality of superpixel-based image segmentation.

In this chapter, we proposed a method for improving the superpixel-based image segmentation algorithm. The experiments show that our algorithm is competitive to the state of the art, and performs better especially in the foreground-background segmentation. Figure 3.1 gives a quick comparison of our algorithm and SAS (Li *et al.*, 2012). Note that the tiger is split into different chunks by SAS, but not by our method.

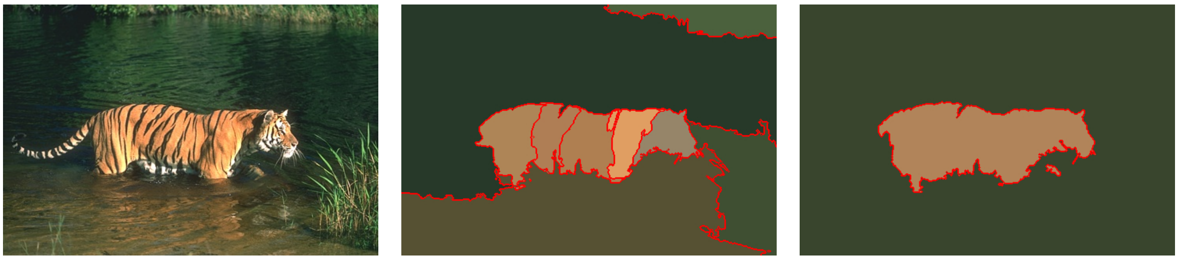

(a) (b) (c)

Figure 3.1: Visual comparison of the best segmentation: (a) original image; (b) SAS; (c) our method.

The main contributions are as follows:

- We first propose a colour covariance matrix as a kind of feature for superpixel, and, since the covariance matrix is a kind of tensor lying on a Riemannian manifold, we find a proper distance metric for it.
- We then propose several ways of fusing the similarity matrices of the superpixels which are measured in two different feature spaces and adopt a few empirical tests for them.

For the rest of this chapter, Section 3.2 is a brief introduction of ensemble segmentation with superpixels; Section 3.3 introduces our CCM algorithm; Section 3.4 gives the details about the experiments; and Section 3.5 is the summary of the chapter.

3.2 Superpixel ensemble

The HBGF algorithm (i.e., Algorithm 2.3) is employed to model the structure of the pixel data by the given superpixel segmentations.

Let $I = \{p_i, \cdots, p_m\}$ be an image and $\mathcal{S} = \{S^1, \cdots, S^N\}$ be a collection of superpixel segmentations, where $S^i = \{s_1^i, \cdots, s_{K_i}^i\}$ is a superpixel segmentation that contains K_i superpixels. Obviously, $\forall s_k^i, s_l^i, (k, l = 1, \cdots, K_i)$, we have $s_k^i \cap s_l^i = \emptyset$ for $k \neq l$ and $\cup_{k=1}^{K_i} s_k^i = I$.

Let $G(V^X, V^Y, W)$ be a bipartite graph for superpixel ensemble, where V^X and V^Y are two subsets of the vertices that satisfy $V^X \cup V^Y = V$ and $V^X \cap V^Y = \emptyset$; W is the weighted cross-adjacency matrix. Similar to the original HBGF model, we set $V^Y = \cup_{i=1}^N S^i$, but for V^X, we set it as an union of pixels and superpixels, that is, $V^X = I \cup (\cup_{i=1}^N S^i)$. With this setting, the bipartite graph is not only influenced by the relations between pixel and superpixel but also among the superpixels. Let v_i^X and v_j^Y represent vertices in V^X and V^Y respectively, then, the weight w_{ij} on the edge between v_i^X and v_j^Y is defined as

$$w_{ij} = \begin{cases} \alpha, & \text{if } v_i^X \in I \text{ and } v_i^X \in v_j^Y, \\ sim(v_i^X, v_j^Y), & \text{if } v_i^X \in S^i \text{ and } v_j^Y \in S^i, \\ 0 & \text{otherwise,} \end{cases} \tag{3.1}$$

where α is a constant, and $sim(x, y)$ is a function that returns the similarity of input x and y. From Eq. 3.1, W can be considered as a concatenation of two matrices, that is,

$$W = \begin{bmatrix} W^{ps} \\ W^{ss} \end{bmatrix}, \tag{3.2}$$

where W^{ps} represents the similarities between pixel and superpixel, and W^{ss} is the superpixel-wise similarity matrix. Moreover, it always holds $|V^X| \gg |V^Y|$ since the number of pixels are far more than that of superpixels. So, the spectral clustering on G can be applied via *T-cut* (i.e., Algorithm 2.4), which is more efficient than SVD (Li *et al.*, 2012).

3.3 The CCM algorithm

Figure 3.2 shows the framework of the CCM algorithm. The algorithm is named as CCM because it employs colour covariance matrix of the superpixels as one feature for similarity measuring among the superpixels.

In the first step, the input image is partitioned into a few oversegmentations by the superpixel algorithms. And then, the covariance descriptors are extracted from the superpixels. Thirdly, a bipartite graph is constructed based on the extracted covariance feature. Finally, the ensemble segmentation is run by the *T-cut* algorithm. The details of feature extraction and graph construction are elaborated in the following subsections.

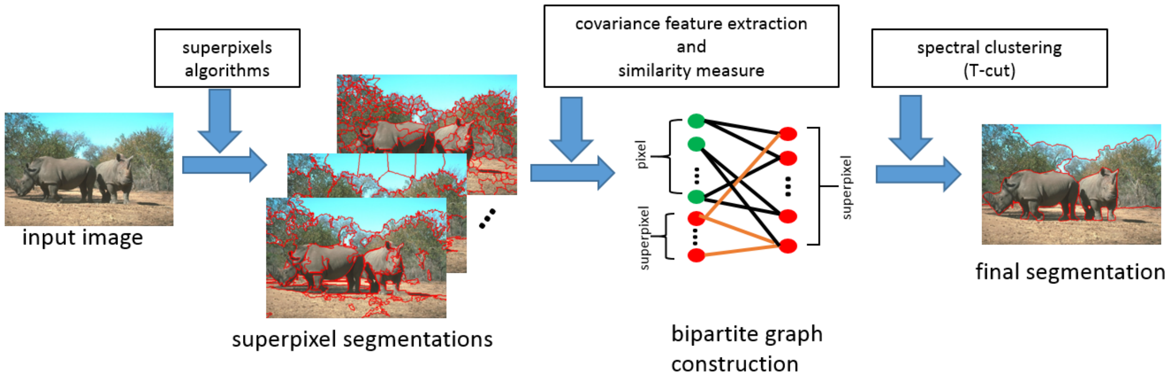

Figure 3.2: The framework of CCM.

3.3.1 Feature extraction

One of the key issues in superpixel-based segmentation is what kind of features can be extracted from superpixels. Intuitively, colour is the most important cue for humans to identify different objects, and in computer vision, the colour space is one of the most natural ways for representing an image. Particularly, it has been shown that the *Lab* colour can provide a good approximation of the colour difference in human vision (Jain, 1989). Therefore in CCM, the method for extracting feature descriptors is delivered based on the *Lab* colour space, but actually for other colour spaces, it is also adaptive.

Let $s_i = \{\mathbf{x}_1, \mathbf{x}_2, \cdots, \mathbf{x}_R\}$ be a superpixel of R pixels in the *Lab* colour space, where, $\mathbf{x}_i = (l_i, a_i, b_i)^T$ is a 3-dimension vector. The first feature we used to represent a superpixel is simply the average value of the colour vectors inside the superpixel. Given a superpixel s_i, the colour feature is defined as

$$\mathbf{c}_i = E(\mathbf{x}_r), \tag{3.3}$$

where $\mathbf{x}_r \in s_i$.

However, using colour information alone may not be enough for generating good segmentation because the high variations of lights and contrast in the real world always make the colour values unstable in the digital images. In fact, many researchers incorporate the colour cue with some other cues for getting a better image segmentation. For example, Li *et al.* (2012) use the spatial cues, that is, the neighbourhoods of the superpixel. But such a kind of spatial cues always fail to catch the long-range relations between the superpixels.

Different from others, we consider using the colour covariance matrix as a feature for the superpixel. The colour covariance matrix of superpixel s_i is defined as

$$\Sigma_i = E((\mathbf{x}_r - \mathbf{c}_i)(\mathbf{x}_r - \mathbf{c}_i)^T), \tag{3.4}$$

where $\mathbf{x}_r \in s_i$.

Covariance matrix is a kind of tensor that lies on a smooth manifold, hence requiring a non-Euclidean distance metric. Since they are symmetric and positive semi-definite, we can use the Förstner and Moonen metric (Förstner and Moonen, 2003) given as

$$d(\Sigma_A, \Sigma_B) = \sqrt{\sum_{r=1}^{n} \ln^2 \lambda_r}, \tag{3.5}$$

where Σ_A, Σ_B are two covariance matrices of dimension $n \times n$, and $\lambda_r (r = 1, \cdots, n)$ are eigenvalues from the generalized eigenvalue problem $|\lambda \Sigma_A - \Sigma_B| = 0$ (Please note that '$|\cdot|$' represents the determinant here).

3.3.2 The similarity measure

Another difference between the CCM and other related works is in the similarity measure of the superpixels. In Li *et al.* (2012), each superpixel is connected with the nearest neighbourhood among its spatially adjacent superpixels, which fails to catch the relationship of those vertices that are separated by spatial distance but close in the feature space. In Wang *et al.* (2013), this weakness was overcome by measuring the similarity of the superpixels with their ℓ_0 sparse coding representation. However, this problem can also be solved in another way. In the CCM approach, the colour covariance matrices are employed to strengthen the colour representations of superpixels so that the spatial constraint can be removed.

Let d_{ij} denote the distance between superpixel s_i and s_j. The similarity function $sim(s_i, s_j)$ between the two superpixels, then, is defined as follows:

$$sim(s_i, s_j) = \begin{cases} e^{-\beta \min(d_{ij}, d_{ji})}, & \text{if } i \neq j, \\ 1, & \text{otherwise,} \end{cases} \tag{3.6}$$

where β is a coefficient of the Gaussian-like kernel, and d_{ij} is normalized into [0,1].

Because the superpixels are represented by two features and they are in two different feature spaces, one is Euclidean and the other is non-Euclidean, it is more desirable to compute the similarity separately than to concatenate them as a vector. Specifically, the distance of the superpixels (i.e., d_{ij}) is represented by Euclidean distance in colour space, and for the representation in the covariance matrix space, Eq. 3.5 is hired.

Let sim^C denote the similarity in *Lab* colour space and sim^Σ be the similarity in the covariance manifold; $Sim = [sim_{ij}]$ denotes the similarity matrix over all superpixels. There are three algorithms for fusing the similarity matrices. The first is by means of the entry-wise product (*aka* Hadamard product):

$$Sim^{\mathrm{HP}} = Sim^C \circ Sim^\Sigma. \tag{3.7}$$

The second approach is proposed by de Sa (2005), which adopts the direct matrix product to similarity matrices:

$$Sim^{\mathrm{DP}} = Sim^c \times Sim^\Sigma. \tag{3.8}$$

The third one is to combine two individual modalities by simply adding them together, which is proposed by Joachims (2003):

$$Sim^{\mathrm{AD}} = Sim^c + Sim^\Sigma. \tag{3.9}$$

In practice, we try all three approaches and choose the one that gives the best performance as the fusing method. The overall algorithm of CCM is given in Algorithm 3.1

Algorithm 3.1 Superpixel-based Segmentation via Colour Covariance Matrix

Input: An image $I = \{p_1, \cdots, p_m\}$, a collection of superpixel segmentations $\mathcal{S} = \{S^1, \cdots, S^N\}$, the cluster number k of the final clustering

Output: Final clustering $S = (s_1, ..., s_k)$

```
Set V^X = I ∪ (∪_{i=1}^N S^i), V^Y = ∪_{i=1}^N S^i, n = Σ_{i=1}^N K_i;
W = ∅;
for i = 1, ··· , m do
    for j = 1, ··· , n do
        Compute the similarity of the superpixels via Eq. 3.6;
        Fuse similarities via Eq. 3.7, Eq. 3.8, or Eq 3.9;
        Compute w_ij via Eq. 3.1;
        W = W ∪ w_ij;
    end for
end for
Apply T-cut to obtain S.
```

Let m be the number of pixels, n be the total number of superpixels, N be the number of superpixel segmentations, and K_i be the numbers of superpixels in the

i-th superpixel segmentation and $K = \max\{K_i\}$. In CCM, the graph construction takes $N(m+n)$ operations + $\mathcal{O}(NK^2)$, and the computational complexity of *T-cut* is $\mathcal{O}(n^{3/2})$ (Li *et al.*, 2012). The computational complexity of CCM is $\mathcal{O}\left(n^{3/2} + NK^2\right)$.

3.4 Experiments

3.4.1 Data sets and settings

The experiments are conducted on two public image segmentation datasets: the Berkeley Segmentation Data Set 300 (BSDS300), and its update, the Berkeley Segmentation Data Set 500 (BSDS500) (Martin *et al.*, 2001; Arbelaez *et al.*, 2011).

In order to compare the performance of the CCM and the state of the art, the parameters are set as the same as those in Li *et al.* (2012) and Wang *et al.* (2013). Specifically, the superpixel segmentations are created by Mean Shift and F-H algorithm. There are three superpixel segmentations generated by Mean Shift with the parameters $(h_s, h_r, M) \in \{(7,7,100), (7,9,100), (7,11,100)\}$ where h_s and h_r are the bandwidth parameters, and M represents the minimum size of the superpixel, and two or three superpixel segmentations produced by the F-H algorithm based on the image variance in the *Lab* colour space with a given threshold; the parameters are set to be $(\sigma, c, M) \in \{(0.5,100,50), (0.8,200,100)\}$ for the two-segmentation case, or $(\sigma, c, M) \in \{(0.8,150,50), (0.8,200,100), (0.8,300,100)\}$ for the three-segmentation case, where σ and c are the parameters for smoothing and scale; M is the minimum size of the superpixel.

For the edge weights in Eq. 3.1, α is set to be 1×10^{-3}, and the parameter β in Eq. 3.6, we set $\beta = 20$ for all feature spaces. We also adopt a nearest-neighbour filter on the similarity matrix of the superpixels, so each superpixel is only connected to its closest neighbour in the final similarity matrix, which is the same as in Li *et al.* (2012) and Wang *et al.* (2013).

The experiments are conducted in two parts. First, for each algorithm, we gradually increase the number of segments K from 2 to 40 for every image to find the best value of K that gives it the highest performance, and we compare the algorithms by manually setting the K to its best value for each image in the experiments. Second, we fix the segment number $K = 2$, which is considered as a foreground and background segmentation.

3.4.2 Results

We compare the CCM with the SAS(Li *et al.*, 2012) and ℓ_0-sparse (Wang *et al.*, 2013). The evaluation is based on four popular methods, that is, PRI (Unnikrishnan *et al.*, 2007), VoI (Meilă, 2005), GCE (Martin *et al.*, 2001), and BDE (Freixenet *et al.*, 2002). The overall performance is represented by Avg.R, that is, the average rank. Moreover, we would like to mention that for PRI a higher value means better, and for VoI, GCE and BDE, the lower value is better.

Table 3.1 and Table 3.2 show the scores of the four evaluation indices with the K manually adjusted on BSDS300 and BSDS500. And, the results of $K = 2$ are listed in Table 3.3 and Table 3.4 separately. Here, we note that some of the scores of the SAS algorithm and ℓ_0-sparse representation methods are directly obtained from the reports in (Li *et al.*, 2012; Wang *et al.*, 2013), and the symbol '$-$' means there are no published results available.

Table 3.1: Performance over BSDS300 with K adjusted manually

Algorithms	PRI	VoI	GCE	BDE	Avg.R
SAS	0.8319	1.6849	**0.1779**	11.2900	2.5
ℓ_0-sparse	0.8355	1.9935	0.2297	**11.1955**	2.5
CCM(W_{HP})	**0.8495**	**1.6260**	0.1785	12.3034	**2.25**
CCM(W_{DP})	0.8345	2.1169	0.2341	12.0008	4.5
CCM(W_{AD})	0.8397	2.0359	0.2308	11.8868	3.25

Table 3.2: Performance over BSDS500 with K adjusted manually

Algorithms	PRI	VoI	GCE	BDE	Avg.R
SAS	0.8372	**1.6914**	**0.1813**	12.6599	2
ℓ_0-sparse	-	-	-	-	-
CCM(W_{HP})	**0.8407**	2.0399	0.2359	**10.7800**	**1**
CCM(W_{DP})	0.8275	2.5169	0.2541	11.5002	3.5
CCM(W_{AD})	0.8370	2.0490	0.2503	10.8868	2.75

In both scenarios our method gives a competitive performance. Our method ranks the first place with PRI and VoI when the cluster number K is manually set, and when K is fixed to 2, it gets the best scores in PRI, VoI, and GCE. We also examine the performance of all three fusion methods in the experiments. The Hadamard product

Table 3.3: Performance over BSDS300 with K fixed to 2

Algorithms	PRI	VoI	GCE	BDE	Avg.R
SAS	0.6179	2.0110	0.1106	42.2877	4.25
ℓ_0-sparse	0.6270	2.0299	0.1050	**23.1298**	3
CCM(W_{HP})	**0.6312**	**1.9350**	**0.0820**	35.8760	**1.75**
CCM(W_{DP})	0.5998	2.0336	0.0892	29.1803	3.5
CCM(W_{AD})	0.6284	1.997	0.0940	24.6991	2.25

Table 3.4: Performance over BSDS500 with K fixed to 2

Algorithms	PRI	VoI	GCE	BDE	Avg.R
SAS	0.6094	2.0701	0.1130	43.7731	3.5
ℓ_0-sparse	-	-	-	-	-
CCM(W_{HP})	**0.6234**	**1.9961**	**0.0870**	36.4631	**1.5**
CCM(W_{DP})	0.5961	2.0841	0.0923	28.6858	3
CCM(W_{AD})	0.6203	2.0461	0.0972	25.3790	2

seems to perform the best among the three fusing schemes with the best Avg.R, but the difference is marginal.

Moreover, the effects of different colour spaces are also investigated. As shown in Table 3.5, the choice of the colour space does not seem to be critical, since the use of the colour covariance matrices seems to boost the performance significantly to a competitive level, even for RGB and HSV. SAS, on the other hand, reports worse results in VoI and GCE when using these two colour spaces compared with using *Lab*.

Table 3.5: Performance in different colour spaces (on BSDS300, $K = 2$)

Algorithms	PRI	VoI	GCE	BDE	Avg.R
Lab (SAS)	0.6179	2.011	0.1106	42.2877	5
RBG (SAS)	0.6189	2.0224	0.1138	42.5141	4.5
HSV (SAS)	0.6182	2.0450	0.1203	42.0903	5.5
Lab (CCM(W_{HP}))	0.6312	**1.9350**	0.0820	35.8760	2
RBG (CCM(W_{HP}))	0.6289	1.9426	**0.0815**	33.9353	2
HSV (CCM(W_{HP}))	**0.6317**	1.9549	0.0838	**30.2480**	2

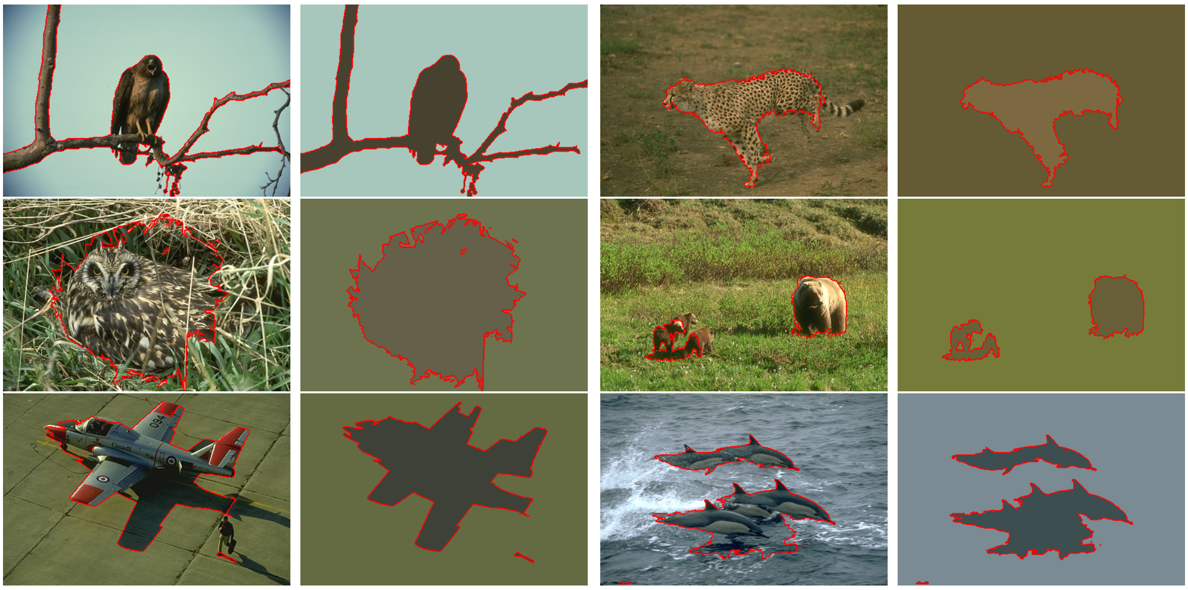

Figure 3.3: Some segmentation results of CCM ($K = 2$).

The experiment results on the BSDS data sets show that the new superpixel feature extracted by a covariance matrix apparently improves the average performance of the bipartite graph-based algorithm when combined with colour cues. By removing the spatial constraints, our method seems to handle long-range homogeneity well, forming superpixels well aligned with object contours. Figure 3.3 shows more experimental results of our algorithm when K is set to 2. And, Figure 3.4 demonstrates the results of the K when set manually. The method seems to be quite effective in foreground-background separation.

When the superpixel segmentations are given, the runtime of the CCM is about 3 seconds per image with Matlab 2014a and a desktop equipped with an Intel i5 CPU and 16GB RAM.

3.5 Conclusion

In this chapter, we present a superpixel-based segmentation approach that uses colour covariance matrices to boost the performance of graph-based image segmentation. A non-Euclidean metric is employed for the covariance matrix space, and the new feature is then integrated with colour information to form the affinity graph for segmentation. The empirical results show that the new approach produces better or competitive segmentation results compared with the state-of-the-art approaches. It is not sensitive to the choice of colour space, different from the previous work (Li *et al.*, 2012).

Figure 3.4: Some segmentation results of CCM (K manually set).

But, there are two issues that need to be considered further. The first one is the methods for merging the similarity matrix of the superpixels. We would like to explore some other information fusing approaches rather than the three intuitive methods used in this chapter. The second one is about the covariance matrix itself, that is, what kind of covariance matrix is better for superpixel representation. These issues will be discussed in the next two chapters.

Chapter 4

Improving the Colour Covariance Matrix-based Segmentation with Subspace Representation

4.1 Introduction

In the CCM algorithm proposed in Chapter 3, the colour covariance matrix is employed to represent the superpixels, by which the similarities between the superpixels can be measured on a Riemannian manifold. The segmentation quality is improved by fusing the superpixel-wise similarities measured in the colour space and the Riemannian manifold. Although the CCM algorithm shows that the covariance descriptor is a useful representation for superpixels, one thing still needs to be considered. Because different features may have different data structures, for example, the covariance descriptors of the superpixels are lying on an manifold while the *Lab* colour features are points in a 3-D Euclidean space, it may not be appropriate to fuse the superpixel descriptors from different feature spaces directly in a Euclidean space. A new feature-fusing method is needed for improving the CCM algorithm.

The research in subspace representation has been blooming in recent years, and some works in that region shed light on the problem mentioned above. Actually, in the literature this problem is also called feature embedding (Zhang *et al.*, 2015). Most of the proposed solutions are based on the dimensionality reduction technologies, by which the redundancy among features can be reduced while preserving the important discriminative information. Tang *et al.* (2009) modelled the relations from different features with different graphs, and the common factors of the multiple graphs are extracted by linked matrix factorization. Dong *et al.* (2014) formulated the multiple features by a multi-layer graph, but differently, they merge the different layers via the regularization on a Grassmann manifold. Zhou and Burges (2007) proposed multiple-graph merging models based on the graph random walk, and the kernel methods are also employed for fusing the information from multiple sources (Wang *et al.*, 2012; Nguyen *et al.*, 2015).

In this chapter we propose one method for fusing superpixel descriptors extracted from different feature spaces, and this method improves the performance of the CCM. Our contributions are as follows:

- we propose a multi-layer bipartite graph to formulate structure information provided by the colour and the covariance descriptors of the superpixels;
- we develop an algorithm for clustering multi-layer bipartite graph.

In the rest of the chapter, Section 4.2 contains the introductions of the necessary background knowledge for elaborating our algorithms. Section 4.3 is the multi-layer bipartite graph-based CCM algorithm (MBG-CCM) and Section 4.4 shows the results of the experiments. In Section 4.5, we give the conclusion.

4.2 Preliminary

4.2.1 The subspace representation

Given a graph $G(V, E)$ and letting W be the adjacency matrix of G, we set the degree matrix $D = \mathrm{diag}(W\mathbf{1})$, where $\mathbf{1}$ is a vector of ones of appropriate size. Then, the graph Laplacian of G is defined as

$$L = D - W. \tag{4.1}$$

For a graph, L is a representation of its structure, i.e., the relations between the vertices. The spectral decomposition of L can map the graph into a Euclidean space with the structure information preserved (Von Luxburg, 2007). Moreover, if we replace the graph Laplacian with $L = D^{-\frac{1}{2}}WD^{-\frac{1}{2}}$, the eigenvectors of the k largest eigenvalues of L will still contain most structure information of the graph (Dong *et al.*, 2014).

Let $U = [u_1, \cdots, u_k]$ be a set of the first k eigenvectors of L. Since the eigenvectors are orthogonal to each other and k is smaller than the rank of L, we say U is a subspace representation of L .

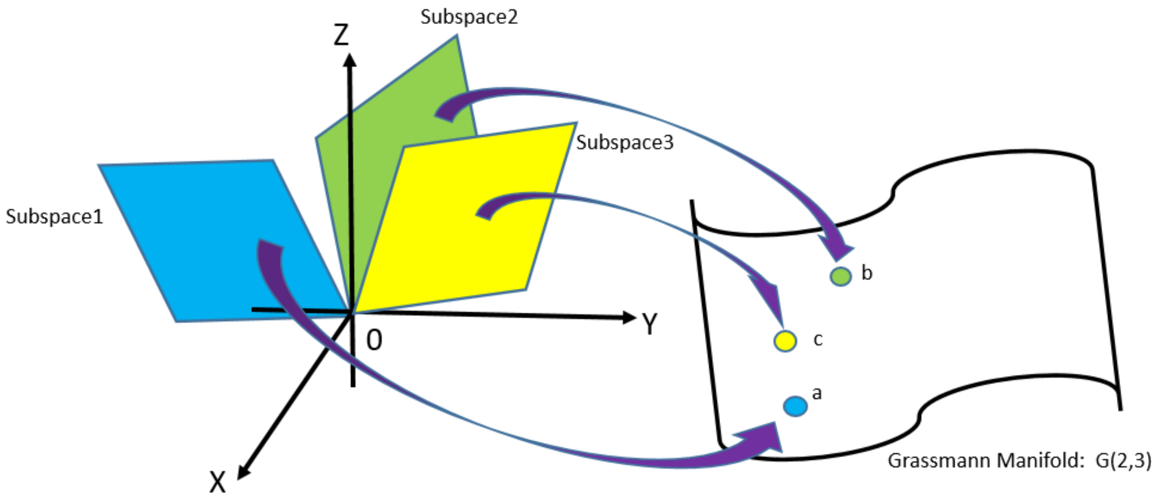

Figure 4.1: An example of Grassmann manifold $\mathcal{G}(2,3)$. The subspace representations are points on $\mathcal{G}(2,3)$.

4.2.2 Grassmann manifold

A Grassmann manifold $\mathcal{G}(k,n)$ is defined as the set of k-dimensional linear subspace of $\mathbb{R}^n$ (Hamm and Lee, 2008). Figure 4.1 demonstrates an example of Grassmann manifold $\mathcal{G}(2,3)$.

Obviously, the subspace representation of L can be considered as a point on a Grassmann manifold.

4.3 Multi-layer graph-based CCM

A number of low-level features can be extracted from superpixels, such as colours, covariance descriptors, each of which is a source of segmentation information. They can be formulated by a multi-layer bipartite graph, with which the structure information from each feature space is represented by a single graph layer independently.

We first introduce the clustering method of a normal multi-layer graph, then, propose the clustering algorithm for the bipartite case.

4.3.1 The multi-layer graph

A multi-layer graph is used to model a graph that processes multiple views. Given a data set $X = \{x_1, \cdots, x_n\}$, let $G(V,E)$ be a graph built on X, where V is the vertex set, each vertex represents a point in X, and E is the set of edges, representing the relationships between the vertices.

Suppose the data set X has M different properties which lead to M different relationships among the vertices; naturally, they can be represented by a set of weighted edges on the common set of vertices. So, a multi-layer graph G with M-layer is defined as

$$G = \{G_i\}_{i=1}^{M}, \tag{4.2}$$

where G_i is a single layer built on the i-th property and defined as

$$G_i = G(V, W_i), \tag{4.3}$$

where W_i is the weight associated to the i-th edge set E_i.

4.3.2 Clustering on multi-layer graph

The clustering on the multi-layer graph G is actually an ensemble of the clusterings on all single graph G_i. Since a graph can be represented by its subspace representation, we achieve the ensemble via a Grassmann manifold.

Let U_i be the subspace representation of $G_i \in G$; the subspace representation of a M-layer graph is written as

$$\mathcal{U} = \{U_i\}_{i=1}^{M}. \tag{4.4}$$

Since each U_i is a point on a Grassmann manifold, the fusion of the $U_i \in \mathcal{U}$ can be straightforwardly modelled as a minimization problem (Dong *et al.*, 2014),

$$U = \arg\min_{U} \sum_{i=1}^{M} f(U_i, U) \tag{4.5}$$

where U is the final representation of $\mathcal{U}$, and, $f(\cdot, \cdot)$ is the cost function. Same as Dong *et al.* (2014), we use the squared projection distance as the cost function, and Eq. 4.5 can be rewritten as

$$U = \arg\min_{U} \sum_{i=1}^{M} d_{proj}^2(U_i, U), \tag{4.6}$$

where $d_{proj}(\cdot, \cdot)$ is the projection distance.

Using Eq. 4.6 is based on two facts. Firstly, the spectral clustering is equal to a trace minimization problem (Dhillon *et al.*, 2004), that is,

$$\begin{aligned} &\min_{U \in R^{n \times k}} \operatorname{tr}(U^T L U), \\ &\text{s.t. } U^T U = I. \end{aligned} \tag{4.7}$$

where n, k are the numbers of vertices and clusters respectively; $\text{tr}(\cdot)$ returns the trace of the input. Secondly, projection distance is a measurement on the Grassmann manifolds, which is related to trace. The defined of projection distance is

$$d_{proj}(X_1, X_2) = (\sum_{i=1}^{k} \sin^2 \theta_i)^{1/2} \tag{4.8}$$

where X_1, X_2 are the orthonormal matrices representing two subspaces; $\{\theta_i\}_{i=1}^{k}$ is the set of principal angles between two subspaces. So, for the squared projection distance, we have (Hamm and Lee, 2008)

$$\begin{aligned} d^2_{proj}(X_1, X_2) &= \sum_{i=1}^{k} \sin^2 \theta_i \\ &= k - \sum_{i=1}^{k} \cos^2 \theta_i \\ &= k - \text{tr}(X_1 X_1^T X_2 X_2^T). \end{aligned} \tag{4.9}$$

And so, Eq. 4.6 can be written as

$$U = \arg\min_{U} \left[kM - \sum_{i=1}^{M} \text{tr}(UU^T U_i, U_i^T) \right]. \tag{4.10}$$

Because U needs to satisfy both Eq. 4.7 and Eq. 4.10, we can combine them together as follows:

$$\begin{aligned} &\min_{U \in R^{n \times k}} \sum_{i=1}^{M} \text{tr}(U^T L_i U) + \gamma \left[kM - \sum_{i=1}^{M} \text{tr}(UU^T U_i U_i^T) \right], \\ &\text{s.t. } UU^T = I, \end{aligned} \tag{4.11}$$

where L_i is the i-th Laplacian of G and U_i is the respective subspace representation, and γ is a weight parameter that balances the effects of two terms in the equation. Moreover, by ignoring the constant term in Eq. 4.11 and considering the fact that $\text{tr}(X) = \text{tr}(X^T)$, we have

$$\begin{aligned} &\min_{U \in R^{n \times k}} tr \left[U^T (\sum_{i=1}^{M} L_i - \gamma \sum_{i=1}^{M} U_i U_i^T) U \right], \\ &\text{s.t. } U^T U = I. \end{aligned} \tag{4.12}$$

If we set

$$L_{mod} = \sum_{i=1}^{M} L_i - \gamma \sum_{i=1}^{M} U_i U_i^T, \tag{4.13}$$

then, the solution of Eq. 4.12 is the first k eigenvectors of the modified Laplacian L_{mod}.

4.3.3 The multi-layer bipartite graph

Given a multi-layer graph G, if each layer G_i is a bipartite graph, then we say G is a multi-layer bipartite graph.

Let $I = \{p_1, \cdots, p_m\}$ be an image with m pixels, and $\mathcal{S} = \{S^1, \cdots, S^N\}$ be a collection of superpixel clusterings of the image, where $S^i = \{s^i_1, \cdots, s^i_{k_i}\}$ is the i-th superpixel clustering with k_i superpixels. Suppose there are M different features extracted from the superpixels, and let G be the multi-layer bipartite graph, which is written as

$$G = \{G_i\}_{i=1}^M = \{G(V^X, V^Y, W_i)\}_{i=1}^M, \tag{4.14}$$

where W_i is the cross-adjacency matrix corresponding to the i-th feature. And each single layer G_i is constructed by setting $V^X = I \cup \mathcal{S}$ and $V^Y = \mathcal{S}$.

One straightforward way to merge the $\{G_i\}$ is treating every G_i as a normal graph, that is, extending W_i into a $(m+n) \times (m+n)$ matrix, so Eq. 4.13 can directly work on G. However, this could be intractable in image segmentation because the huge number of pixel results in high complexity both in computation and memory.

Actually, the spectral clustering of each $G_i \in G$ can be done via singular value decomposition (SVD) of the normalized W_i, and the clustering of V^X can be obtained from the clustering of V^Y (Li *et al.*, 2012; Dhillon, 2001). Fortunately, with the following lemma, this is also applicable for the multi-lay bipartite graph.

Lemma 4.3.1. *Given a matrix* $A = \begin{bmatrix} a_{11} & \cdots & a_{1n} \\ \vdots & & \vdots \\ a_{m1} & \cdots & a_{mn} \end{bmatrix}$, *let* $D_X = diag(A)$ *be a* $m \times m$ *diagonal matrix with the* i*-th entry of the main diagonal is the sum of the* i*-th row of* A *(i.e.,* $\sum_{j=1}^n a_{ij}$*), and* $D_Y = diag(A^T)$ *be a* $n \times n$ *diagonal matrix with the* j*-th entry of the main diagonal is the sum of* j*-th column of* A *(i.e.,* $\sum_{i=1}^m a_{ij}$*), then, it holds* $D_Y = diag(A^T D_X^{-1} A)$.

Proof. The proof is straightforward. $A^T D_X^{-1} A =$

$$\begin{bmatrix} a_{11} & \cdots & a_{m1} \\ \vdots & & \vdots \\ a_{1n} & \cdots & a_{mn} \end{bmatrix} \begin{bmatrix} (\sum_{j=1}^n a_{1j})^{-1} & & \\ & \ddots & \\ & & (\sum_{j=1}^n a_{mj})^{-1} \end{bmatrix} \begin{bmatrix} a_{11} & \cdots & a_{1n} \\ \vdots & & \vdots \\ a_{m1} & \cdots & a_{mn} \end{bmatrix}$$

$$= \begin{bmatrix} \frac{a_{11}^2}{\sum_{j=1}^n a_{1j}} + \cdots + \frac{a_{m1}^2}{\sum_{j=1}^n a_{mj}} & \cdots & \frac{a_{11}a_{1n}}{\sum_{j=1}^n a_{1j}} + \cdots + \frac{a_{m1}a_{mn}}{\sum_{j=1}^n a_{mj}} \\ \vdots & & \vdots \\ \frac{a_{1n}a_{11}}{\sum_{j=1}^n a_{1j}} + \cdots + \frac{a_{mn}a_{m1}}{\sum_{j=1}^n a_{mj}} & \cdots & \frac{a_{1n}^2}{\sum_{j=1}^n a_{1j}} + \cdots + \frac{a_{mn}^2}{\sum_{j=1}^n a_{mj}} \end{bmatrix},$$

$$\text{so, } \mathrm{diag}(A^T D_X^{-1} A) = \begin{bmatrix} \sum_{i=1}^m a_{i1} \frac{\sum_{j=1}^n a_{ij}}{\sum_{j=1}^n a_{ij}} & & \\ & \ddots & \\ & & \sum_{i=1}^m a_{in} \frac{\sum_{j=1}^n a_{ij}}{\sum_{j=1}^n a_{ij}} \end{bmatrix} = D_Y. \qquad \square$$

Let W_{in} be the i-th normalized cross-adjacency matrix, according to the definition we have

$$W_{in} = D_{iX}^{-\frac{1}{2}} W_i D_{iY}^{-\frac{1}{2}}, \tag{4.15}$$

where $D_{iX} = \mathrm{diag}(W_i \mathbf{1})$ and $D_{iY} = \mathrm{diag}(W_i^T \mathbf{1})$, and $\mathbf{1}$ is a vector of ones in proper size; $\mathrm{diag}(\cdot)$ is a diagonal matrix whose nonzero entries represented by '$(\cdot)$'. Then, we define W_{iYn}, whose eigenvectors are the right singular vectors of W_{in}:

$$W_{iYn} = W_{in}^T W_{in} = D_{iY}^{-\frac{1}{2}} W_i^T D_{iX}^{-1} W_i D_{iY}^{-\frac{1}{2}}, \tag{4.16}$$

If we set $W_{iY} = W_i^T D_{iX}^{-1} W_i$, from Lemma 4.3.1, we know $D_{iY} = \mathrm{diag}(W_i^T D_{iX}^{-1} W_i)$, then, the normalized graph Laplacian of $G_{iY}(V^Y, W_{iY})$ is

$$L_{iYn} = I - W_{iYn}. \tag{4.17}$$

Therefore, for a multi-layer bipartite graph G, the layers can be merged by Eq. 4.13 with the Laplacian in Eq. 4.17. Because the pixel-superpixel relations (i.e., W^{ps} in Eq. 3.2) in each graph layer are the same, the clustering of V^X can be obtained from the clustering of V^Y by the *T-cut*. Algorithm 4.1 shows the details.

Algorithm 4.1 MBG-CCM

Input: A set of weighted cross-adjacency matrix $\{W_i\}_{i=1}^M$ of multi-layer bipartite graph G, merging weight parameter γ, number of clusters k;

Output: A final clustering $\mathcal{C} = \{C_1, \cdots, C_n\}$

1: **for** $i = 1, \cdots, M$ **do**
2: Convert W_i into W_{iYn} by Eq. 4.16
3: Compute the normalized Laplacian L_i of G_i by Eq. 4.17.
4: Compute the first k eigenvectors of L_i as U_i.
5: **end for**
6: Compute the merged Laplacian L_{mod}^Y by Eq. 4.13.
7: Compute the first k eigenvectors of L_{mod}^Y as U.
8: Apply the *T-cut* (i.e., Algorithm 2.4) to obtain the final clustering $\mathcal{C}$.

The computational cost of MBG-CCM contains three parts: the graph construction, the layer merging, and *T-cut*. Let m be the number of pixels, n be the total number of superpixels, M be the number of superpixel segmentations (i.e., the number of layers), and K_i be the numbers of superpixels in the i-th superpixel segmentation and $K = \max\{K_i\}$. For graph construction, there are M(m+n) operations + $\mathcal{O}(MK^2)$ operations. The layer merging takes $\mathcal{O}(Mn^{3/2})$, and the cost of *T-cuts* is $\mathcal{O}(n^{3/2})$. Therefore, the total computational complexity of MBG-CCM is $\mathcal{O}\left((M+1)n^{3/2} + MK^2\right)$, which is M times higher than the CCM.

4.4 Experiments

4.4.1 Data sets and settings

The experiments are conducted on two public image segmentation datasets: the Berkeley Segmentation Data Set 300 (BSDS300), and its update, the Berkeley Segmentation Data Set 500 (BSDS500) (Martin *et al.*, 2001; Arbelaez *et al.*, 2011).

For comparison purposes, we set the parameters to the same values as those used in CCM. Specifically, the superpixel segmentations are created by Mean Shift and F-H algorithm with the same parameter settings. There are three superpixel segmentations generated by Mean Shift with the parameters $(h_s, h_r, M) \in \{(7, 7, 100), (7, 9, 100), (7, 11, 100)\}$ where h_s and h_r are the bandwidth parameters, and M represents the minimum size of the superpixel, and two or three superpixel segmentations produced by F-H algorithm based on the image variance in the *Lab* colour space with a given threshold; the parameters are set to be $(\sigma, c, M) \in \{(0.5, 100, 50), (0.8, 200, 100)\}$ for the two-segmentation case, or $(\sigma, c, M) \in \{(0.8, 150, 50), (0.8, 200, 100), (0.8, 300, 100)\}$ for the three-segmentation case, where σ and c are the parameters for smoothing and scale; M is the minimum size of the superpixel.

For MBG-CCM, each single bipartite graph layer is constructed by following the Algorithm 3.1 in Chapter 3. The edge-weights parameter α is set to be 1×10^{-3} and the scale parameter β is set to be 20 for all feature spaces. In addition, the γ in Eq. 4.13 is set to $\gamma = 1$.

The experiments are conducted in two parts. First, for each algorithm, we gradually increase the number of segments K from 2 to 40 for every image to find the best value of K that gives it the highest performance, and we compare the algorithms by setting the K to it best value for each image in the experiments. Second, we fix the segment number $K = 2$, which is considered as a way for foreground-background segmentation.

4.4.2 Results

We compare the performance of MBG-CCM with CCM. And the evaluation is based on four popular methods, that is, PRI (Unnikrishnan *et al.*, 2007), VoI (Meilă, 2005), GCE (Martin *et al.*, 2001), and BDE (Freixenet *et al.*, 2002). The overall performance is represented by Avg.R, that is, the average rank.

Table 4.1 and Table 4.2 show the results of foreground-background segmentation (i.e., $K = 2$). In this case, the scores of MBG-CCM rank first in PRI on both data sets and second in VoI and BDE with performance quite close to the best one. And the Avg.R score of MBG-CCM is equal to CCM/HP. Moreover, Table 4.3 and Table 4.4 show the performance of K manually adjusted. MBG-CCM also performs competitively. Figure 4.2 and Figure 4.3 give more visual results of MBG-CCM algorithm with $K = 2$ and K manually set respectively.

Table 4.1: Performance over the BSDS300 with K fixed to 2

Algorithms	PRI	VoI	GCE	BDE	Avg.R
CCM/HP	0.631	**1.935**	**0.082**	35.876	2
CCM/DP	0.599	2.033	0.089	29.180	3.75
CCM/AD	0.628	1.997	0.094	24.699	2.75
MBG-CCM	**0.641**	2.018	0.104	**21.426**	2

Table 4.2: Performance over the BSDS500 with K fixed to 2

Algorithms	PRI	VoI	GCE	BDE	Avg.R
CCM/HP	0.623	**1.996**	**0.087**	36.463	2
CCM/DP	0.596	2.084	0.092	28.685	3.75
CCM/AD	0.620	2.054	0.097	25.379	2.75
MBG-CCM	**0.635**	2.067	0.108	**21.610**	2

Table 4.3: Performance over the BSDS300 with K manually adjusted

Algorithms	PRI	VoI	GCE	BDE	Avg.R
CCM/HP	**0.8495**	**1.6260**	**0.1785**	12.3034	1.75
CCM/DP	0.8345	2.1169	0.2341	12.0008	3.75
CCM/AD	0.8397	2.0359	0.2308	11.8868	2.75
MBG-CCM	0.8421	2.0220	0.2231	**11.5773**	1.75

Figure 4.2: More visual results of MBG-CCM on foreground background segmentation

Table 4.4: Performance over the BSDS500 with K manually adjusted

Algorithms	PRI	VoI	GCE	BDE	Avg.R
CCM/HP	0.8407	**2.0399**	0.2359	**10.7800**	1.5
CCM/DP	0.8275	2.5169	0.2541	11.5002	4
CCM/AD	0.8370	2.0490	0.2503	10.8868	3.5
MBG-CCM	**0.8418**	2.0430	**0.2263**	11.1650	1.75

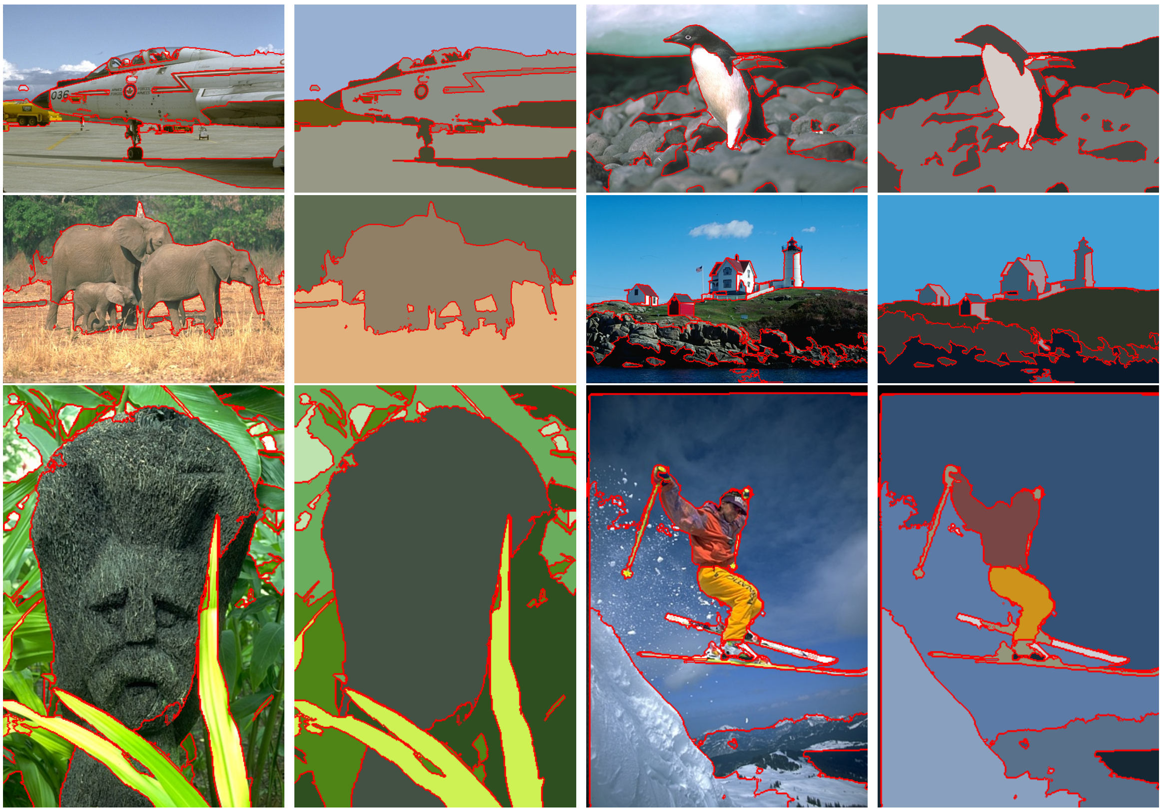

Figure 4.3: More visual results of MBG-CCM with K manually set.

When the superpixel segmentations are given, the runtime of the MBG-CCM is about 11 seconds per image with Matlab 2014a and a desktop equipped with an Intel i5 CPU and 16GB RAM.

4.5 Conclusion

We have presented a novel approach, MBG-CCM, for improving the CCM. In the MBG-CCM, we employ a multi-layer bipartite graph for modelling the segmentation information provided by superpixel features extracted from different feature spaces and merge the different graph layers via a Grassmann manifold.

Use of this algorithm is motivated by the fact that the cross-adjacency matrices of a multi-layer bipartite graph can be converted into a set of positive semidefinite matrices so that it can be decomposed into eigenvectors and eigenvalues, by which the subspace representations of the matrices can be found. And the algorithm provides a strong theoretical support for using different features in the original CCM.

The experiment results show that the performance of MBG-CCM is competitive with CCM. And if there are multiple features, the MBG-CCM is undoubtedly a better option than trying the matrix operators one by one as in the original CCM given in the previous chapter.

There is, however, a shortcoming of the MBG-CCM. It needs to compute the eigenvectors for each graph layer, which makes the computation cost higher than for CCM. Actually in both MBG-CCM and CCM, the final segmentation is carried out by spectral clustering techniques, so for them, computing the eigenvectors is an inevitable procedure. Moreover, for spectral clustering, an exact number of clusters should be given as prior knowledge. But this may be inapplicable in many image segmentation applications. To solve these problems, we need to develop a new ensemble segmentation method, which can formulate the pixel-superpixel relations without bipartite graph and determine the number of clusters automatically.

Chapter 5

Low-rank Representation for Covariance Descriptor

5.1 Introduction

Apart from the feature fusing problem, there is another issue in the CCM that needs to be considered, that is, how to find a 'good' covariance descriptor that produces the stable performance. Actually, this is not only an issue for CCM but all the segmentation algorithms that take handcrafted covariance descriptors as features. Similar to MBG-CCM in Chapter 4, we also plan to convert this issue into an embedding problem. Specifically, we aim to represent the covariance descriptors in some subspace so that the discriminative information should be kept while the redundancies are removed.

The low-rank representation (LRR) is one of the techniques that may solve the problem mentioned above. LRR was proposed for finding a robust subspace representation for the data represented in the linear feature spaces. Since the linear space is the most common choice for data presentation, the application of LRR involves numerous research fields, such as machine learning and computer vision (Liu *et al.*, 2010). For different applications, the LRR algorithm is developed by different motivations (Liu *et al.*, 2013). In some works, the subspaces are modelled as a mixture of Gaussian distributions, and the data structure can be obtained by the parameter estimation of the mixture Gaussian model (Gruber and Weiss, 2004; Ho *et al.*, 2003; Fischler and Bolles, 1981). And, some researchers proposed an algebraic way to model the data with LRR and showed that the LRR is a generalized principal component analysis problem (Ma *et al.*, 2008; Wright *et al.*, 2009). Moreover, an augmented Lagrange multipliers (ALM) method is proposed by Lin *et al.* (2010) to solve the LRR model. Fu *et al.* (2015) extended the LRR model to the Riemannian manifold, which is nonlinear.

In this chapter we propose a low-rank representation method for the covariance descriptors extracted from superpixels. Our contributions are as follows:

- we propose a LRR model to find the subspace structure of the covariance features;
- we improve the CCM algorithm by measuring the similarities of the superpixels with LRR.

In the rest of the chapter, Section 5.2 gives the introductions of the necessary background knowledge for elaborating our algorithms. Section 5.3 is the low-rank representation-based CCM algorithm (LRR-CCM). Section 5.4 shows the results of the experiments; in Section 5.5, we give the conclusion.

5.2 Preliminary

5.2.1 Low-rank representation

The low-rank representation (LRR) can be considered as a generalized principle component analysis (PCA) problem. One basic assumption of the LRR theory is that the given high-dimensional data lie near a lower-dimensional linear subspace. Mathematically, given a data set $X = \{\mathbf{x}_1, \cdots, \mathbf{x}_n\}$ and $\mathbf{x}_i$ be a d-dimension column vector, i.e., $\mathbf{x}_i \in \mathbb{R}^d$, suppose X is sampled from a subspace, then, X can be decomposed into

$$X = X_0 + E, \tag{5.1}$$

where X_0 is the origin of X and holds $\text{rank}(X_0) < \text{rank}(X)$, and, E is a matrix representing the difference between X_0 and X, also called corruption. The goal of LRR is to estimate the low-dimensional subspace efficiently and accurately. However, modelling this problem depends on the intrinsic structure of the data set X.

If the corruption is caused by additive i.i.d. Gaussian noise with small magnitude, then, Eq. 5.1 can be modelled as an optimization problem, that is,

$$\begin{aligned} &\min ||E||_F, \\ &\text{s.t. } \text{rank}(D) \leq k, \text{and, } X = D + E, \end{aligned} \tag{5.2}$$

where D is the low-rank representation of X, k is the target dimension of the subspace, and $||\cdot||_F$ is the Frobenius norm. Actually, Eq. 5.2 is equivalent to a PCA problem (Lin *et al.*, 2010).

But Eq. 5.2 will fail to find the proper $\hat{D}$ when there exists large corruption in X, even though the corruption affects only a few of the entities. In this case, Eq. 5.1 can be solved by the following minimization problem (Lin *et al.*, 2010; Wright *et al.*, 2009), that is,

$$\begin{aligned} &\min_{D,E} ||D||_* + \lambda ||E||_1, \\ &\text{s.t. } X = D + E, \end{aligned} \tag{5.3}$$

where $||\cdot||_*$ is the nuclear norm of a matrix (i.e., the sum of its sigular values), $||\cdot||_1$ is the sum of absolute values of matrix entries, and λ is a positive weighting parameter.

In Liu *et al.* (2013), a more generalized version of Eq. 5.3 is given, which is based on the fact that many real-world data sets contain multiple subspace structures. Let $\mathcal{S} = \{\mathcal{S}_1, \cdots, \mathcal{S}_k\}$ be a set of subspaces, and we assume X is drawn from a union of these subspaces, denoted as $\mathcal{S} = \cup_{i=1}^k \mathcal{S}_i$; let $A = [A_1, \cdots, A_k]$ be a 'dictionary' that linearly spans the data space, and A_i is the dictionary for the i-th subspace, then, Eq. 5.1 can be modelled as

$$\begin{aligned} &\min_{Z,E} ||Z||_* + \lambda ||E||_\ell, \\ &\text{s.t. } X = AZ + E, \end{aligned} \tag{5.4}$$

where $||\cdot||_*$ is the nuclear norm, and,

$$Z = \begin{bmatrix} Z_1 & & & \\ & Z_2 & & \\ & & \ddots & \\ & & & Z_k \end{bmatrix}$$

is called the low-rank representation of X; $\lambda > 0$ is a parameter and $||\cdot||_\ell$ represents some regularization strategy for modelling the noise, such as the squared Frobenius norm. And, we note that if set $A = I$ and $||\cdot||_\ell$ to be $||\cdot||_1$, then, Eq. 5.4 is equivalent to Eq. 5.3.

Eq. 5.4 can be solved by the augmented Lagrange multiplier (ALM) method proposed in (Liu *et al.*, 2013). First, Eq. 5.4 is rewritten into the following equivalent formation, that is,

$$\begin{aligned} &\min_{Z,E,J} ||J||_* + \lambda ||E||_{2,1}, \\ &\text{s.t. } X = AZ + E, Z = J, \end{aligned} \tag{5.5}$$

where $||E||_{2,1} = \sum_{j=1}^{n} \sqrt{\sum_{i=n}^{n}([E]_{ij})^2}$ is called $\ell_{2,1}$ norm. Then, the augmented Lagrange function is written as

$$\begin{aligned} \mathcal{L} = & ||J||_* + \lambda||E||_{2,1} + \mathrm{tr}(Y_1^T(X - AZ - E)) \\ & + \mathrm{tr}(Y_2^T(Z - J)) + \frac{\mu}{2}(||X - AZ - E||_F^2 + ||Z - J||_F^2) \end{aligned} \tag{5.6}$$

where $\mathrm{tr}(\cdot)$ is the trace operator, Y_1 and Y_2 are the Lagrange multipliers, and $\mu > 0$ is the penalty parameter. So, Eq. 5.5 can be solved by iteratively updating one variable while fixing the others each time until the convergence conditions are met. The inexact ALM method is shown in Algorithm 5.1, which is a variation of ALM method for an unsmooth object function (Liu *et al.*, 2013).

Algorithm 5.1 Inexact ALM for Eq 5.4

Input: A data set $X = \{\mathbf{x}_1, \cdots, \mathbf{x}_m\}$, parameter λ, dictionary A.

Output: The lowest-rank representation Z^*

Initialization: $Z = J = 0$, $E = 0$, $Y_1 = 0$, $Y_2 = 0$, $\mu = 10^{-6}$, $\mu_{max} = 10^6$, $\rho = 1.1$, and $\epsilon = 10^{-8}$
while not converged **do**
  Fix the others and update J by $J = \mathrm{argmin}\frac{1}{\mu}||J||_* + \frac{1}{2}||J - (Z + Y_2/\mu)||_F^2$.
  Fix the others and update Z by $Z = (I + A^T A)^{-1}(A^T(X - E) + J + (A^T Y_1 - Y_2)/\mu)$
  Fix the others and update E by $E = \mathrm{argmin}\frac{\lambda}{\mu}||E||_{2,1} + \frac{1}{2}||E - (X - AZ + Y_1/\mu)||_F^2$.
  Update Y_1 and Y_2 by $Y_1 = Y_1 + \mu(X - AZ - E)$, $Y_2 = Y_2 + \mu(Z - J)$
  Update μ by $\mu = \min(\rho\mu, \mu_{max})$
  Check convergence conditions, $||X - AZ - E||_\infty < \epsilon$ and $||Z - J||_\infty < \epsilon$.
end while

5.2.2 Covariance descriptor and collinearity

Covariance Descriptor and Sym_d^+

Covariance descriptor maps feature functions to a symmetric positive definite matrix space.

Specifically, let $\mathbf{F} = (\mathbf{f}_1, ..., \mathbf{f}_d)^T$ be a feature array, where $\mathbf{f}_i$ is a vector whose entries are the observations of the i-th feature. A covariance descriptor is the covariance matrix of $\mathbf{F}$, which is defined as

$$cov(\mathbf{F}) = \left[E((\mathbf{f}_i - \mu_i)^T(\mathbf{f}_j - \mu_j))\right]_{d\times d}, \tag{5.7}$$

where μ_i is the mean of the *i-th* feature $\mathbf{f}_i$, $[\cdot]_{d\times d}$ indicates an $d \times d$ matrix. Apparently, different sets of $\mathbf{f}_i$ generate different $cov(\mathbf{F})$, which brings a different performance.

Moreover, since the $d \times d$ covariance matrix is symmetric and semi-positive definite, the space of $d \times d$ covariance matrix is a convex cone in the d^2-dimensional Euclidean space, that is, a manifold embedding in d^2-dimensional Euclidean space, written as Sym_d^+.

Collinearity

Collinearity (or multi-collinearity), a term from statistics, refers to a linear association between two (or more) variables. Specifically, given a feature array $\mathbf{F}$, suppose there exists a set of not-all-zero scalar $\lambda_1, ..., \lambda_n$ that makes the following equation hold

$$\lambda_1 \mathbf{f}_1 + \lambda_2 \mathbf{f}_2 + \cdots + \lambda_n \mathbf{f}_n + u = 0. \tag{5.8}$$

If $u = 0$, $\mathbf{F}$ is perfect multi-collinearity, while if $u \sim N(0, \sigma)$, $\mathbf{F}$ is nearly multi-collinearity.

In image segmentation, this multi-collinearity phenomenon is common when building the covariance descriptors. For example, if we use the RGB value and intensity value as two features for covariance descriptor construction, the covariance matrix generated by Eq.5.7 is not full rank. Because the intensity value can be converted from the RGB value via a linear transformation, the covariance matrix generated by Eq.5.7 is not full rank. This means there are redundant entries and noises in the covariance descriptor.

5.3 LRR-based CCM

In CCM, a colour covariance matrix is used as a descriptor of the superpixels. Obviously, it is not the only covariance descriptor available for superpixels. By using different covariance descriptors, the performance of CCM may vary. In many applications, the most suitable covariance descriptor are often chosen in an empirical way, that is, trying different selections of them and taking the one that gives the best performance (Habiboğlu *et al.*, 2012; Kviatkovsky *et al.*, 2013). This may work in practice but lacks theoretical support. In this section, the LRR is used to reduce the noises in the covariance descriptor set.

5.3.1 Refine covariance descriptors with LRR

The low-rank representation (LRR) is proposed for finding a stable and compact representation for a given data set, which has been proved an efficient method for noise reduction in the Euclidean space (Candès *et al.*, 2011; Wright *et al.*, 2009; Ganesh *et al.*, 2009; Chen and Yang, 2014; Liu and Yan, 2011). Recently, it has been extended into the non-Euclidean space, such as Riemannian manifold (Fu *et al.*, 2015; Wang *et al.*, 2015a,b).

The covariance descriptors are the points lying on a Sym_d^+, and in this case, the *Frobenius* norm is used as the metric for it. So, the Sym_d^+ is embedded into the d^2-dimensional Euclidean space. Although this *Frobenius* metric is not geodesic, which may lose the intrinsic structure of the data set in embedding, it allows all the methods from Euclidean space to be applied to the manifold directly.

LRR for covariance matrices

Given a set of covariance descriptors $\mathcal{X} = \{X_1, \cdots, X_n\}$, where X_i is a covariance matrix of size $d \times d$, if we stack the X_i in a third dimension, then, $\mathcal{X}$ become a 3-order tensor, i.e., a cube. By the *Frobenius* metric, we can embed $\mathcal{X}$ into the d^2-dimensional Euclidean space, so the LRR model, Eq.5.4, is written as follows:

$$\begin{aligned} &\min_{E,Z} \|E\|_F^2 + \lambda \|Z\|_*, \\ &s.t. \quad \mathcal{X} = \mathcal{X}_{\times_3} Z + E, \end{aligned} \tag{5.9}$$

where $\|\cdot\|_F$ is the *Frobenius* norm; $\|\cdot\|_*$ is the *nuclear* norm; λ is the balance parameter; $\times_3$ means mode-3 multiplication of a tensor and matrix (Kolda and Bader, 2009). Eq. 5.9 can be solved via augment Lagrangian multiplier (ALM) and the solution is as follows (Wang *et al.*, 2015b):
for the error term E, we have $\|E\|_F^2 = \|\mathcal{X} - \mathcal{X}_{\times 3} Z\|_F^2$, and we can rewrite $\|E\|_F^2$ as,

$$\|E\|_F^2 = \sum_i^N \|E_i\|_F^2, \tag{5.10}$$

where $E_i = X_i - \sum_j^N z_{ij} X_j$, i.e., the i-th slice of E. Note that for matrix A, it holds

$\|A\|_F^2 = \mathrm{tr}(A^T A)$, and X_i is symmetric, so, Eq. 5.10 can be expanded as

$$\|E_i\|_F^2 = \mathrm{tr}[(X_i - \sum_j^N z_{ij} X_j)^T (X_i - \sum_j^N z_{ij} X_j)]$$
$$= \mathrm{tr}(X_i^T X_i) - \mathrm{tr}(X_i^T \sum_j^N z_{ij} X_j) - \mathrm{tr}(\sum_j^N z_{ij} X_j^T X_i)$$
$$+ \mathrm{tr}(\sum_{j_1}^N z_{ij_1} X_{j_1}^T \sum_{j_2}^N z_{ij_2} X_{j_2})$$
$$= \mathrm{tr}(X_i X_i) - 2\mathrm{tr}(\sum_j^N z_{ij} X_i X_j) + tr(\sum_{j_1,j_2}^N z_{ij_1} z_{ij_2} X_{j_1} X_{j_2}).$$

Let Δ be a symmetric matrix of size $N \times N$, whose entries are $\Delta_{ij} = \Delta_{ji} = \mathrm{tr}(X_i X_j)$ and $P = \Delta^{\frac{1}{2}}$. Because X_i is a symmetric matrix, Δ_{ij} can be written as $\Delta_{ij} = \mathrm{vec}(X_i)^T \mathrm{vec}(X_j)$, where $\mathrm{vec}(\cdot)$ is an operator that vectorized a matrix. As a Gram matrix, Δ is positive semidefinite. So, we have

$$\|E_i\|_F^2 = \Delta_{ii} - 2\sum_{j=1}^N z_{ij}\Delta_{ij} + \sum_{j_1}^N \sum_{j_2}^N z_{ij_1} z_{ij_2} \Delta_{j_1 j_2}$$
$$= \Delta ii - 2\sum_{j=1}^N z_{ij}\Delta_{ij} + \mathbf{z}_i \Delta \mathbf{z}_i^T.$$

For $\Delta = PP^T$,

$$\|E\|_F^2 = \sum_{i=1}^N \Delta_{ii} - 2\mathrm{tr}[Z\Delta] + \mathrm{tr}[Z\Delta Z^T]$$
$$= C + \|ZP - P\|_F^2,$$

where C is a constant. The optimization Eq.5.9 is equivalent:

$$\min_Z \|ZP - P\|_F^2 + \lambda \|Z\|_*. \tag{5.11}$$

We transform the Eq.5.11 into an equivalent formulation

$$\begin{aligned} \min_Z \ & \frac{1}{\lambda}\|ZP - P\|_F^2 + \|J\|_*, \\ \text{s.t.} \quad & J = Z. \end{aligned} \tag{5.12}$$

Then by ALM (Argument Lagrange Multiplier), we have

$$\min_{Z,J} \frac{1}{\lambda}\|ZP - P\|_F^2 + \|J\|_* + < Y, Z - J > + \frac{\mu}{2}\|Z - J\|_F^2, \tag{5.13}$$

where Y is the Lagrange coefficient; λ and μ are scale parameters. Eq.5.13 can be solved by the following two subproblems (Lin *et al.*, 2010):

$$J_{k+1} = \min_{J}(\|J\|_{*} + < Y, Z_k - J > + \frac{\mu}{2}\|Z_k - J\|_F^2)$$

and,

$$Z_{k+1} = \min_{Z}(\frac{1}{\lambda}\|ZP - P\|_F^2 + < Y, Z - J_k > + \frac{\mu}{2}\|Z - J\|_F^2).$$

Fortunately, according to Cai *et al.* (2010), the solutions for the above subproblems have the following close forms:

$$J = \Theta(Z + \frac{Y}{\mu}),$$

$$Z = (\lambda\mu J - \lambda Y + 2\Delta)(2\Delta + \lambda\mu I)^{-1},$$

where $\Theta(\cdot)$ is the singular value thresholding operator (Cai *et al.*, 2010). Thus, by iteratively updating J and Z until the converge conditions are satisfied, a solution for Eq.5.9 can be found.

5.3.2 LRR-CCM algorithm

In the graph construction step of the CCM algorithm, the superpixels-wise similarity matrix W^{ss} in Eq. 3.2 is obtained by measuring the similarity between the superpixels within the same superpixel segmentation. Let $S^i = \{s_1^i, \cdots, s_{K_i}^i\}$ be a set of covariance descriptors of the i-th superpixel segmentation; it is easy to see S^i is a 3-order tensor. Thus, we can get the LRR of S^i by solving Eq. 5.9, i.e. using Algorithm 5.1. Let Z^i be the LRR coefficient matrix of S^i and $\widetilde{U}_i$ be the row-normalized singular vectors of Z^i. The same as Ma *et al.* (2007), we define a similarity matrix for the superpixels as

$$Sim_{K_i \times K_i} = (\widetilde{U}_i \widetilde{U}_i^T)^2. \tag{5.14}$$

and, the entry at (m, n) of matrix Sim is the similarity between superpixel descriptor s_m^i and s_n^i, written as $Sim(m, n)$. By setting the entries of W^{ss} to the respective $Sim(m, n)$, the superpixel-wise similarity matrix can be obtained. The LRR-CCM algorithm is shown in Algorithm 5.2.

5.4 Experiments

5.4.1 Data sets and settings

The experiments are conducted on two public image segmentation data sets: the Berkeley Segmentation Data Set 300 (BSDS300), and its update, the Berkeley Segmentation

Algorithm 5.2 The LRR-CCM Algorithm

Input: An image I, a collection of superpixel segmentations $\mathcal{S}$, the number of clusters k;

Output: A final clustering $\mathcal{C} = \{C_1, \cdots, C_n\}$

1: Compute the LRR (i.e., Z) for every superpixel segmentation by Algorithm 5.1.

2: Build the bipartite graph G via Algorithm 3.1, in which the superpixel-wise similarity matrix W^{ss} obtained by Eq.5.14.

3: Apply Algorithm 2.4 (i.e., *T-cut*) on G and obtain the final clustering $\mathcal{C}$.

Data Set 500 (BSDS500) (Martin *et al.*, 2001; Arbelaez *et al.*, 2011).

For comparison purposes, we set the parameters to the same values as those used in CCM. Specifically, the superpixel segmentations are created by Mean Shift and the F-H method with the same parameter settings. There are three superpixel segmentations generated by Mean Shift with the parameters $(h_s, h_r, M) \in \{(7, 7, 100), (7, 9, 100), (7, 11, 100)\}$ where h_s and h_r are the bandwidth parameters, and M represents the minimum size of the superpixel, and two or three superpixel segmentations produced by F-H method based on the image variance in the *Lab* colour space with a given threshold; the parameters are set to be $(\sigma, c, M) \in \{(0.5, 100, 50), (0.8, 200, 100)\}$ for the two-segmentation case, or $(\sigma, c, M) \in \{(0.8, 150, 50), (0.8, 200, 100), (0.8, 300, 100)\}$ for the three-segmentation case, where σ and c are the parameters for smoothing and scale; M is the minimum size of the superpixel.

For LRR-CCM, the parameter λ in Eq. 5.9 is chosen by a grid search among $\{1, 0.1, 0.01, 0.001\}$ for every image, that is, we select the value that gives the highest performance.

Moreover, for the LRR-based CCM algorithm, three different covariance descriptors are used:

- CovI : $[R, G, B]$,
- CovII : $[R, G, B, I, \frac{\partial I}{\partial x}, \frac{\partial I}{\partial y}, \frac{\partial I}{\partial^2 x}, \frac{\partial I}{\partial^2 y}]$,
- CovIII :$[R, G, B, \frac{\partial R}{\partial x}, \frac{\partial R}{\partial y}, \frac{\partial G}{\partial x}, \frac{\partial G}{\partial y}, \frac{\partial B}{\partial x}, \frac{\partial B}{\partial y}, \frac{\partial R}{\partial^2 x}, \frac{\partial R}{\partial^2 y}, \frac{\partial G}{\partial^2 x}, \frac{\partial G}{\partial^2 y}, \frac{\partial B}{\partial^2 x}, \frac{\partial B}{\partial^2 y}]$.

From CovI to CovIII, the dimensionality of the covariance descriptor is increasing. For example, CovI contains the patterns in the R, G, B channels, while in CovIII, the patterns of their derivatives are also included. This means the covariance descriptors

Table 5.1: Performance of LRR with different covariance descriptors

Algorithms	PRI	VoI	GCE	BDE	Avg.R
CovI+LRR	0.8454	1.7564	**0.1885**	13.0427	2
CovII+LRR	**0.8499**	**1.7418**	0.1915	12.7635	1.5
CovIII+LRR	0.8451	1.7698	0.1932	**12.4837**	2.5

become more discriminative. But since the partial derivatives are directly computed from other contained features, the tendencies of multi-collinearity are also growing.

The main purpose of our experiments is to evaluate the ability of LRR method in extracting the subspace structure of covariance descriptors. Because the subspace structure of each image may be different, therefore, we partition every image into K regions with $K \in [2; 40]$. And, the reported evaluation results are based on the K that provides the best performance of the algorithms.

5.4.2 Results

The LRR-CCM can successfully run over all images in the BSDS300 but not all images in the BSDS500 since ALM (i.e., Algorithm 5.1) failed to converge when running with a few images in BSDS500. One possible reason is there is too much noise in the covariance descriptor sets of those images, which makes it hard to find the stable subspace structure. And, an incorrect subspace representation may result in a problematic superpixel-wise similarity matrix, which causes a failure in the spectral clustering procedure in *T-cut*.

Table 5.1 shows the results of LRR-CCM with different types of covariance descriptors over BSDS300. With CovII descriptor, the PRI and VoI of LRR-CCM reach the best, and, GCE and BDE reach the best with CovI and CovIII respectively. But the overall performance of the three descriptors are very close.

Table 5.2 shows the comparison between the state-of-the-art algorithms with LRR-CCM on BSDS300. The CCM has the highest overall performance but LRR-CCM performs best on PRI. In order to run the experiments of LRR-CCM on BSDS500, we use Gaussian filter to smooth the images that failed on ALM. Table 5.3 shows the corresponding performance. The LRR-CCM has the second-highest average rank, and its performance on PRI is still the highest overall. Figure 5.1 demonstrates a few results of the LRR-CCM.

When the superpixel segmentations are given, it takes about 15 seconds to run

Table 5.2: Performance of different algorithms over BSDS300

Algorithms	PRI	VoI	GCE	BDE	Avg.R
SAS	0.8319	1.6849	**0.1779**	11.2900	2.5
ℓ_0-sparse	0.8355	1.9935	0.2297	**11.1955**	3.5
CCM	0.8495	**1.6260**	0.1785	12.3034	2.25
MBG-CCM	0.8421	2.0223	0.2231	11.5771	3.75
LRR-CCM	**0.8499**	1.7418	0.1915	12.7635	3

Table 5.3: Performance of different algorithms over BSDS500

Algorithms	PRI	VoI	GCE	BDE	Avg.R
SAS	0.8372	1.6914	0.1813	12.6599	3.25
ℓ_0-sparse	-	-	-	-	
CCM	0.8495	**1.6260**	**0.1785**	12.3034	1.75
MBG-CCM	0.8418	2.0430	0.2263	**11.1650**	3
LRR-CCM	**0.8498**	1.7858	0.1948	11.9848	2

Note: The symbol '$-$' means there are no published results available.

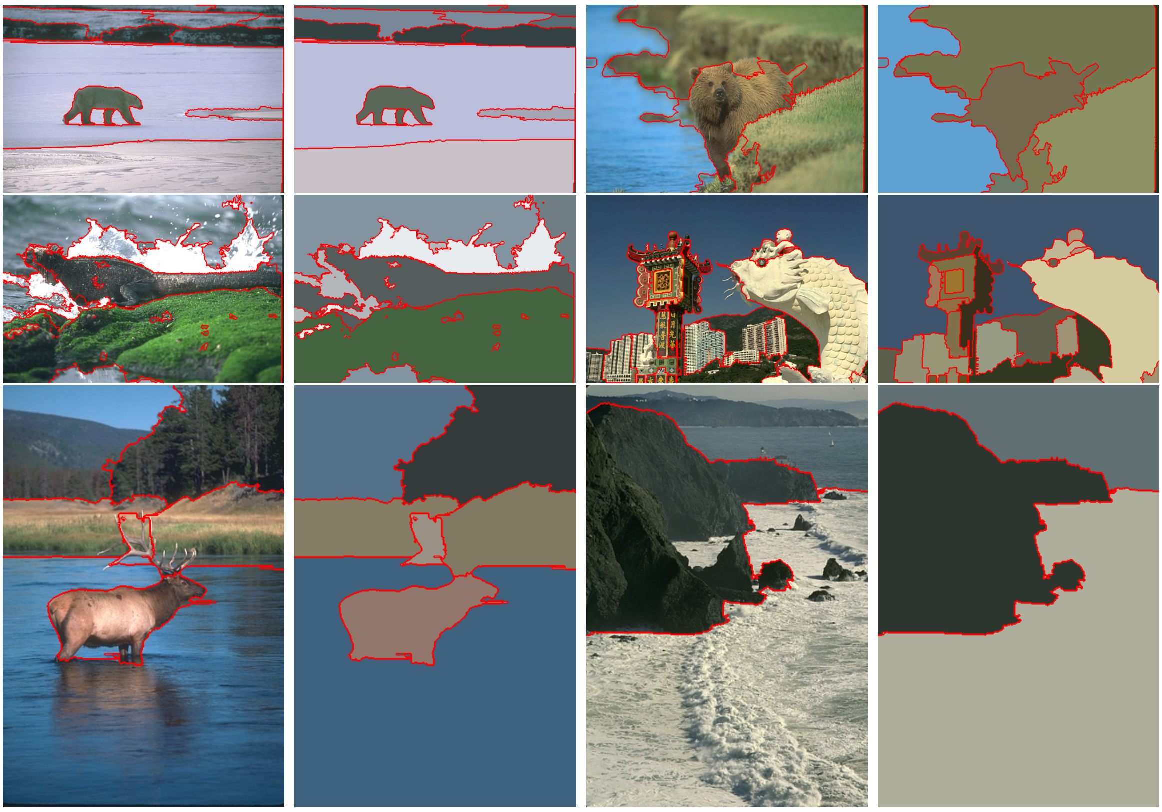

Figure 5.1: Some visualized results of LRR-CCM.

LRR-CCM on one image with Matlab 2014a and a desktop equipped with an Intel i5 CPU and 16GB RAM.

5.5 Conclusion

We have presented a novel approach, LRR-CCM, for improving the CCM algorithm. In LRR-CCM, we apply the augmented Lagrange multiplier (ALM) method to find the low-rank representation of the covariance descriptor set and build the superpixel-wise similarity matrix based on the low-rank representation.

We test the LRR-CCM with three different covariance descriptors. Each of them contains noise due to collinearity. The experiment results show that the performance of LRR-CCM with these covariance descriptors are relatively stable, which means the LRR method we proposed is able to extract the robust subspace representation for the covariance descriptors. And for covariance descriptors, the low-rank representation may be the 'good' descriptor.

But the shortcomings of the MBG-CCM also happen on LRR-CCM. It needs spectral clustering for generating the final segmentation and a specified number of clusters. Moreover, in order to find the most suitable parameters, LRR needs to search over the parameter space, which is a significant overhead for a segmentation algorithm. So, a new algorithm that can avoid these problems is needed. This is the purpose of our next chapter.

Chapter 6

Superpixel Association

6.1 Introduction

As a group of pixels with perceptual similarities, superpixel is widely used in computer vision applications. In many works, the superpixels are used as primitives for image processing tasks. For example, Gould et al. developed a few of object recognition algorithms based on superpixels (Gould *et al.*, 2008, 2014, 2009); Kluckner *et al.* (2009) proposed an image segmentation algorithm that working with superpixels via the random forests. While in some other research, different superpixel segmentations are regarded as segmentation clues, and the ensemble clustering algorithms are applied to them and produce the final segmentation. Kim *et al.* (2010) proposed an algorithm in which the superpixel segmentations are incorporated in a dense affinity matrix over pixels, and the final segmentation is obtained by spectral clustering on the pixels. A bipartite graph is used to solve the information fusing problem by which both the pixels and superpixels are set as graph vertices (Li *et al.*, 2012; Wang *et al.*, 2013), and the final clustering information of the pixels is delivered from a spectral clustering-based algorithm, named *T-cut* (Li *et al.*, 2012).

Although most of the superpixel-based algorithms are well-tuned to provide good performance, there are still a few issues to be addressed. The first one is the selection of superpixel segmentations. Since different superpixel algorithms (or, different parameter settings) generate different superpixel segmentations, the performance of those algorithms varies, especially for those algorithms that work on a single superpixel segmentation directly. Secondly, many superpixel-based algorithms employ graph models and the final segmentation is often obtained via spectral clustering. So, they need a specified cluster number for the final segmentation. However, even for a human, it is still not easy to give an exact cluster number for image segmentation, because for an image, the 'correct' segmentation is not unique, especially for natural images. Figure 6.1 demonstrates this phenomenon: the first left column is the original image, and the rest are the different segmentations made by a human. It is easy to notice that some people partition the sky into a few regions while others don't. Actually, all these segmentations are considered to be 'correct'. This phenomenon encourages researchers to model the segmentation with a hierarchical structure. For example, Arbelaez *et al.* (2011) proposed the ultrametric contour map (UGM) algorithm in which a hierarchical segmentation tree is built to capture the possible segmentations with different scales.

Figure 6.1: An example of the multiple 'correct' segmentations.

In this chapter, we also propose a hierarchical tree model for image segmentation, which is named superpixel-based hierarchical segmentation tree (SHST). With this algorithm, we can generate segmentations with different scales. Different to the UGM in which the tree is constructed from the contours, our algorithm builds the tree with the superpixel associations. To our knowledge, this method has not been sufficiently explored. Our contributions mainly contain the following:

- we propose the concept of superpixel association and show some nice properties of it;
- we propose the SHST algorithm by which a hierarchical segmentation tree can be built with superpixel associations;
- we propose a strategy for determining the number of segments with the SHST.

The rest of the chapter is organized as follows. Section 6.2 is about the superpixel association and its properties. In Section 6.3, we propose the SHST algorithm and give the details for building the SHST. The experiment results are reported in Section 6.4. And Section 6.5 summarizes the chapter.

6.2 Superpixel association

The concept of superpixel association is proposed with the inspiration from the Hybrid Bipartite Graph Formation (HBGF) algorithm. In HBGF-based image segmentation algorithms, like SAS (Li *et al.*, 2012) and CCM, we find that those pixels having the same pixel-superpixel relations are always partitioned into the same segment in the final segmentation. This indicates those pixels can be considered as a unit in the HBGF-based algorithm. Actually, we will prove that the segmentation result from an HBGF-based algorithm will not change if we take the superpixel associations instead of pixels as primitives for segmentation. Firstly, we give the definitions of superpixel association.

Let $I = \{p_u\}_{u=1}^{m}$ represent an image of m pixels. A superpixel segmentation is a clustering on I denoted by $S = \{s_1, \cdots, s_K\}$, where s_i is a subset of I, called a superpixel, and K is the number of superpixels in S; for $\forall s_i, s_j \in S$, where $i \neq j$, we have $s_i \cap s_j = \emptyset$. We denote $\mathcal{S} = \{S^1, \cdots, S^N\}$ as a collection of superpixel segmentations, where N is the number of superpixel segmentations. And, let $SL^i = \{1, 2, \cdots, K_i\}$ represent the set of superpixel labels of S^i, where K_i is the number of superpixels in S^i.

For a given $S^i \in \mathcal{S}$, we define an indicator $Id : I \to SL^i$, which assigns a superpixel label $l \in SL^i$ to pixel p_u. Then, we have the following definition:

Definition 6.2.1 (Superpixel association). *A set of pixels $Sa = \{p_u\}_{u=1}^{n_{Sa}}$ is called a superpixel association if it satisfies the following conditions:*

(i) $\forall p_u, p_v \in Sa$, $\forall S^i \in \mathcal{S}$, it holds that $Id(p_u) = Id(p_v)$;

(ii) $\forall p_u \in Sa$ and $p_v \notin Sa$, $\exists S^i \in \mathcal{S}$, such that $Id(p_u) \neq Id(p_v)$;

where n_{Sa} is the number of pixels in the superpixel association.

For a given $\mathcal{S}$, there exists a unique collection of Sa, which is denoted as $\mathcal{A} = \{Sa_1, ..., Sa_M\}$, where M is the number of superpixel associations. Two pixels are in the same Sa if and only if they are in the same superpixel in all of the given superpixel segmentations; Figure 6.2 gives an example. Besides, for a given threshold $\tau \geq 0$, we say Sa is a tiny superpixel association, if $n_{sa} < \tau$ holds.

Theoretically, we can take superpixel associations as primitives for segmentation instead of pixels because of the following Theorem 6.2.1.

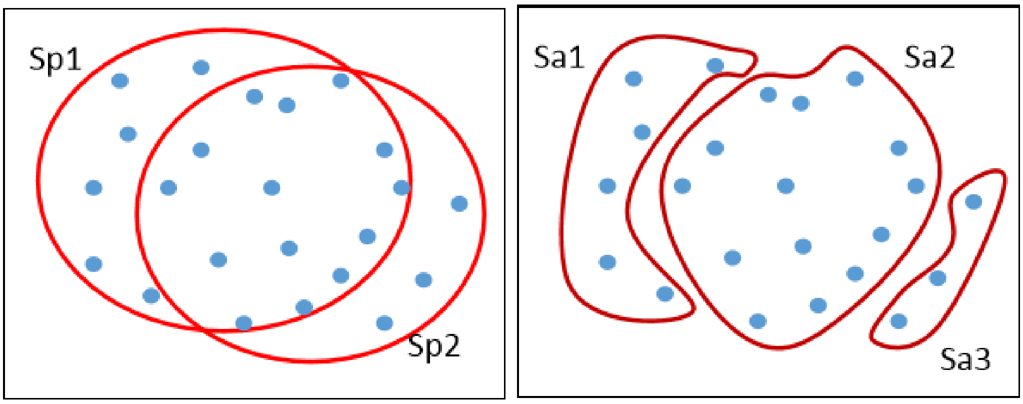

(a) (b)

Figure 6.2: An example for superpixel association: (a) two superpixels; (b) the corresponding superpixel associations. Intuitively, the superpixel associations are the intersected and non-intersected parts of the given superpixels.

Theorem 6.2.1. *For a given I and a collection of its clusterings $\mathcal{S}$, let $G^p(V_p^X, V_p^Y, E_p)$ and $G^{Sa}(V_{Sa}^X, V_{Sa}^Y, E_{Sa})$ denote two bipartite graphs constructed according to the HBGF algorithm, and, S'_{sp} and $S'_{spassoc}$ denote the final clusterings obtained from the respective graphs. For the spectral clustering on G^p and G^{Sa} with a given cluster number k, it holds that $S'_{sp} = S'_{spassoc}$, if G^p and G^{Sa} satisfy the following conditions:*

(i) vertices in V_p^X and V_{Sa}^X represent $p_i \in I$ for G^p and $Sa_i \in \mathcal{A}$ for G^{Sa} respectively;

(ii) weights on the $E_p = \{e_r\}_{r=1}^{R_p}$ and $E_{Sa} = \{e_r\}_{r=1}^{R_{Sa}}$ are set to be $\mathbf{C}$ for G^p and $\{n_{Sa}^r \mathbf{C}\}_{r=1}^{R_{Sa}}$ for G^{Sa} respectively;

where $\mathbf{C}$ is a positive constant; R_p and R_{Sa} are the numbers of edges; and, n_{Sa}^r is the number of pixels in the Sa that is connected to some superpixel by e_r.

Proof. Without loss of generality, for image $I = \{p_1, \cdots, p_m\}$, we make the following settings to simplify the proof,

1. the superpixels $\mathcal{S}_p = \{s_1, \cdots, s_n\}$;
2. the superpixel associations $\mathcal{A} = \{Sa_1, \cdots, Sa_M\}$;
3. G^p is built with Algorithm 2.3 by $V^I = I$, and the weights on the edges are set to be 1;
4. G^{Sa} is built with Algorithm 2.3 by $V^I = \mathcal{A}$, and, the number of pixels in Sa_i, denoted as t_i, is set to be the edge weight that connects Sa_i and s_j, if $Sa_i \subseteq s_j$.

Let B^p and B^{Sa} be the respective cross-adjacency matrices. Since the order of the rows is irrelevant to the result, we arrange the rows of B^p into blocks according to the superpixel associations, that is, those pixels belonging to a same superpixel association will stay together. Let Z_i be a set of subscripts of the superpixels in $\mathcal{S}_p$ that cover Sa_i, and, we set $\mathcal{Z} = \{Z_1, \cdots, Z_M\}$. Then, we suppose B^p and B^{Sa} are as follows,

$$B^p = \begin{array}{c} \\ p_1 \\ \vdots \\ p_{t_1} \\ p_{t_1+1} \\ \vdots \\ p_{t_1+t_2} \\ \vdots \\ p_m \end{array} \begin{array}{c} \begin{array}{ccccccc} s_1 & \cdots & s_u & \cdots & s_v & \cdots & s_n \end{array} \\ \begin{bmatrix} 1 & \cdots & 0 & \cdots & 1 & \cdots & 0 \\ \vdots & & \vdots & & \vdots & & \vdots \\ 1 & \cdots & 0 & \cdots & 1 & \cdots & 0 \\ 0 & \cdots & 1 & \cdots & 1 & \cdots & 0 \\ \vdots & & \vdots & & \vdots & & \vdots \\ 0 & \cdots & 1 & \cdots & 1 & \cdots & 0 \\ \vdots & & \vdots & & \vdots & & \vdots \\ 1 & \cdots & 0 & \cdots & 1 & \cdots & 1 \end{bmatrix}_{m\times n} \end{array},$$

and,

$$B^{Sa} = \begin{array}{c} \\ Sa_1 \\ Sa_2 \\ \vdots \\ Sa_M \end{array} \begin{array}{c} \begin{array}{ccccccc} s_1 & \cdots & s_u & \cdots & s_v & \cdots & s_n \end{array} \\ \begin{bmatrix} t_1 & \cdots & 0 & \cdots & t_1 & \cdots & 0 \\ 0 & \cdots & t_2 & \cdots & t_2 & \cdots & 0 \\ \vdots & & \vdots & & \vdots & & \vdots \\ t_M & \cdots & 0 & \cdots & t_M & \cdots & t_M \end{bmatrix}_{M\times n} \end{array}.$$

We denote $D_X = diag(B\mathbf{1})$ and $D_Y = diag(B^T\mathbf{1})$ are two degree matrices corresponding to V^I and V^C, where $\mathbf{1}$ is a vector of ones in proper size and diag$(\cdot)$ is a diagonal matrix whose nonzero entries represented by '$(\cdot)$'. Obviously, we have $D_Y^p = D_Y^{Sa}$. Besides, we have

$$D_X^p = \begin{array}{c} \\ 1 \\ \vdots \\ t_1 \\ t_1{+}1 \\ \vdots \\ t_1{+}t_2 \\ \vdots \\ m \end{array} \begin{array}{c} \begin{array}{cccccccc} 1 & \cdots & t_1 & t_1{+}1 & \cdots & t_1{+}t_2 & \cdots & m \end{array} \\ \begin{bmatrix} |Z_1| & & & & & & \\ & \ddots & & & & & \\ & & |Z_1| & & & & \\ & & & |Z_2| & & & \\ & & & & \ddots & & \\ & & & & & |Z_2| & \\ & & & & & & \ddots & \\ & & & & & & & |Z_M| \end{bmatrix}_{m\times m} \end{array},$$

where $|Z_i|$ represents the number of entries in Z_i, and,

$$D_X^{Sa} = \begin{array}{c} \\ 1 \\ 2 \\ \vdots \\ M \end{array} \begin{array}{c} \begin{array}{cccc} 1 & 2 & \cdots & M \end{array} \\ \begin{bmatrix} |Z_1|t_1 & & & \\ & |Z_2|t_2 & & \\ & & \ddots & \\ & & & |Z_M|t_M \end{bmatrix}_{M\times M} \end{array}.$$

So,

$$(B^p)^T\left[(D_X^p)^{-1}B^p\right] =$$

$$\begin{array}{c|c} & \begin{array}{cccccccc} p_1 & \cdots & p_{t_1} & p_{t_1+1} & \cdots & p_{t_1+t_2} & \cdots & p_m \end{array} \\ \begin{array}{c} s_1 \\ \vdots \\ s_u \\ \vdots \\ s_v \\ \vdots \\ s_n \end{array} & \begin{bmatrix} 1 & \cdots & 1 & 0 & \cdots & 0 & \cdots & 1 \\ \vdots & & \vdots & \vdots & & \vdots & & \vdots \\ 0 & \cdots & 0 & 1 & \cdots & 1 & \cdots & 0 \\ \vdots & & \vdots & \vdots & & \vdots & & \vdots \\ 1 & \cdots & 1 & 1 & \cdots & 1 & \cdots & 1 \\ \vdots & & \vdots & \vdots & & \vdots & & \vdots \\ 0 & \cdots & 0 & 0 & \cdots & 0 & \cdots & 1 \end{bmatrix} \end{array} \times \begin{array}{c|c} & \begin{array}{ccccccc} s_1 & \cdots & s_u & \cdots & s_v & \cdots & s_n \end{array} \\ \begin{array}{c} p_1 \\ \vdots \\ p_{t_1} \\ p_{t_1+1} \\ \vdots \\ p_{t_1+t_2} \\ \vdots \\ p_m \end{array} & \begin{bmatrix} \frac{1}{|Z_1|} & \cdots & 0 & \cdots & \frac{1}{|Z_1|} & \cdots & 0 \\ \vdots & & \vdots & & \vdots & & \vdots \\ \frac{1}{|Z_1|} & \cdots & 0 & \cdots & \frac{1}{|Z_1|} & \cdots & 0 \\ 0 & \cdots & \frac{1}{|Z_2|} & \cdots & \frac{1}{|Z_2|} & \cdots & 0 \\ \vdots & & \vdots & & \vdots & & \vdots \\ 0 & \cdots & \frac{1}{|Z_2|} & \cdots & \frac{1}{|Z_2|} & \cdots & 0 \\ \vdots & & \vdots & & \vdots & & \vdots \\ \frac{1}{|Z_M|} & \cdots & 0 & \cdots & \frac{1}{|Z_M|} & \cdots & \frac{1}{|Z_M|} \end{bmatrix} \end{array}$$

$$= \begin{array}{c} \\ 1 \\ \vdots \\ n \end{array} \begin{array}{c} \begin{array}{ccc} 1 & \cdots & n \end{array} \\ \begin{bmatrix} \sum_{q=1}^M \left(\frac{t_q}{|Z_q|}\delta(1\in Z_q)\delta(1\in Z_q)\right) & \cdots & \sum_{i=q}^M \left(\frac{t_q}{|Z_q|}\delta(1\in Z_q)\delta(n\in Z_q)\right) \\ \vdots & & \vdots \\ \sum_{q=1}^M \left(\frac{t_q}{|Z_q|}\delta(n\in Z_q)\delta(1\in Z_q)\right) & \cdots & \sum_{q=1}^M \left(\frac{t_q}{|Z_q|}\delta(n\in Z_q)\delta(n\in Z_q)\right) \end{bmatrix} \end{array}$$

$$= \left[\left(\sum_{q=1}^M \frac{t_q}{|Z_q|}\delta(i\in Z_q)\delta(j\in Z_q)\right)_{ij}\right]_{n\times n},$$

where the value of $\delta(\cdot)$ is 1 if the condition '$(\cdot)$' is true, and 0, otherwise; $i,j \in \{1,2,\cdots,n\}$. And,

$$(B^{Sa})^T\left[(D_X^{Sa})^{-1}B^{Sa}\right] =$$

$$\begin{array}{c|c} & \begin{array}{cccc} Sa_1 & Sa_2 & \cdots & Sa_M \end{array} \\ \begin{array}{c} s_1 \\ \vdots \\ s_u \\ \vdots \\ s_v \\ \vdots \\ s_n \end{array} & \begin{bmatrix} t_1 & 0 & \cdots & t_M \\ \vdots & \vdots & & \vdots \\ 0 & t_2 & \cdots & 0 \\ \vdots & \vdots & & \vdots \\ t_1 & t_2 & \cdots & t_M \\ \vdots & \vdots & & \vdots \\ 0 & 0 & \cdots & t_M \end{bmatrix} \end{array} \times \begin{array}{c|c} & \begin{array}{ccccccc} s_1 & \cdots & s_u & \cdots & s_v & \cdots & s_n \end{array} \\ \begin{array}{c} Sa_1 \\ Sa_2 \\ \vdots \\ Sa_M \end{array} & \begin{bmatrix} \frac{1}{|Z_1|} & \cdots & 0 & \cdots & \frac{1}{|Z_1|} & \cdots & 0 \\ 0 & \cdots & \frac{1}{|Z_2|} & \cdots & \frac{1}{|Z_2|} & \cdots & 0 \\ \vdots & & \vdots & & \vdots & & \vdots \\ \frac{1}{|Z_M|} & \cdots & 0 & \cdots & \frac{1}{|Z_M|} & \cdots & \frac{1}{|Z_M|} \end{bmatrix} \end{array}$$

$$= \left[\left(\sum_{q=1}^M \frac{t_q}{|Z_q|}\delta(i\in Z_q)\delta(j\in Z_q)\right)_{ij}\right]_{n\times n}.$$

So, for

$$L_Y^{p(sym)} = (D_Y^p)^{-\frac{1}{2}}(B^p)^T(D_X^p)^{-1}B^p(D_Y^p)^{-\frac{1}{2}}$$

and

$$L_Y^{Sa(sym)} = (D_Y^{Sa})^{-\frac{1}{2}}(B^{Sa})^T(D_X^{Sa})^{-1}B^{Sa}(D_Y^{Sa})^{-\frac{1}{2}},$$

we have

$$L_Y^p = L_Y^{Sa}.$$

Let u_i and v_i be the i-th eigenvector of L_X and L_Y and λ_i be the respective eigenvalue of L_Y. According to Theorem 1 in Li *et al.* (2012), $u_i = \frac{1}{1-\gamma_i}D_X^{-1}Bv_i$, where $\gamma_i(2-\gamma_i) = \lambda_i$. So,

$$u_i^p = \frac{1}{1-\gamma_i}(D_X^p)^{-1}B^p v_i^p,$$

and,

$$u_i^{Sa} = \frac{1}{1-\gamma_i}(D_X^{Sa})^{-1}B^{Sa}v_i^{Sa},$$

Because the eigenvectors of L_Y^p and L_Y^{Sa} are the same (i.e., $v_i^p = v_i^{Sa}$), the m-th element in v_i^p is same to the n-th element in v_i^{Sa} if $p_m \in Sa_n$. Thus, G^p and G^{Sa} are equivalent in representing the data structure of the pixel set P. □

For those HBGF-based segmentation algorithms, Theorem 6.2.1 indicates that we can get same clustering result if we take superpixel associations instead of pixels as the vertices in G. But if we are using superpixels, there is not such a guarantee. This means, as primitives, superpixel associations are better than superpixels.

6.3 Segmentation with superpixel associations

Since the superpixel associations is a kind of primitives for ensemble clustering, for hierarchical image segmentation, one intuitive idea is to generate the segmentation by merging the superpixel association gradually (i.e., by a bottom-up process). Moreover, this can be easily done with a tree-growing algorithm. Thus, we propose a novel image segmentation algorithm which works on the superpixel association level, named superpixel-based hierarchical segmentation tree (SHST). In our algorithm, the superpixel associations are regarded as the leaves, and, the tree is constructed based on a similarity matrix of the superpixel associations.

The framework of SHST can simply be divided into two parts: measuring the similarities among the superpixel associations and merging them according to the similarities. However, this algorithm has three characteristics that are different from the state of the art. The first one is the method for similarity measure. The second one is a two-stage merging strategy that allows balancing between the local and globe similarity. Finally, SHST is able to determine the number of segmentations automatically by setting a cluster lifetime. The details are elaborated as follows.

6.3.1 The similarity measure

We propose a voting strategy for measuring the similarity between two superpixel associations. Given a set of superpixel segmentations $\mathcal{S}$, $Sa_i = \{p^i_1, \cdots, p^i_{K_i}\}$ and $Sa_j = \{p^j_1, \cdots, p^j_{K_j}\}$ are two superpixel associations obtained from $\mathcal{S}$ that contain K_i and K_j pixels respectively. Moreover, let $\Pi = \{\pi^1, \cdots, \pi^M\}$ be a set of segmentations of the image I and $\pi^m = \{R^m_1, \cdots, R^m_{r_m}\}$ be a segmentation containing r_m regions. We define a δ function as

$$\delta^m(p_i, p_j) = \begin{cases} 1, & \text{if } p_i \in R^m_r, p_j \in R^m_r, \text{ and, } R^m_r \in \pi^m \\ 0, & \text{otherwise,} \end{cases} \tag{6.1}$$

where p_i and p_j are pixels in I. Then, the co-occurrence p_i and p_j on a given Π is

$$\Delta(p_i, p_j) = \sum_{m=1}^{M} \sum_{r=1}^{r_m} \delta^m(p_i, p_j). \tag{6.2}$$

And, the similarity between Sa_i and Sa_j is defined as,

$$sim(Sa_i, Sa_j) = \frac{\sum_{p^i \in Sa_i} \sum_{p^j \in Sa_j} \Delta(p^i, p^j)}{|Sa_i| \cdot |Sa_j|}, \tag{6.3}$$

where $|Sa_i|$ represents the number of pixels in Sa_i. Actually, if we set H to be a histogram of N bins where N is the total number of regions in Π, and each bin is represented by the number of pixels belonging to the respective region, then, Eq. 6.3 can be rewritten as

$$sim(Sa_i, Sa_j) = \frac{H_{Sa_i} H^T_{Sa_j}}{|Sa_i| \cdot |Sa_j|}, \tag{6.4}$$

where H_{Sa_i} is a row vector representing the histogram of occurrence of pixels in Sa_i on Π.

There are a few nice properties for our similarity function. First, the similarity is computed purely from the co-occurrence of the pixels, which is simple and easy to adopt. Given $\mathcal{S}$, we can get the similarity without any other extra feature extraction procedures. Moreover, according to Eq. 6.4, the similarity is actually a normalized inner product, which is quite easy to compute. Second, we can balance the similarity in different scales by using different base segmentations Π, which may benefit image segmentation.

6.3.2 Two-stage merging

From Eq. 6.3 it is clear that different segmentation sets Π will bring different similarities. Thus, we developed a two-stage merging strategy that merges the superpixel associations in two steps with two different Π. In the first stage, the superpixel associations are refined with the given superpixel segmentations $\mathcal{S}$, and in the second stage, the refined superpixel associations are merged to final segmentation based on a few clusterings of $\mathcal{S}$, which contain the long-range relations of the superpixel associations.

Refining superpixel association with $\mathcal{S}$

The whole merging procedure starts with the refining step based on $\mathcal{S}$. There are two reasons for doing this. First, there always exists some tiny superpixel associations, that is, superpixel association with very small size, because noise or complexity in real-world images makes the superpixel boundaries unstable. Second, many superpixel algorithms tend to oversegment the image, which makes H in Eq. 6.4 (the occurrence histogram on $\mathcal{S}$) sparse. This means $\mathcal{S}$ contains strong local similarity information while weak long-range relations. Therefore, a refining procedure based on $\mathcal{S}$ is necessary and good for producing the stable performance.

We refine the superpixel associations by merging the tiny entries into their nearest neighbours according to the similarity measure in Eq. 6.3. For a given threshold τ, the tiny superpixel association is merged with the one that is most similar to it. Since it is possible for two tiny superpixel associations to be merged into one but the new one is still tiny, the merging process is done in an iterative manner. In this chapter, we set τ as a p-quantile of the superpixel associations' size sequence, where $p \in [0, 1]$. This makes the selection of τ more adapting.

Long-range similarity

Since many superpixel algorithms tend to oversegment the image, the base segmentation set $\mathcal{S}$ tends to lose the long-range similarities among the superpixel associations, which means the H based on $\mathcal{S}$ is sparse and Eq. 6.4 cannot work properly. The solution for this problem is intuitive, that is, making a set of clusterings on $\mathcal{S}$ and computing the similarities based on them. Fortunately, we can obtain the clusterings on $\mathcal{S}$ easily with an algorithm similar to HBGF, which models the pixel-superpixel relations with a bipartite graph and get the clusterings via spectral clustering. Algorithm 6.1 shows the details. Besides, it is worthy to mention that, in Algorithm 6.1, we can fuse dif-

Algorithm 6.1 The spectral clustering on $\mathcal{S}$

Input: Image $I = \{p_1, \cdots, p_m\}$, Superpixel clusterings $\mathcal{S} = \{S^1, \cdots, S^N\}$, a set of number of clusters $K = \{K_1, \cdots, K_M\}$;

Output: A set of clusterings on $\mathcal{S}$: $\mathcal{C} = \{C^1, \cdots, C^M\}$.

/$*$Part I: Graph construction.$*$/
Set $V^X = I \cup \mathcal{S}$, $V^Y = \mathcal{S}$, $W = \emptyset$; //Another option is $V^X = I$.
Compute $n = \sum_{i=1}^{N} K_i$; // K_i is the number of superpixels in S^i.
for $v_i^X \in V^X, i = 1, \cdots, m + n$ **do**
  for $v_j^Y \in V^Y, j = 1, \cdots, n$ **do**
    $w_{ij} = similar(v_i^X, v_j^Y)$ //$similar(\cdot, \cdot)$ is the similarity measure.
  end for
end for
/$*$ Part II: Partition Superpixels$*$/
Compute the adjacency matrix on V^Y: $W_Y = W^T D_x^{-1} W$.
Apply spectral clustering on W^Y with $K_i \in K$, and obtain $\mathcal{C}$.

ferent features of the superpixels by the function $similar(\cdot, \cdot)$, then, the segmentation information from different features will transfer into the final segmentation via Eq. 6.3.

Construction of SHST

The tree is built on the refined superpixel associations by a minimum spanning tree algorithm (MST). Let Z be the similarity matrix of the refined superpixel associations; the tree construction process is summarized in Algorithm 6.2.

6.3.3 The cluster lifetime

We define the k-cluster lifetime for the SHST. Let $T = \{t_1, \cdots, t_M | t_1 \leq t_2 \leq \cdots \leq t_M\}$ denote the set of sorted edge weights of the SHST, and a cluster lifetime is defined as $\delta_i = (t_{i+1} - t_i)$. Since the SHST is constructed by a MST algorithm, we say δ_i is a k-cluster lifetime if the SHST is separated into k subtrees when removing the edges whose weights t satisfy $t > t_i$.

According to the highest lifetime criterion proposed in ?? (fre), a higher value of a k-cluster lifetime indicates the k is closer to the true cluster number of the data set. Thus, given a sorted cluster lifetime set $\Delta = \{\delta_1, \cdots, \delta_{M-1} | \delta_1 \geq \delta_2 \geq \cdots \geq \delta_{M-1}\}$, we can obtain the image segmentation by specifying the lifetime level, which is more flexible

Algorithm 6.2 Construction of SHST

Input: Superpixel associations $\mathcal{A} = \{Sa_1, \cdots, Sa_M\}$, Size threshold τ, base clusterings $\mathcal{S} = \{S^1, \cdots, S^N\}$, a set of number of clusters $K = \{K_1, \cdots, K_M\}$;

Output: A hierarchical segmentation tree H

/* The first stage of merging*/

$\mathcal{A}^* = \emptyset$, $Z = [Z_{ij}]$

for $Sa_i \in \mathcal{A}$ **do**

  $Sa = Sa_i$, remove Sa_i from $\mathcal{A}$;

  repeat

    Compute the $sim(Sa, Sa_j)$ by Eq. 6.4 based on $\mathcal{S}$ for all $i \neq j$;

    Find the most similar Sa_j of Sa;

    $Sa = Sa \cup Sa_j$;

    Remove Sa_j from A^*;

  until $|Sa| > \tau$

  $A^* = A^* \cup Sa$;

end for

/* Computer a set of clusterings of $\mathcal{S}$ */

Apply Algorithm 6.1 on $\mathcal{S}$ with K;

Obtain $\mathcal{C}$;

/* The second stage of merging*/

Compute the similarity matrix Z of $\mathcal{A}^*$ by Eq. 6.4 based on $\mathcal{C}$;

Apply MST on $(-Z)$ and get H //note:$(-Z)$ is the dissimilarity matrix.

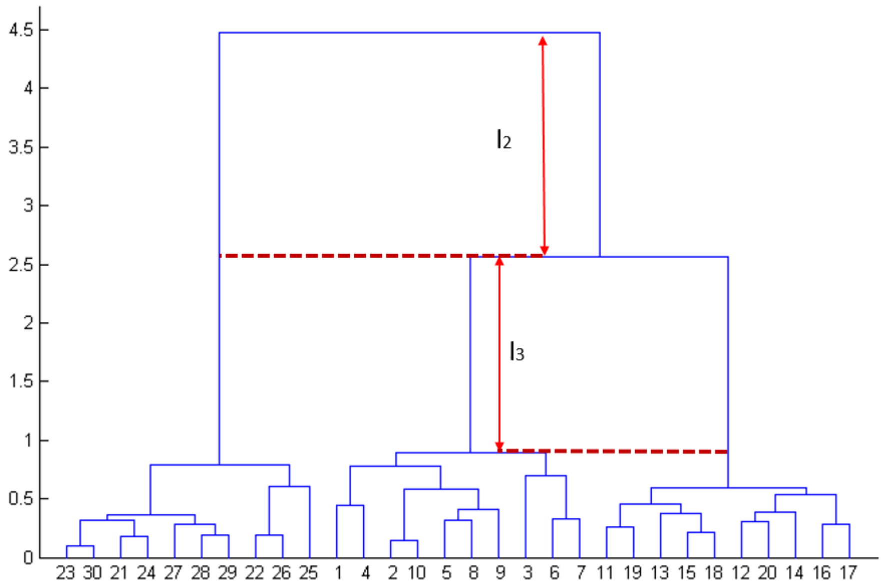

Figure 6.3: A dendrogram produced from SHST. If we remove the edges at l_2 level, the SHST will be partitioned into 2 subtrees. And, if we remove the edges at l_3, the SHST will be partitioned into 3 subtrees.

and objective than those algorithms that only work with specified cluster numbers. Figure 6.3 demonstrates the lifetime criterion.

Therefore, we have two ways for getting the segmentation result from SHST. One is cutting the tree with a specified cluster number, another is partitioning the tree with a given lifetime level.

6.4 Experiments

6.4.1 Data sets and settings

The experiments are conducted on two public image segmentation data sets: the Berkeley Segmentation Data Set 300 (BSDS300), and its update, the Berkeley Segmentation Data Set 500 (BSDS500) (Martin *et al.*, 2001; Arbelaez *et al.*, 2011).

For the similarity measure between superpixels, colour and texture are two significant clues. We take *Lab* colour space to compare the colours, in which the Euclidean distance can represent the difference of colours in the human visual system, while for the texture feature, we use texton (Arbelaez *et al.*, 2011) and colour covariance matrix (Gu *et al.*, 2014a). In addition, we also consider the geometry relations of the superpixels, that is, the neighbourhoods of the superpixels and take it as a cue in graph construction (Li *et al.*, 2012).

For the parameters in Algorithm 6.1, they are set to the same values as those in Li *et al.* (2012) and Gu *et al.* (2014a). For τ in Algorithm 6.2, we set it as the p-quantile of the input superpixel associations' size sequence, and we adopt a grid search in $[0.1, 0.9]$ with the step of 0.1 for finding the best p. We set the cluster number K from 2 to 20 for base clustering generation, which gives 19 different clusterings for all the superpixels.

Furthermore, we use two classical superpixel algorithms to generate the superpixel segmentations: the F-H method (Felzenszwalb and Huttenlocher, 2004) and Mean Shift (Comaniciu and Meer, 2002); and the parameters for superpixel generation are set to be the same as those in Chapter 3.

6.4.2 Results

We test the SHST with PRI (Unnikrishnan *et al.*, 2007), VoI (Meilă, 2005), GCE (Martin *et al.*, 2001), and BDE (Freixenet *et al.*, 2002). And in some tables, we also listed the performance of the state of the art for comparison, which includes, SAS(Li *et al.*, 2012) and ℓ_0-sparse algorithm (Wang *et al.*, 2013), and CCM.

Firstly, we test the algorithm with different features, segmentation information, and different combinations of them, which includes the *Lab* colour (Col), texton (Tex), colour covariance matrix (CovMat) and geometry relations of the superpixels(Geo). The performance of SHST is stable with those features over the two data sets; and the indices values indicate that the combination of Col, Tex, and Geo is better than others. The mean values of each index are demonstrated in Table 6.1 and Table 6.2.

Secondly, the comparisons against other state-of-the-art algorithms are conducted. SHST gets higher performance on PRI, VoI and GCE except BDE, which implies our approach is good at partitioning the regions containing the objects but with rough boundaries. Table 6.3 and Table 6.4 show the average values of each index over the data sets.

Finally, we test the algorithm by varying the tiny superpixel association threshold p. Figure 6.4 displays the result on BSDS500, which is conducted by combing the Col, Tex and Geo features. And, we find the the performance gets better with the increasing of p.

In addition, we note that, in all the tables, $(\cdot)^*$ and $(\cdot)^\dagger$ represent the results that were obtained by the lifetime criterion and specified segment numbers respectively; the parameters are well tuned for the highest performance on PRI. And, Figure 6.5 is an

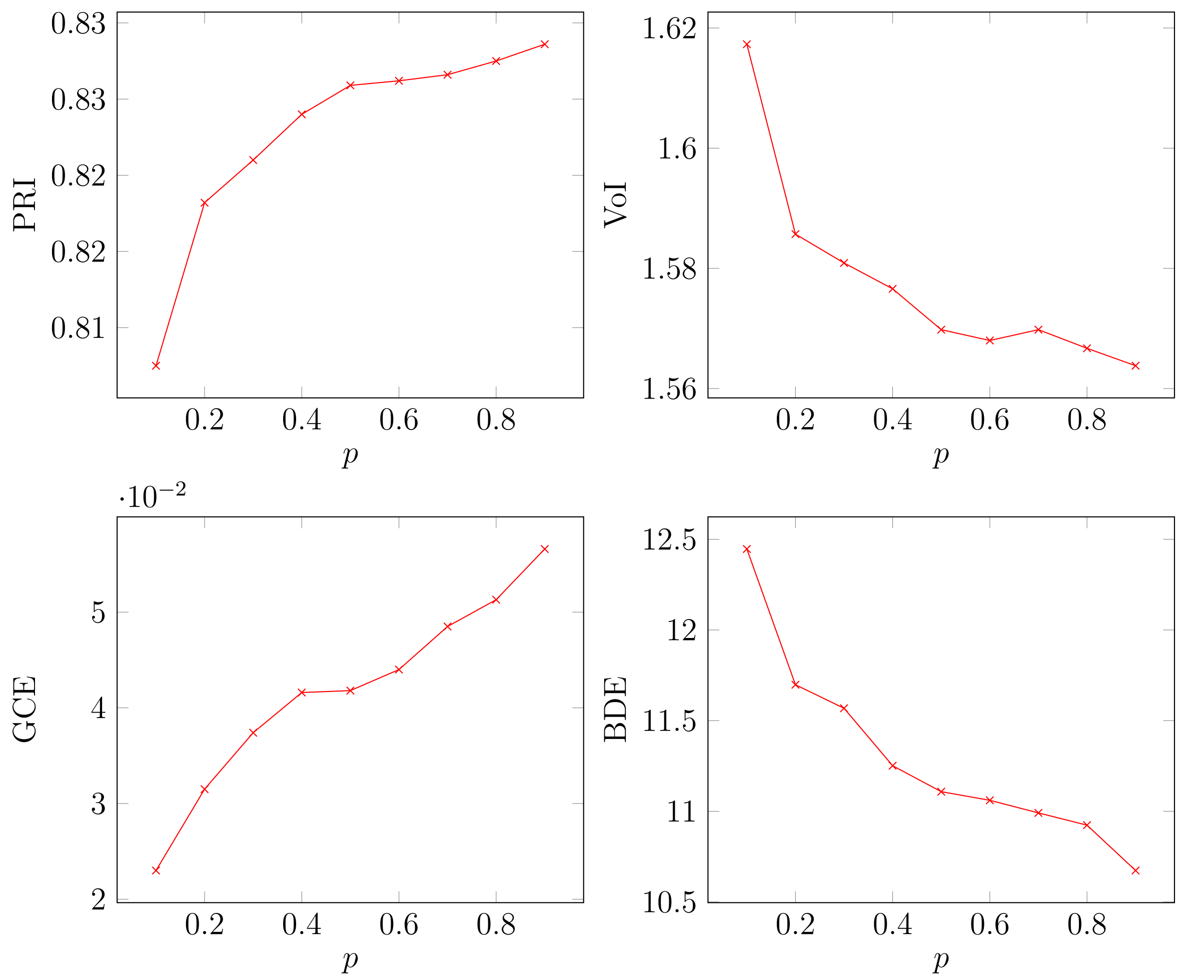

Figure 6.4: Testing on the size threshold parameter p of tiny superpixel association. The four charts correspond to the average scores of PRI, VoI, GCE and BDE on BSDS500; Lab colour, texton and geometry relations are used in the test.

example of hierarchical segmentation tree; Figure 6.6 shows a few of the segmentations generated by different algorithms. On a desktop equipped with an Intel i5 CPU and 16GB RAM, the run time of the Matlab code for building a SHST on one image is about 20 seconds when the superpixel segmentations are given.

6.5 Conclusion

We propose a novel concept, named superpixel association, which is the overlap of superpixels from different superpixel segmentations. Then, a similarity measure function is defined based on the majority voting algorithm. And with this similarity measure,

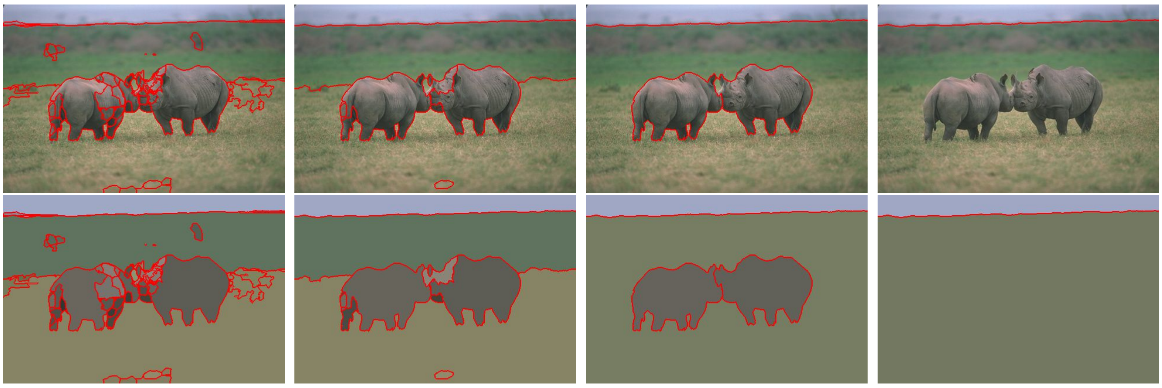

Figure 6.5: An example of the hierarchical structure; from left to right, the number of segments is decreasing.

Table 6.1: Performance of SHST with different features on BSDS300

Features	PRI	VoI	GCE	BDE
(Col+Geo)*	0.8422	1.4668	0.1502	18.2738
(Col+CovMat)*	0.8368	2.3072	0.1945	12.5409
(Col+Tex)*	0.8374	2.2240	0.1939	**11.7387**
(Col+Geo+Tex)*	**0.8416**	**1.4308**	**0.1449**	21.9028
(Col+Geo)†	0.8465	1.4491	0.1465	18.2901
(Col+CovMat)†	0.8335	1.9257	0.2120	12.5758
(Col+Tex)†	0.8339	1.8597	0.2081	**11.3832**
(Col+Geo+Tex)†	**0.8452**	**1.4209**	**0.1420**	23.1781

Table 6.2: Performance of SHST with different features on BSDS500

Features	PRI	VoI	GCE	BDE
(Col+Geo)*	0.8399	1.5458	0.1612	15.7963
(Col+CovMat)*	0.8369	2.3513	0.1948	11.8055
(Col+Tex)*	0.8367	2.2909	0.1964	**11.1386**
(Col+Geo+Tex)*	**0.8417**	**1.4846**	**0.1497**	18.1900
(Col+Geo)†	0.8443	1.5264	0.1588	15.6898
(Col+CovMat)†	0.8337	1.9473	0.2158	11.5977
(Col+Tex)†	0.8331	1.9066	0.2152	**10.8030**
(Col+Geo+Tex)†	**0.8451**	**1.4749**	**0.1483**	19.0004

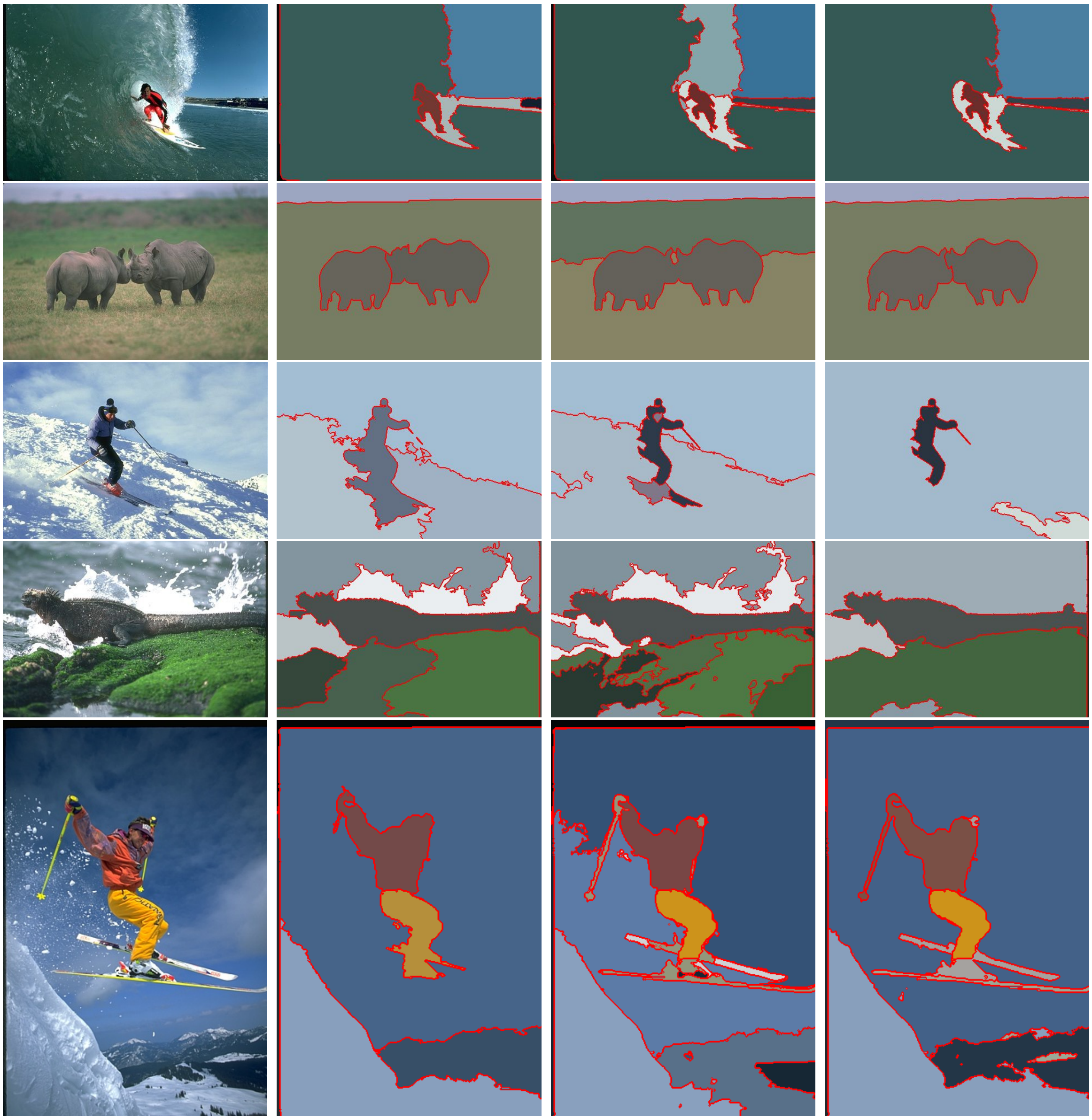

(a) (b) (c) (d)

Figure 6.6: Segmentations from different approach: (a) the original (b) SAS (c) CCM (d) SHST*. SHST* tends to partition the image with fewer segments.

Table 6.3: Performance of Different Algorithms on BSDS300

Algorithms	PRI	VoI	GCE	BDE	Avg.R
SAS	0.8319	1.6849	0.1779	11.2900	3.5
CCM	**0.8495**	1.6260	0.1785	12.3034	2.75
ℓ_0-sparse	0.8335	1.9935	0.2297	**11.1955**	4
SHST*	0.8422	1.4668	0.1502	18.2738	2.75
SHST†	0.8465	**1.4491**	**0.1465**	18.2901	2.25

Table 6.4: Performance of Different Algorithms on BSDS500

Algorithms	PRI	VoI	GCE	BDE	Avg.R
SAS	0.8372	1.6914	0.1813	12.6599	3
CCM	0.8407	2.0399	0.2359	**10.7829**	3
ℓ_0-sparse	-	-	-	-	-
SHST*	0.8417	1.4846	0.1497	18.1900	2.25
SHST†	**0.8451**	**1.4749**	**0.1483**	19.0004	1.75

Note: The symbol '$-$' means there are no published results available.

the tiny superpixel associations can be merged into their neighbours so that a more robust oversegmentation of the image (i.e., a set of refined superpixel associations) can be obtained.

And, we also proposed a segmentation tree algorithm (i.e., SHST), which can build a hierarchical segmentation tree on the superpixel associations (or, refined superpixel associations). SHST has two advantages. First, it is more flexible in partitioning the image since it can generate the segmentation with a specified number of segments or a scale level. Second, SHST is built with the superpixel associations, which makes the computational cost affordable.

Extensive experiments have been conducted and the results have shown that our method gets stable performance with different features; and compared with other state-of-the-art segmentation algorithms, the outputs of SHST are competitive. Moreover, the grid search of the size threshold τ for the tiny superpixel association shows this parameter has a strong connection with the performance of SHST. So, as a parameter for balancing the quantity and quality of superpixel associations, it is efficient and effective.

Chapter 7

Semantic Segmentation with Unsupervised Segmentation

7.1 Introduction

Semantic segmentation is one of the frontiers in computer vision that attempts to partition the image into semantically meaningful parts and classify each part into one of the predetermined classes. Compared with unsupervised segmentation, semantic segmentation not only partitions the image into several 'coherent' parts but also tries to understand what these parts represent. To this extent, semantic segmentation and unsupervised segmentation are different in solving the segmentation problem. For semantic segmentation, it is more like a classification task, while for unsupervised image segmentation, it is a task of clustering.

A wide range of semantic segmentation algorithms has been published in the past few years. In many early works, great efforts have been made to building frameworks for the semantic segmentation. Shotton *et al.* (2008) proposed the semantic random forests, which labels every pixel by a set of decision trees simply with a few low-level features. Fulkerson *et al.* (2009) proposed a two-stage model to do the semantic segmentation on superpixel-level, in which the superpixels are labelled by a support vector machine and then the labels are refined by a conditional random field (CRF). Krähenbühl and Koltun (Krähenbühl and Koltun) built a fully connected CRF over the pixels, and they proposed an efficient inference algorithm to label every pixel. Another focus in this region is the features extraction. Gould *et al.* (2008) proposed a superpixel-based algorithm in which the relative location prior is incorporated into the CRF. And Liu et al. employed a convolutional neural network to extract the 'deep features', and the performance of the state of art is improved when replacing the traditional features with those 'deep' ones (Liu *et al.*, 2015).

Moreover, the unsupervised segmentation also draws the attention of researchers in semantic segmentation. Because the image cues contained in the unsupervised segmentations, such as contours and object shape, are informative, they may be helpful in deciding the pixel labels. Kohli *et al.* (2009) proposed a higher-order conditional random field, which expands the basic CRF framework to incorporate higher-order potentials defined on superpixels. This higher-order CRF incorporates the superpixels from different superpixel segmentations and improves object segmentation with better boundaries. Kluckner *et al.* (2009) also take use of the region consistency extracted from superpixels to improve the labelling accuracy.

In this chapter, we propose an algorithm that integrates the superpixel associations into semantic segmentation. In our algorithm, we adopt a random forests algorithm which provides structured labels, and the final labelling is generated via a puzzle game framework. The rest of the chapter is organized as follows. Section 7.2 is a brief introduction of semantic segmentation. In Section 7.3, we propose a generalized puzzle game framework, and Section 7.4 specifies the algorithm we proposed for semantic segmentation. In Section 7.5, the results of the experiments are reported. And in Section 7.6, the conclusion is given.

7.2 Semantic image segmentation

An image always contains one or more objects, including things like animals, people, sky, water, and mountains. The appearances of the objects generate intensity edges between one object and its neighbours in the image, and semantic image segmentation aims to split the image into regions corresponding to the objects and label them with the relevant object category simultaneously.

Usually, this task is approached with supervised machine learning techniques, which use a set of training images with manually segmented and labelled ground-truth to learn the parameters for discriminating different regions.

7.2.1 Overview

Essentially, the semantic segmentation task is a pixel-classification problem. A variety of methods have been proposed for solving this problem in recent years. However, based on the relationships of encoding between different pixels, these methods can be

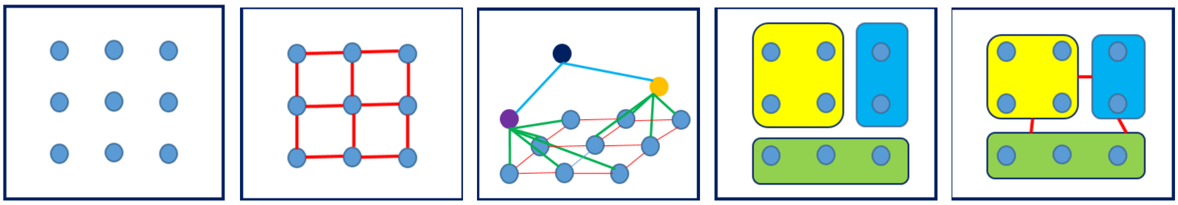

(a) (b) (c) (d) (e)

Figure 7.1: Methods of modelling pixel relationships: (a) pixels are independent, (b) pairwise relationships between pixels, (c) higher-order relationships between pixels, (d) using superpixels, (e) pairwise relationships between superpixels. Random field models are built on different pixel relationships.

categorized into two classes. In the first class, the pixel-labelling problem is solved by classifying each pixel independently, that is, with a pixel-level model, such as Shotton *et al.* (2006, 2008). While in the second class, the algorithms work with pixel groups (i.e., superpixels) and assign a label to each group; we call them region-level models (Gould *et al.*, 2008). Compared with those pixel-level algorithms, the region-based methods are more computationally efficient but may lead to an incorrect final labelling.

Many semantic segmentation algorithms for both two categories have a common framework, which is considered as a two-stage process (Fulkerson *et al.*, 2009; Gould *et al.*, 2008). The first stage is for extracting the unary potentials, and the second stage is to label the pixel based on its relationships between the neighbouring pixels. The second stage is modelled by a pairwise Markov Random Field (MRF) or Conditional Random Field (CRF) (Lafferty *et al.*, 2001; Kumar *et al.*, 2003). These models encourage the adjacent pixels to take the same semantic label, which leads the smooth boundaries in the segmentation results. In Kohli *et al.* (2009) and Ladický *et al.* (2010), the pairwise interaction between pixels are replaced by higher-order relationships between pixels (or pixel groups), which improves the segmentation results with better object boundaries. Figure 7.1 shows different ways of using the pixel (or pixel group) relationships. The random field models are constructed on those relationships.

Moreover, from Shotton *et al.* (2006), we know that the unary potential has a significant influence on the success of a segmentation algorithm. Much effort has been put into the generation of good unary potentials. In some early works, many classical classifiers are used as unary classifiers, such as support vector machine, logistic regression, and random forests (Shotton *et al.*, 2006; Verbeek and Triggs, 2007; Gould *et al.*, 2008;

Fulkerson *et al.*, 2009). Recently, structured prediction algorithms are also introduced to training the unary classifiers, for example, the structured support vector machine in Liu *et al.* (2015) and the structured random forests in Kontschieder *et al.* (2011, 2014).

7.2.2 Features

Feature extraction is one critical issue in image segmentation. There are many informative image cues that can be used for semantic segmentation.

Obviously, the most widely used features are the low-level features, such as intensity, colour, texture. These features are easy to get and always computed on a per-pixel basis and incorporate local colour or texture statistics. Other popular descriptors are the mid-level features, which are extracted from regions (i.e., superpixels) to provide shape, continuity or symmetry information. For example, in Kluckner *et al.* (2009), the covariance descriptors extracted from superpixels are used to train the random forests. In addition, many handcrafted features are also involved in generating mid-level descriptors. For example, the density of SIFT and HoG feature is used to represent the superpixels (Fulkerson *et al.*, 2009; Ladický *et al.*, 2010), and Bo *et al.* (2011) encode the pixels by a multi-layer sparse coding algorithm. A stronger mid-level feature is the deep feature introduced by Liu *et al.* (2015). This feature is extracted by a well-trained convolutional neural network and improves the performance of the CRF-based semantic segmentation model.

In addition to the abovementioned features, the context information is also prevailing in semantic segmentation (Johnson *et al.*, 2013; Torralba *et al.*, 2003; Rabinovich *et al.*, 2007). The motivation behind using this feature is the perceptual psychology, which claims that the global image statistics and information about the contextual relations can help to seek the proper configurations of the objects in images.

7.2.3 Training data issues

To a large extent, the quality of the training data set is also related to the performance of the semantic segmentation algorithms. Most techniques require a variety of training images with full pixel-wise labels. Unfortunately, such a kind of data set is expensive to obtain. But Shotton *et al.* (2008) showed that the performance of the algorithm can be improved by a random transform of the training images, which includes rotating with some random angles, rescaling with random ratios, and adding Gaussian noises.

Actually, with such transfer operations, the number of training images is increased. So, the random transform is a simple but effective method which may bring a boost in performance of the semantic segmentation algorithm.

7.3 Generalized puzzle game for semantic segmentation

Kontschieder *et al.* (2011) proposed a framework for semantic segmentation with squared label patches, and they named it as label puzzle game. We generalize this framework and make it integrated with unsupervised segmentation. To avoid unnecessary confusions, we inherit part of the notations from Kontschieder *et al.* (2011) in this section.

7.3.1 The generalized puzzle game

An image is a function $f : D \rightarrow R^d$ mapping the pixels in a 2-dimensional lattice $D \subseteq Z^2$ to d-dimensional feature vectors. Let $Y = \{1, \cdots, k\}$ be the class label set, and a labelling for an image is a function $\ell : D \rightarrow Y$ mapping the pixels to labels. A (label) puzzle piece is a label configuration, which is defined as a function $p : P \rightarrow Y \cup \{\perp\}$ mapping 2-dimensional points to labels or void (i.e., $\{\perp\}$, the absence of label), where $P \subseteq Z^2$ is a neighbourhood of the pixel. Since one pixel can be associated to multiple puzzle pieces, we set $\mathcal{P}$ to represent the set of puzzle piece associating to one pixel.

We set $\mathscr{F}$, $\mathscr{L}$ and $\mathscr{P}$ to denote the set of images, labellings and puzzle pieces respectively. Then, a puzzle configuration is defined as a function $z : D \rightarrow \mathscr{P}$ assigning each pixel in D with a puzzle piece in $\mathscr{P}$. And, the set of puzzle configuration is denoted by $\mathscr{Z}$.

Moreover, let (i, j) and (u, v) represent the coordinates on D, and the puzzle piece at (i, j) is written as $p_{i,j}$ and by setting (i, j) be the centre of $p_{i,j}$, we denote $p_{i,j}(u-i, v-j)$ the label in position (u, v), and this denotation also holds for the puzzle configuration z. Let $S \subseteq D$ be a region on image D, and the set of S is written as $\mathscr{S}$. We denote $\mathcal{S}_{i,j} = \{S \in \mathscr{S} | S \sim \mathcal{P}_{i,j} \neq \emptyset\}$ the regions associated with (i, j), where the symbol '$\sim$' indicates some relation. And, given a labelling ℓ, $\ell(S)$ is the label configuration of S.

The generalized puzzle game of semantic segmentation has three components: the puzzle generator, the agreement, and the game solver. They are given by the following four definitions.

Definition 7.3.1 (puzzle generator)**.** *For semantic segmentation, a puzzle generator is a function* π *that maps each pixel* $(i, j) \in D$ *to a non-empty set of puzzle pieces* $\mathcal{P}_{i,j} \subseteq \mathscr{P}$*.*

Let π be a puzzle game, then from Definition 7.3.1, all possible puzzle configurations obtained from π can be written as

$$\mathscr{Z}|_\pi = \{z \in \mathscr{Z} | z_{i,j} \in \mathcal{P}_{i,j}\}.$$

Definition 7.3.2 (generalized agreement)**.** *Given an image labelling* ℓ *and a set of region* $\mathcal{S}$ *respecting to the puzzle piece* p*, the agreement of* p *is defined as*

$$\phi(p, \ell, \mathcal{S}) = \sum_{S \in \mathcal{S}} similarity(p, \ell(S)), \tag{7.1}$$

where $similarity(\cdot, \cdot)$ *is a function measure the similarity between* p *and* $\ell(S)$*.*

Moreover, for a puzzle piece configuration, we define a total agreement as the sum of its puzzle piece agreements, that is,

Definition 7.3.3 (total agreement)**.** *Given a puzzle piece configuration* z*, a labelling* ℓ *and the region set* $\mathscr{S} = \{\mathcal{S}_{i,j}\}$*, the total agreement of* z *is*

$$\Phi(z, \ell, \mathscr{S}) = \sum_{z_{i,j} \in z} \phi(z_{i,j}, \ell, \mathcal{S}_{i,j}). \tag{7.2}$$

Here, we note that Definition 7.3.2 and Definition 7.3.3 are the generalized versions of the respective definitions in (Kontschieder *et al.*, 2011), which extend the similarity measured with a region set $\mathscr{S}$.

Then, the solution for the puzzle game can be defined as an optimization problem of Eq. 7.2.

Definition 7.3.4 (game solver)**.** *Given a labelling set* $\mathscr{L} = \{\ell^{(1)}, \cdots, \ell^{(T)}\}$ *respected to* $\mathscr{Z}|_\pi$ *and a region set* $\mathscr{S}$*, the solution* (z^*, ℓ^*) *of the puzzle game satisfies*

$$(z^*, \ell^*) = arg \max_{(z,\ell)} \{\Phi(z, \ell, \mathscr{S}) | (z, l) \in \mathscr{Z}|_\pi \times \mathscr{L}\}. \tag{7.3}$$

In our puzzle game definitions, the unsupervised segmentation is able to affect the labelling updating via the agreement, which is different from those proposed by Kontschieder *et al.* (2011). Figure 7.2 shows the framework.

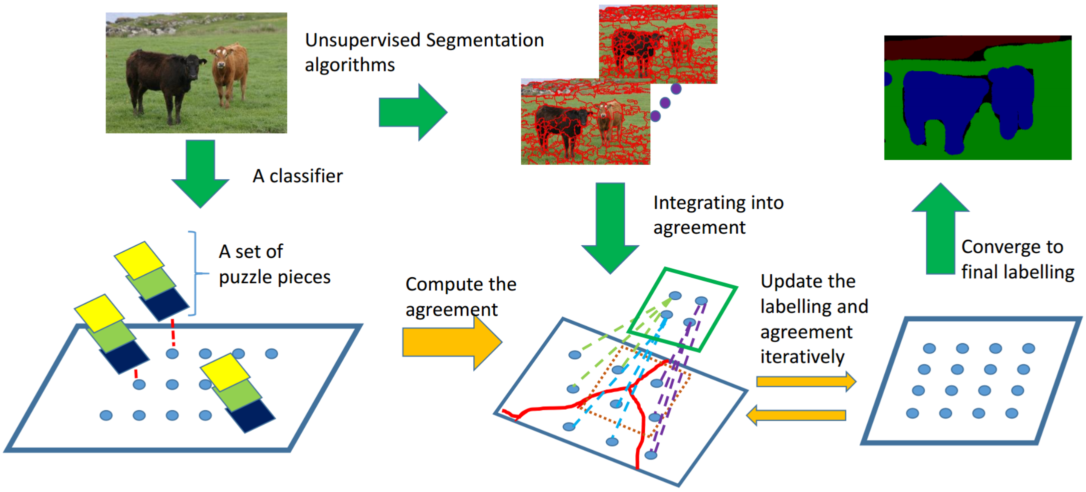

Figure 7.2: The framework of our algorithm. From left to right: first, a classifier generates a few puzzle pieces for each pixel; meanwhile, a few unsupervised segmentation algorithms produce some unsupervised segmentations; second, we compute the agreement by integrating the unsupervised segmentation and alternatively update the labelling and agreement; finally, the labelling converges to the final result.

7.3.2 Agreement with unsupervised segmentation

The agreement is critical for solving the puzzle game. With the generalized agreement (i.e., Definition 7.3.2), we can integrate the information provided by the unsupervised segmentation into the game solver.

The puzzle piece is set to be in a square patch shape with the size of $d \times d$, which is same as Kontschieder *et al.* (2011). But for the regions associated with pixel (i, j), we define them as $\mathcal{S}_{i,j} = \{S^D \in \mathscr{S}^D | S^D \cap \mathcal{P}_{i,j} \neq \emptyset\}$, where $\mathscr{S}^D$ is a given unsupervised segmentation $\mathscr{S}^D = \{S_1^D, \cdots, S_K^D\}$. Intuitively, those pixel labels within one region should be the same, so, given a labelling ℓ, we set the label of a segmentation S_k^D by a majority vote on the labels within it, written as $\text{Vote}[\ell(S_k^D)]$. Therefore, the similarity is defined as the coincidence of the labels of $p_{i,j} \cap S_{i,j}$ in $p_{i,j}$ and $\ell(S_{i,j})$, which is

$$\phi_{i,j}(p_{i,j}, \ell, \mathcal{S}_{i,j}) = \sum_{(u,v)\in D} \sum_{S_{i,j}\in\mathcal{S}_{i,j}} \delta[p_{i,j}(u-i, v-j) = \text{Vote}[\ell(S_{i,j})] | (u,v) \in S_{i,j}], \quad (7.4)$$

where $\delta[\cdot]$ is a delta function which yields 1 if the input is true, 0 otherwise.

7.3.3 Optimization of game solver

We follow the algorithm in (Kontschieder *et al.*, 2011) to find the solution for the puzzle game. Specifically, the optimization of game solver (i.e., Eq. 7.3) is obtained by iteratively switching between optimizing the labelling $\ell \in \mathscr{L}$ and the puzzle configuration $z \in \mathscr{Z}|\pi$.

Let $\ell^{(t)}$ be the labelling of the image at time $t \geq 0$. The entries in puzzle configuration $z^{(t+1)}$ at time $t+1$ are individually updated via

$$z_{i,j}^{(t+1)} \in \arg\max_{p_{i,j}} \left\{ \phi_{i,j}(p_{i,j}, \ell^{(t)}, \mathcal{S}_{i,j}) | p_{i,j} \in \mathcal{P}_{i,j} \right\}. \tag{7.5}$$

And then, the $\ell^{(t+1)}$ is computed with the given $z^{(t+1)}$ by taking a majority vote over all puzzle pieces in z. Let C be the set of puzzle pieces z that cover pixel px_i and $z(i)$ be the label of px_i in z, we have

$$\ell^{(t+1)}(u,v) \in \arg\max_{y} \left\{ \sum_{(i,j)\in D} \delta[z_{i,j}^{(t+1)}(u-i, v-j) = y | y \in Y] \right\}. \tag{7.6}$$

Given an initial labelling $L^{(0)}$, then, by updating the z and ℓ alternatively, it will reach the local maximum of the game solver, which is proofed as **Theorem** 1 in (Kontschieder *et al.*, 2011).

7.4 Integrating unsupervised segmentations

In our generalized puzzle game for semantic segmentation, we employ a structured prediction random forests algorithm as the game generator. Theoretically, a structured prediction algorithm is able to produce more candidates for the puzzle piece and enrich the searching space. The unsupervised segmentation is generated from superpixel associations via the SHST algorithm in Chapter 6.

7.4.1 Structured prediction with random forests

The random forests algorithm is an ensemble learning method for classification proposed in Breiman (2001), which has a few appealing properties, such as robustness to noise and resistance to overfitting. Traditionally, the random forests algorithm assigns the input data samples with single, atomic class labels, but for many computer vision application, this kind of prediction models is limited because the inherent topological structure in the label space is ignored. Kontschieder *et al.* (2014) propose a random forests algorithm for structured prediction, that is, a random forests algorithm predicts structured objects rather than scalar discrete or real values. Here, we refer to the traditional random forests as *standard* random forests, while for the one providing structured predictions, we refer to it as *structured* random forests.

Basically, the two types of random forests have common structures, that is, they are both an ensemble of decision trees. Let $\mathcal{X}$ be a data set, $\mathcal{Y} = \{y_i\}$ represent the class labels and π be a prediction of the class label. A decision tree t is a tree-structured classifier which makes a prediction by routing a sample $x \in \mathcal{X}$ through the nodes to a leaf, where the final prediction is proposed. A leaf $L_F(\pi) \in t$ is a node without any children nodes and is able to cast a class prediction π for any x that reaches it. For all other nodes, written as $N_D(\psi, t_l, t_r) \in t$, each of them is associated with a decision binary split function $\psi(x) : \mathcal{X} \to \{0, 1\}$, which determines the next route of sample x. If $\psi(x) = 0$, x will be forwarded to the left sub-tree $t_l \subset t$, or sent to the right sub-tree $t_r \subset t$, if $\psi(x) = 1$. And, a random forest is written as $F = \cup_{i=1}^{k} t_i$, that is, an ensemble of a couple of decision trees.

The main difference between *standard* and *structured* random forests is in the training of split function. In the following, we first introduce the prediction function and then show the difference between the *standard* and *structured* random forests.

Formally, the prediction function $h(x|t) : \mathcal{X} \to \mathcal{Y}$ for the nodes in a decision tree T is written as

$$\begin{aligned} h(x|N_D(\psi, t_l, t_r)) &= \begin{cases} h(x|t_l), & \text{if } \psi(x) = 0, \\ h(x|t_r), & \text{if } \psi(x) = 1, \end{cases} \\ h(x|L_F(\pi)) &= \pi. \end{aligned} \tag{7.7}$$

A sample x is branched recursively, and the procedure stops until x reaches a leaf. Obviously, the split function ψ is critical for the prediction, and different ψ leads different outputs. In computer vision, there are four types of ψ commonly used; let $f(x)$ be the feature vector of sample x and $f(x)_\theta$ be the value at the θ-th dimension.

$$\begin{aligned} &\psi^{(1)}(x|\theta_1, \tau) = [f(x)_{\theta_1} > \tau], \\ &\psi^{(2)}(x|\theta_1, \theta_2, \tau) = [f(x)_{\theta_1} - f(x)_{\theta_2} > \tau], \\ &\psi^{(3)}(x|\theta_1, \theta_2, \tau) = [f(x)_{\theta_1} + f(x)_{\theta_2} > \tau], \\ &\psi^{(4)}(x|\theta_1, \theta_2, \tau) = [|f(x)_{\theta_1} - f(x)_{\theta_2}| > \tau], \end{aligned}$$

where τ is a threshold, and $[\cdot]$ is an operator that gives 1 if the '$\cdot$' is true and 0 otherwise. The split function ψ and the parameters θ and τ are learned based on the information gain theory, which is computed from the class label distribution. Let $\mathcal{P}$ be the samples reached node N_D in the training, $E(\mathcal{P})$ represent the entropy of the class label distribution of N_D, and Ψ be the set of ψ. When training the random forests, firstly, a ψ is selected from Ψ randomly, and then, the algorithm randomly generates a few sets of θ and τ, by which the $\mathcal{P}$ is split into $\{\mathcal{P}_l, \mathcal{P}_r\}$. The information gain is defined as (Shotton *et al.*, 2008)

$$\Delta E = -\frac{|\mathcal{P}_l|}{|\mathcal{P}|}E(\mathcal{P}_l) - \frac{|\mathcal{P}_r|}{|\mathcal{P}|}E(\mathcal{P}_r), \tag{7.8}$$

and, $\{\psi, \tau\}$ is selected to maximize the ΔE.

In *standard* random forests, every sample in the training data is assigned with exactly one label, so the entropy $E(\mathcal{P})$ is computed on the distribution of one variable. But for the *structured* random forests, the samples for training are associated with a batch of labels, which means the $E(\mathcal{P})$ is computed on a distribution of multiple variables (i.e., a joint distribution). This makes the computation cost of the *structured* random forests higher than the *standard* one. But, it has been pointed out that by randomly choosing a (marginal) distribution from the joint distribution, the output of the *structured* random forests remains as effective as the one using joint distribution (Kontschieder *et al.*, 2011).

Moreover, the leaf node of *structured* random forests is also different from the *standard* one. Because the samples reached the leaves are assigned to multiple labels, the label presentation of a leaf should also be a set of labels. In this chapter, we extract the label representations for the leaves in the same way as in (Kontschieder *et al.*, 2011). Specifically, let $\mathcal{P}_t = \{\mathbf{p}_1 \cdots, \mathbf{p}_k\}$ be the puzzle pieces that reach leaf L_{Ft} during the training process. The joint probability of the labels in $\mathbf{p} \in \mathcal{P}_t$ is defined as

$$Pr(\mathbf{p}|\mathcal{P}_t) = \prod_{i,j} Pr^{(i,j)}(\mathbf{p}(i,j)|\mathcal{P}_t), \tag{7.9}$$

where $Pr^{(i,j)}(\mathbf{p}(i,j)|\mathcal{P}_t)$ is the marginal probability over all $\mathbf{p} \in \mathcal{P}$ of the label at position (i,j). Then, the label representation π of leaf L_{Ft} will be the one puzzle piece that maximizing the joint probability, that is,

$$\pi = \arg\max_{\mathbf{p}\in\mathcal{P}_t} Pr(\mathbf{p}|\mathcal{P}). \tag{7.10}$$

7.4.2 Integrating the unsupervised segmentation

We take the superpixel associations as the unsupervised segmentation for integration into the puzzle game.

The superpixel association is the intersections of superpixels from different over-segmentations and has been proved to be a good replacement of pixels for region-level models. The main motivation for using superpixel associations is because the probability of the pixels having the same labelling inside the superpixel association is higher than those regions obtained from single superpixel segmentation.

To obtain superpixel associations, we first use two classical superpixel algorithms to generate the superpixel segmentations, i.e., the F-H method (Felzenszwalb and Huttenlocher, 2004) and Mean Shift (Comaniciu and Meer, 2002), and the parameters in the superpixel generation procedure are set to be the same as those in Chapter 6. And then, following the Definition 6.2.1 in Chapter 6, we can get the superpixel associations.

Moreover, for those superpixel associations whose size is smaller than a given threshold, that is, the tiny superpixel associations, we can adopt an optimization option to merge them into their nearest neighbours.

7.5 Experiment

For semantic segmentation, the feature representations have a significant influence on the success of a labelling algorithm. However, in this chapter, since the primary intention of our experiments is to demonstrate the effects of integrating the unsupervised segmentation, we simply use the *Lab* colour and a multi-layer sparse coding feature to be the pixel representation. The effect of the integration of unsupervised segmentation can still be observed, even with this simple feature.

7.5.1 Data set and settings

The experiments of our algorithm are conducted on MSRC21. Following the protocol of previous works using MSRC21 (Shotton *et al.*, 2008; Gould *et al.*, 2008; Kohli *et al.*, 2009), we split the data into 276 training and 256 test samples and ignore those pixels with the void label during both training and evaluation. The results are evaluated with recall and precision (i.e., Avg(Class) and Global).

In our experiment, each pixel is represented by a vector that incorporates the colour and texture features. For the colour feature, we concatenate the Lab colour values of pixels within the $d_{col} \times d_{col}$ neighbour (centred at the current pixel).

As for the texture feature, we employ the sparse coding algorithm with a spatial pyramid. Specifically, we first use the sparse coding techniques to extract a sparse representation for each pixel, and then adopt a few spatial max pooling procedures on the sparse representations, that is, a spatial pyramid. Finally, the texture feature is generated by concatenating the coefficients of different layers of the spatial pyramid.

After all, the parameters are empirically set to be those providing the highest performance. For the colour feature, the neighbourhood size is set to be 23×23; while for the texture feature, the patch size for sparse coding is set to be 15×15, the spatial max pooling is adopted within a 2×2 grid of each pixel, and the number of the layers in spatial pyramid is set to be 3. Besides, the training samples are collected on a regular lattice with a stride of 4, which leads to approximately 500,000 training samples. Each forest contains ten trees.

7.5.2 Results

In order to demonstrate the effects of integrating unsupervised segmentation, the experiments are conducted with different algorithms on MSRC21. We set RF_{std} as the standard random forests, and RF_{str} as the structured random forests. For different *agreement* definitions, '*reg*' represents the definition proposed by Kontschieder *et al.* (2011), and, '*usp*' denotes the one proposed in this chapter. Particularly, we use 'usp_{all}' represents the superpixel associations without optimization, and 'usp_{100}' and 'usp_{40}' represent the superpixel associations that are merged into 100 units and 40 units based on the SHST algorithm (i.e., Algorithm 6.2) respectively.

Table 7.1 shows the results of experiments. The results obtained from our algorithms are visualized in Figure 7.3 and Figure 7.4; each row shows the results of one class. Also, Figure 7.5 demonstrates a few failures of our algorithm.

From the visualized results, we can see the outputs of $RF_{str}(usp_{40})$ have the clearest object boundaries. Moreover, the object labels obtained from $RF_{str}(usp_{40})$ are more accurate than those of others. Actually, when comparing the results of RF_{str}, it is easy to find that the higher performance of $RF_{str}(usp_{40})$ algorithm mainly comes from the integration of the unsupervised segmentation.

However, there are also some failed examples in which the objects (or parts of the object) are well marked but labelled incorrectly. This is most likely due to the weak feature scheme we used in the experiments.

Finally, in our experiments, the run time for the trained $RF_{str}(usp_4 0)$ labelling one image is about 7 seconds on a desktop equipped with an Intel i5 CPU and 16 GB RAM with Matlab 2014a.

Table 7.1: Performance of Different Random Forests on MSRC21

Algorithm	RF_{std}	$RF_{str}(reg)$	$RF_{str}(usp_{all})$	$RF_{str}(usp_{100})$	$RF_{str}(usp_{40})$
building	26.09%	29.84%	31.64%	32.21%	31.98%
grass	92.47%	93.85%	94.30%	94.22%	94.41%
tree	73.14%	77.64%	75.81%	78.19%	78.23%
cow	43.19%	48.26%	45.14%	46.94%	45.29%
sheep	54.94%	63.29%	65.27%	65.40%	68.86%
sky	91.25%	93.54%	95.98%	95.63%	95.45%
aeroplane	44.67%	55.41%	58.44%	58.79%	61.53%
water	51.07%	53.94%	59.39%	55.31%	55.70%
face	58.24%	64.00%	66.53%	67.62%	68.69%
car	32.84%	39.68%	42.97%	47.81%	48.88%
bicycle	60.66%	68.31%	68.46%	71.45%	74.12%
flower	37.06%	41.44%	40.48%	40.29%	40.97%
sign	23.35%	27.28%	39.30%	37.24%	37.66%
bird	7.81%	6.32%	2.38%	5.51%	3.57%
book	41.28%	49.55%	51.57%	53.05%	55.36%
chair	18.52%	21.85%	22.78%	22.98%	23.82%
road	58.74%	64.22%	74.51%	70.30%	73.28%
cat	43.38%	52.25%	55.52%	55.43%	59.76%
dog	20.11%	19.63%	24.43%	20.01%	20.53%
body	17.03%	18.79%	20.73%	20.28%	19.84%
boat	12.79%	10.05%	5.74%	5.39%	4.03%
Avg(Class)	43.27%	47.57%	49.59%	49.72%	50.57%
Global	57.77%	61.57%	63.91%	63.72%	64.37%

Figure 7.3: Semantic segmentation from different random forests: (a) the original, (b) *standard* random forest, (c) *structured* random forest, (d) *structured* random forest with unsupervised segmentation, (e) the ground truth with class labels shown in colour (the void label is in black).

(a) (b) (c) (d) (e)

Figure 7.4: Semantic segmentation from different random forests: (a) the original, (b) *standard* random forest, (c) *structured* random forests, (d) *structured* random forest with unsupervised segmentation, (e) the ground truth with class labels shown in colour (the void label is in black).

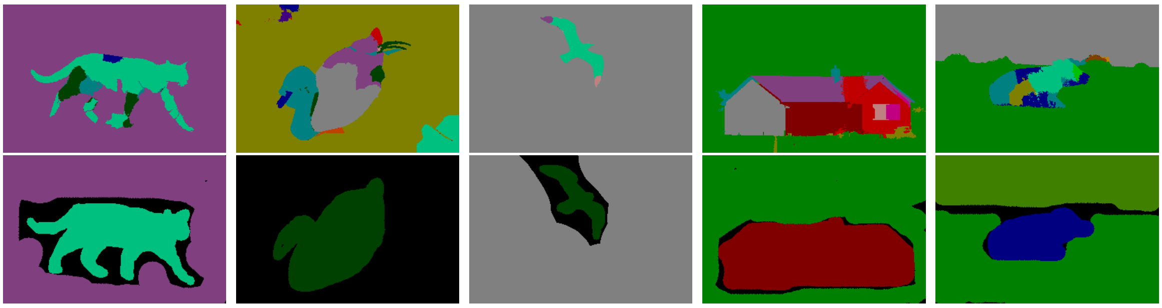

Figure 7.5: A few failures of our algorithm. The outputs of our algorithm are listed in the upper row, and their respective ground-truth segmentations are in the lower row with class labels shown in colour (the void label is in black). Most objects are properly figured out but with wrong labels, which is most likely due to the weak feature scheme used in the experiments.

7.6 Conclusion

In this chapter, we proposed a generalized puzzle game framework for semantic segmentation, by which the unsupervised segmentations can be easily integrated into the labelling procedure. The experiment results show that the integration of unsupervised segmentation brings obvious improvement for the labelling algorithm. Compared with the *standard* random forests, the *structured* random forests improves the average class and the global accuracy by 4.3% and 3.8% respectively; while integrating the unsupervised segmentations, the maximum improvements (i.e., $RF_{str}(usp_{40})$) are 7.3% for average class accuracy and 6.6% for global accuracy. Also, within the *structured* random forests, the accuracy increments from using different unsupervised segmentations are around 2%.

The feature scheme we used in the experiments is a concatenation of *Lab* colour values and a texture extracted by sparse coding techniques. When compared with those popular 'deep features', it is less effective in capturing the segmentation information, which results in relatively low performance of out algorithm.

Chapter 8

Conclusion and Future work

8.1 Conclusions

Applications of image segmentation in the foreseeable future will be on demand. For example, automatic car driving, medical imaging, image editing for artistic purposes will require exact pixel-accurate segmentation of an object. Superpixel segmentation, as a preprocessing procedure, is widely used in image segmentation applications, by which object parts or image features can be extracted. In this thesis, we have examined the issues about using superpixels in image segmentation. Our research began by asking the following questions:

- Can we develop an efficient descriptor for superpixels which is able to improve the state-of-the-art segmentation algorithms?
- Can we find some methods for combining the superpixel descriptors that extracted from different feature spaces?
- Is there any method that can improve the performance of the handcrafted superpixel descriptors?
- Is there any new method that can generate image segmentation with superpixels more effectively than the state of the art?
- Can we take use of the image cues in superpixel segmentations to improve the supervised segmentation?

These questions have been explored in one chapter, or relevant chapters jointly, as follows:

- **Proposing a novel covariance descriptor for superpixel and developing a corresponding segmentation algorithm 'CCM' in Chapter 3.**

  The SAS algorithm (Li *et al.*, 2012) is a superpixel-based segmentation algorithm, which employs a bipartite graph to model the pixel-superpixel relations. The performance of this model is critically influenced by the similarity defined on superpixels. So, we proposed a colour covariance matrix, as a representation of superpixel, adding to the discrimination ability of the colour feature. And, we also propose the CCM algorithm, by which the similarity of superpixel covariance descriptor in measured not only in colour space but also a manifold of the covariance matrix. With a properly defined metric for the covariance descriptor, CCM can perform better than SAS.

- **Proposing a multi-layer bipartite graph model 'MBG-CCM' for fusing superpixel descriptors from different feature spaces in Chapter 4.**

  The feature fusing method for bipartite graph has not been sufficiently explored. In the CCM algorithm, the superpixel similarities measured in colour space and covariance manifold are combined by a few matrix operators, which may be inapplicable with multiple features. So, we develop the MBG-CCM algorithm, which employs a multi-layer bipartite graph to formulate the similarities from different features. And, the layers of the graph are fusing by their subspace representation on a Grassmann manifold. Moreover, because of the high computational cost, the spectral clustering algorithm of normal multi-layer graph is intractable on our multi-layer bipartite graph. To solve this problem, we propose a transfer procedure for fusing the subspace representations, which is based on a property of singular value decomposition, that is, the left and right singular vectors can be computed from each other. Theoretically, the MBG-CCM is able to generate robust final segmentation with multiple features.

- **Proposing a low-rank representation model 'LRR-CCM' for utilizing subspace structure of the covariance descriptors of superpixel in Chapter 5.**

  The covariance descriptors are common, handcrafted features for superpixel. But the research about how to use the covariance descriptors effectively is not sufficient. So, we develop a low-rank representation algorithm that can find the subspace structures for the covariance descriptor set. We combine this algorithm with CCM and propose the LRR-CCM algorithm, which measures the similarity between the superpixels via the low-rank representation. The empirical experiments show that LRR-CCM is able to generate stable segmentation with noisy covariance descriptors.

- **Proposing a new oversegmentation method 'superpixel association' and a novel hierarchical segmentation algorithm 'SHST' in Chapter 6.**

  Inspired by the fact that, in HBGF-based segmentation algorithms, the pixels having the same pixel-superpixel relations are always partitioned into the same segment in the final segmentation, we propose the superpixel association method. Moreover, we proved that there exist an explicit relation between superpixel association and the pixels in the HBGF algorithm. This indicates that superpixel association is a good replacement of pixel in superpixel-based segmentation. Thus, we proposed a hierarchical segmentation algorithm (i.e., SHST). This novel segmentation algorithm takes superpixel associations as leaves and grows the segment by iteratively merging those closest regions. Since the number of superpixel associations is far less than that of pixels, the computational cost of the SHST is affordable. Another advantage of SHST is the number of segments in the final segmentation can be determined automatically, while for most of the existing algorithms, a specified number of segments is a prerequisite.

- **Developing a framework for integrating superpixel segmentation into semantic segmentation in Chapter 7.**

  Apart from those unsupervised segmentation methods, we extend our research into semantic segmentation. We propose a semantic segmentation algorithm, by which the superpixel segmentations can be easily integrated into the labeling procedure. This algorithm is named as *generalized puzzle game*, because its framework is inspired from the puzzle game. And, it contains three parts. The first part is called *game generator*, which is in charge of generating *label puzzle pieces* from the given image. The second is named *agreement*, which is a predefined similarity between the puzzle pieces and the current image labelling. The last one is called *game solver*, which is a predefined objective function, that is, the condition that the final labelling should satisfy. A modified random forests algorithm is employed as a *game generator*, which can provide more proposals (i.e., *label puzzle pieces*) than tradition random forests. Moreover, we introduce a new definition of *agreement*, by which the superpixel segmentation can influence the similarity measuring between the *label puzzle pieces* and current labelling. And, the final image labelling is obtained by alternatively updating the selection of puzzle pieces and the respective image labelling until the *game solver* converges.

8.2 Future work

Superpixel-based image segmentation is a research topic with an extensive and multi-faceted scope. In the following, we intend to discuss some current limitations and a few possible future directions that may extend from the work in this thesis.

- Computational cost-related study

  For online segmentation applications or some applications running on devices with low computational capacity, the computational cost is critical. Unfortunately, in our study, this has not been sufficiently considered because our major work is concentrating on improving the accuracy of the segmentation. Actually, there is a conflict between computational cost and segmentation quality. For most existing segmentation models, the high segmentation accuracy will definitely result in the high computational complexity. However, one possible solution for this problem is parallel computing. And, for superpixel-based segmentation, this means new ensemble segmentation techniques should be proposed with the ability to be parallelized and operated on multiple processors.

- Application of superpixel association

  Superpixel association is, in fact, an ensemble of superpixels, which can be considered as a replacement of pixel in many image-processing tasks. It is able to keep more image details, especially the boundary information than superpixel, yet, its amount is far smaller than that of the pixel. To bring about a more accurate segmentation result but with a relatively low computational cost, it may be possible to modify the superpixel-based segmentation algorithms with superpixel association. For example, it would be interesting to see how the performance of the models proposed by Gould *et al.* (2014) might be possibly improved by replacing the superpixels with superpixel associations.

- Deep learning with superpixel

  Supervised image segmentation would benefit from integrating the unsupervised segmentation. In our study, we only combined the unsupervised segmentation into a two-stage labelling framework (i.e., generating proposals and optimizing their combination). But, a more efficient and complicated structure, called deep learning, has been proposed recently (LeCun *et al.*, 2015), which achieves remarkable performance in supervised image segmentation. Moreover, studies in (Zheng *et al.*, 2015; Arnab *et al.*, 2016) show that the performance of VGG-16 network (Simonyan and Zisserman, 2014) is enhanced by considering the information from unsupervised segmentations. In order to boost both the training and inference stages, it may be possible to formulate a framework that integrates the superpixel segmentations with deep neural networks.

References

Achanta, R., Shaji, A., Smith, K., Lucchi, A., Fua, P., and Süsstrunk, S. (2012). SLIC superpixels compared to state-of-the-art superpixel methods. *IEEE Transactions on Pattern Analysis and Machine Intelligence*, *34*(11), 2274–2282.

Alush, A. and Goldberger, J. (2012). Ensemble segmentation using efficient integer linear programming. *IEEE Transactions on Pattern Analysis and Machine Intelligence*, *34*(10), 1966–1977.

Arbelaez, P., Maire, M., Fowlkes, C., and Malik, J. (2011). Contour detection and hierarchical image segmentation. *IEEE Transactions on Pattern Analysis and Machine Intelligence*, *33*(5), 898–916.

Arnab, A., Jayasumana, S., Zheng, S., and Torr, P. H. (2016). Higher order conditional random fields in deep neural networks. In *Proceedings of European Conference on Computer Vision (ECCV)*, 524–540. Springer.

Bo, L., Ren, X., and Fox, D. (2011). Hierarchical matching pursuit for image classification: architecture and fast algorithms. In *Proceedings of Advances in Neural Information Processing Systems (NIPS)*.

Boden, M. A. (2006). *Mind as machine: a history of cognitive science*. Clarendon Press.

Borenstein, E. and Ullman, S. (2008). Combined top-down/bottom-up segmentation. *IEEE Transactions on Pattern Analysis and Machine Intelligence*, *30*(12), 2109–2125.

Borji, A., Cheng, M.-M., Jiang, H., and Li, J. (2014). Salient object detection: a survey. *arXiv preprint arXiv:1411.5878*.

Breiman, L. (2001). Random forests. *Machine Learning*, *45*(1), 5–32.

Cai, J.-F., Candès, E. J., and Shen, Z. (2010). A singular value thresholding algorithm for matrix completion. *SIAM Journal on Optimization*, *20*(4), 1956–1982.

Candès, E. J., Li, X., Ma, Y., and Wright, J. (2011). Robust principal component analysis? *Journal of the ACM*, *58*(3), 11.

Chen, J. and Yang, J. (2014). Robust subspace segmentation via low-rank representation. *IEEE Transactions on Cybernetics*, *44*(8), 1432–1445.

Cheng, B., Liu, G., Wang, J., Huang, Z., and Yan, S. (2011). Multi-task low-rank affinity pursuit for image segmentation. In *Proceedings of IEEE International Conference on Computer Vision (ICCV)*, 2439–2446. IEEE.

Cheng, Y. (1995). Mean shift, mode seeking, and clustering. *IEEE Transactions on Pattern Analysis and Machine Intelligence*, *17*(8), 790–799.

Comaniciu, D. and Meer, P. (2002). Mean shift: a robust approach toward feature space analysis. *IEEE Transactions on Pattern Analysis and Machine Intelligence*, *24*(5), 603–619.

Couprie, C., Grady, L., Najman, L., and Talbot, H. (2009). Power watersheds: a new image segmentation framework extending graph cuts, random walker and optimal spanning forest. In *Proceedings of IEEE International Conference on Computer Vision (ICCV)*, 731–738. IEEE.

Dalal, N. and Triggs, B. (2005). Histograms of oriented gradients for human detection. In *Proceedings of IEEE International Conference on Computer Vision and Pattern Recognition (CVPR)*, Volume 1, 886–893. IEEE.

de Sa, V. R. (2005). Spectral clustering with two views. In *Proceedings of the Workshop on Learning with Multiple Views, the 22nd International Conference on Machine Learning (ICML)*, 20–27.

Dhillon, I. S. (2001). Co-clustering documents and words using bipartite spectral graph partitioning. In *Proceedings of the 7th ACM SIGKDD International Conference on Knowledge Discovery and Data Mining (KDD)*, 269–274. ACM.

Dhillon, I. S., Guan, Y., and Kulis, B. (2004). A unified view of kernel k-means, spectral clustering and graph cuts. Technical Report UTCS TR-04-25, University of Texas at Austin.

Ding, L. and Yilmaz, A. (2008). Image segmentation as learning on hypergraphs. In *Proceedings of The 7th International Conference on Machine Learning and Applications (ICMLA)*, 247–252. IEEE.

Dong, X., Frossard, P., Vandergheynst, P., and Nefedov, N. (2014). Clustering on multi-layer graphs via subspace analysis on Grassmann manifolds. *IEEE Transactions on Signal Processing*, *62*(4), 905–918.

Everingham, M. and Winn, J. (2007). The pascal visual object classes challenge 2007 (voc2007) development kit. *University of Leeds, Tech. Rep.*

Everingham, M. and Winn, J. (2011). The pascal visual object classes challenge 2011 (voc2011) development kit. *Pattern Analysis, Statistical Modelling and Computational Learning, Tech. Rep.*

Felzenszwalb, P. F., Girshick, R. B., McAllester, D., and Ramanan, D. (2010). Object detection with discriminatively trained part based models. *IEEE Transactions on Pattern Analysis and Machine Intelligence*, *32*(9), 1627–1645.

Felzenszwalb, P. F. and Huttenlocher, D. P. (2004). Efficient graph-based image segmentation. *International Journal of Computer Vision*, *59*(2), 167–181.

Fern, X. Z. and Brodley, C. E. (2004). Solving cluster ensemble problems by bipartite graph partitioning. In *Proceedings of the 21st International Conference on Machine Learning*, 36. ACM.

Fidler, S., Mottaghi, R., Yuille, A., and Urtasun, R. (2013). Bottom-up segmentation for top-down detection. In *Proceedings of IEEE International Conference on Computer Vision and Pattern Recognition (CVPR)*, 3294–3301. IEEE.

Fischler, M. A. and Bolles, R. C. (1981). Random sample consensus: a paradigm for model fitting with applications to image analysis and automated cartography. *Communications of the ACM*, *24*(6), 381–395.

Förstner, W. and Moonen, B. (2003). A metric for covariance matrices. In E. Grafarend, F. Krumm, and V. Schwarze (Eds.), *Geodesy - The Challenge of the 3rd Millennium*, 299–309. Springer.

Franek, L., Abdala, D. D., Vega-Pons, S., and Jiang, X. (2010). Image segmentation fusion using general ensemble clustering methods. In *Proceedings of Asian Conference on Computer Vision (ACCV)*, 373–384. Springer.

Freixenet, J., Muñoz, X., Raba, D., Martí, J., and Cufí, X. (2002). Yet another survey on image segmentation: region and boundary information integration. In *Proceedings of European Conference on Computer Vision (ECCV)*, 408–422. Springer.

Fu, Y., Gao, J., Hong, X., and Tien, D. (2015). Low rank representation on Riemannian manifold of symmetric positive definite matrices. In *Proceedings of SIAM International Conference on Data Mining*. SIAM.

Fukunaga, K. and Hostetler, L. (1975). The estimation of the gradient of a density function, with applications in pattern recognition. *IEEE Transactions on Information Theory*, *21*(1), 32–40.

Fulkerson, B., Vedaldi, A., and Soatto, S. (2009). Class segmentation and object localization with superpixel neighborhoods. In *Proceedings of IEEE International Conference on Computer Vision (ICCV)*, 670–677. IEEE.

Ganesh, A., Lin, Z., Wright, J., Wu, L., Chen, M., and Ma, Y. (2009). Fast algorithms for recovering a corrupted low-rank matrix. In *Proceedings of International Workshop on Computational Advances in Multi-Sensor Adaptive Processing (CAMSAP)*, 213–216. IEEE.

Gould, S., Gao, T., and Koller, D. (2009). Region-based segmentation and object detection. In *Proceedings of Advances in Neural Information Processing Systems (NIPS)*, 655–663.

Gould, S., Rodgers, J., Cohen, D., Elidan, G., and Koller, D. (2008). Multi-class segmentation with relative location prior. *International Journal of Computer Vision*, *80*(3), 300–316.

Gould, S., Zhao, J., He, X., and Zhang, Y. (2014). Superpixel graph label transfer with learned distance metric. In *Proceedings of European Conference on Computer Vision (ECCV)*, 632–647. Springer.

Gruber, A. and Weiss, Y. (2004). Multibody factorization with uncertainty and missing data using the EM algorithm. In *Proceedings of IEEE International Conference on Computer Vision and Pattern Recognition (CVPR)*. IEEE.

Gu, X., Deng, J. D., and Purvis, M. K. (2014a). Improving superpixel-based image segmentation by incorporating color covariance matrix manifolds. In *Proceedings of IEEE International Conference on Image Processing (ICIP)*, 4403–4406. IEEE.

Gu, X., Deng, J. D., and Purvis, M. K. (2014b). Superpixel-based segmentation using multi-layer bipartite graphs and Grassmann manifolds. In *Proceedings of The 29th International Conference on Image and Vision Computing New Zealand (IVCNZ)*, 119–123. ACM.

Gu, X., Deng, J. D., and Purvis, M. K. (2016). A hierarchical segmentation tree for superpixel-based image segmentation. In *Proceedings of The 31th International Conference on Image and Vision Computing New Zealand (IVCNZ)*, 1–6. IEEE.

Gu, X. and Purvis, M. (2016). Image segmentation with superpixel based covariance descriptor. In *Proceedings of Pacific-Asia Conference on Knowledge Discovery and Data Mining*, 154–165. Springer.

Habiboğlu, Y. H., Günay, O., and Çetin, A. E. (2012). Covariance matrix-based fire and flame detection method in video. *Machine Vision and Applications*, *23*(6), 1103–1113.

Hamm, J. and Lee, D. D. (2008). Grassmann discriminant analysis: a unifying view on subspace-based learning. In *Proceedings of the 25th International Conference on Machine Learning (ICML)*, 376–383. ACM.

Ho, J., Yang, M.-H., Lim, J., Lee, K.-C., and Kriegman, D. (2003). Clustering appearances of objects under varying illumination conditions. In *Proceedings of IEEE International conference on Computer Vision and Pattern Recognition (CVPR)*. IEEE.

Hoffman, D. D. and Singh, M. (1997). Salience of visual parts. *Cognition*, *63*(1), 29–78.

Hosang, J., Benenson, R., and Schiele, B. (2014). How good are detection proposals, really? *arXiv preprint arXiv:1406.6962*.

Huang, D., Lai, J.-H., Wang, C.-D., and Yuen, P. C. (2016). Ensembling over-segmentations: from weak evidence to strong segmentation. *Neurocomputing*, *207*, 416–427.

Huang, Q., Han, M., Wu, B., and Ioffe, S. (2011). A hierarchical conditional random field model for labeling and segmenting images of street scenes. In *Proceedings of*

IEEE Conference on Computer Vision and Pattern Recognition (CVPR), 1953–1960. IEEE.

Jain, A. K. (1989). *Fundamentals of digital image processing.* Prentice Hall.

Joachims, T. (2003). Transductive learning via spectral graph partitioning. In *Proceedings of the 20th International Conference on Machine Learning (ICML)*, 290–297.

Johnson, M., Shotton, J., and Cipolla, R. (2013). Semantic texton forests for image categorization and segmentation. In *Decision Forests for Computer Vision and Medical Image Analysis*, 211–227. Springer.

Kim, H., Thiagarajan, J. J., and Bremer, P.-T. (2014). Image segmentation using consensus from hierarchical segmentation ensembles. In *Proceedings of IEEE International Conference on Image Processing (ICIP)*, 3272–3276. IEEE.

Kim, T. H., Lee, K. M., and Lee, S. U. (2010). Learning full pairwise affinities for spectral segmentation. In *Proceedings of IEEE International Conference on Computer Vision and Pattern Recognition (CVPR)*, 2101–2108. IEEE.

Kluckner, S., Mauthner, T., Roth, P., and Bischof, H. (2009). Semantic image classification using consistent regions and individual context. In *Proceedings of British Machine Vision Conference (BMVC)*, Volume 6.

Kohli, P., Ladický, L., and Torr, P. H. (2009). Robust higher order potentials for enforcing label consistency. *International Journal of Computer Vision*, *82*(3), 302–324.

Kolda, T. G. and Bader, B. W. (2009). Tensor decompositions and applications. *SIAM review*, *51*(3), 455–500.

Kontschieder, P., Bulo, S. R., Bischof, H., and Pelillo, M. (2011). Structured class-labels in random forests for semantic image labelling. In *Proceedings of IEEE International Conference on Computer Vision (ICCV)*, 2190–2197. IEEE.

Kontschieder, P., Bulò, S. R., Donoser, M., Pelillo, M., and Bischof, H. (2011). Semantic image labelling as a label puzzle game. In *Proceedings of British Machine Vision Conference (BMVC)*, 1–12.

Kontschieder, P., Bulo, S. R., Pelillo, M., and Bischof, H. (2014). Structured labels in random forests for semantic labelling and object detection. *IEEE Transactions on Pattern Analysis and Machine Intelligence*, *36*(10), 2104–2116.

Kontschieder, P., Fiterau, M., Criminisi, A., and Rota Bulo, S. (2015). Deep neural decision forests. In *Proceedings of IEEE International Conference on Computer Vision (ICCV)*, 1467–1475. IEEE.

Krähenbühl, P. and Koltun, V. Efficient inference in fully connected CRFs with Gaussian edge potentials. *Proceedings of Advances in Neural Information Processing Systems (NIPS)*.

Kumar, S. *et al.* (2003). Discriminative random fields: a discriminative framework for contextual interaction in classification. In *Proceedings of IEEE International Conference on Computer Vision (CVPR)*, 1150–1157. IEEE.

Kviatkovsky, I., Adam, A., and Rivlin, E. (2013). Color invariants for person reidentification. *IEEE Transactions on Pattern Analysis and Machine Intelligence*, *35*(7), 1622–1634.

Ladický, L., Russell, C., Kohli, P., and Torr, P. H. (2010). Graph cut based inference with co-occurrence statistics. In *Proceedings of European Conference on Computer Vision (ECCV)*, 239–253. Springer.

Lafferty, J., McCallum, A., Pereira, F., *et al.* (2001). Conditional random fields: probabilistic models for segmenting and labeling sequence data. In *Proceedings of the 8th International Conference on Machine Learning (ICML)*, Volume 1, 282–289.

LeCun, Y., Bengio, Y., and Hinton, G. (2015). Deep learning. *Nature*, *521*(7553), 436–444.

LeCun, Y., Kavukcuoglu, K., and Farabet, C. (2010). Convolutional networks and applications in vision. In *Proceedings of IEEE International Symposium on Circuits and Systems (ISCAS)*, 253–256. IEEE.

Levinshtein, A., Stere, A., Kutulakos, K. N., Fleet, D. J., Dickinson, S. J., and Siddiqi, K. (2009). Turbopixels: fast superpixels using geometric flows. *IEEE Transactions on Pattern Analysis and Machine Intelligence*, *31*(12), 2290–2297.

Li, Z., Wu, X.-M., and Chang, S.-F. (2012). Segmentation using superpixels: a bipartite graph partitioning approach. In *Proceedings of IEEE International Conference on Computer Vision and Pattern Recognition (CVPR)*, 789–796. IEEE.

Lin, Z., Chen, M., and Ma, Y. (2010). The augmented Lagrange multiplier method for exact recovery of corrupted low-rank matrices. *arXiv preprint arXiv:1009.5055*.

Liu, F., Lin, G., and Shen, C. (2015). CRF learning with CNN features for image segmentation. *Pattern Recognition*, *48*(10), 2983–2992.

Liu, G., Lin, Z., Yan, S., Sun, J., Yu, Y., and Ma, Y. (2013). Robust recovery of subspace structures by low-rank representation. *IEEE Transactions on Pattern Analysis and Machine Intelligence*, *35*(1), 171–184.

Liu, G., Lin, Z., and Yu, Y. (2010). Robust subspace segmentation by low-rank representation. In *Proceedings of the 27th International Conference on Machine Learning (ICML)*, 663–670.

Liu, G. and Yan, S. (2011). Latent low-rank representation for subspace segmentation and feature extraction. In *Proceedings of IEEE International Conference on Computer Vision (ICCV)*, 1615–1622. IEEE.

Liu, M.-Y., Tuzel, O., Ramalingam, S., and Chellappa, R. (2011). Entropy rate superpixel segmentation. In *Proceedings of IEEE International Conference on Computer Vision and Pattern Recognition (CVPR)*, 2097–2104. IEEE.

Liu, W., He, J., and Chang, S.-F. (2010). Large graph construction for scalable semi-supervised learning. In *Proceedings of the 27th International Conference on Machine Learning (ICML)*, 679–686.

Liu, Y., Zhang, D., Lu, G., and Ma, W.-Y. (2007). A survey of content-based image retrieval with high-level semantics. *Pattern Recognition*, *40*(1), 262–282.

Ma, Y., Derksen, H., Hong, W., and Wright, J. (2007). Segmentation of multivariate mixed data via lossy data coding and compression. *IEEE Transactions on Pattern Analysis and Machine Intelligence*, (9), 1546–1562.

Ma, Y., Yang, A. Y., Derksen, H., and Fossum, R. (2008). Estimation of subspace arrangements with applications in modeling and segmenting mixed data. *SIAM review*, *50*(3), 413–458.

Malisiewicz, T. and Efros, A. A. Improving spatial support for objects via multiple segmentations. In *Proceedings of British Machine Vision Conference (BMVC)*, 1–10.

Martin, D., Fowlkes, C., Tal, D., and Malik, J. (2001). A database of human segmented natural images and its application to evaluating segmentation algorithms and measuring ecological statistics. In *Proceedings of IEEE International Conference on Computer Vision (ICCV)*, Volume 2, 416–423. IEEE.

Mei, X., Sun, X., Dong, W., Wang, H., and Zhang, X. (2013). Segment-tree based cost aggregation for stereo matching. In *Proceedings of IEEE International Conference on Computer Vision and Pattern Recognition (CVPR)*, 313–320. IEEE.

Meilă, M. (2005). Comparing clusterings: an axiomatic view. In *Proceedings of the 22nd International Conference on Machine Learning (ICML)*, 577–584. ACM.

Mignotte, M. (2008). Segmentation by fusion of histogram-based k-means clusters in different color spaces. *IEEE Transactions on Image Processing*, *17*(5), 780–787.

Mignotte, M. (2014). A label field fusion model with a variation of information estimator for image segmentation. *Information Fusion*, *20*, 7–20.

Moore, A. P., Prince, S. J., and Warrell, J. (2010). "Lattice Cut"-constructing superpixels using layer constraints. In *Proceedings of IEEE International Conference on Computer Vision and Pattern Recognition (CVPR)*, 2117–2124. IEEE.

Moore, A. P., Prince, S. J., Warrell, J., Mohammed, U., and Jones, G. (2008). Superpixel lattices. In *Proceedings of IEEE International Conference on Computer Vision and Pattern Recognition (CVPR)*, 1–8. IEEE.

Ng, P. C. and Henikoff, S. (2003). SIFT: predicting amino acid changes that affect protein function. *Nucleic Acids Research*, *31*(13), 3812–3814.

Nguyen, H., Yang, W., Shen, F., and Sun, C. (2015). Kernel low-rank representation for face recognition. *Neurocomputing*, *155*, 32–42.

Palmer, S. E. (1999). *Vision science: photons to phenomenology.* MIT press.

Panagiotakis, C., Papadakis, H., Grinias, E., Komodakis, N., Fragopoulou, P., and Tziritas, G. (2013). Interactive image segmentation based on synthetic graph coordinates. *Pattern Recognition*, *46*(11), 2940–2952.

Rabinovich, A., Vedaldi, A., Galleguillos, C., Wiewiora, E., and Belongie, S. (2007). Objects in context. In *Proceedings of IEEE International Conference on Computer vision (ICCV)*, 1–8. IEEE.

Rao, S. R., Mobahi, H., Yang, A. Y., Sastry, S. S., and Ma, Y. (2009). Natural image segmentation with adaptive texture and boundary encoding. In *Proceedings of Asian Conference on Computer Vision (ACCV)*, 135–146. Springer.

Ren, X. and Malik, J. (2003). Learning a classification model for segmentation. In *Proceedings of IEEE International Conference on Computer Vision (ICCV)*, 10–17. IEEE.

Rother, C., Kolmogorov, V., and Blake, A. (2004). Grabcut: interactive foreground extraction using iterated graph cuts. In *ACM Transactions on Graphics (TOG)*, Volume 23, 309–314. ACM.

Shi, J. and Malik, J. (2000). Normalized cuts and image segmentation. *IEEE Transactions on Pattern Analysis and Machine Intelligence*, *22*(8), 888–905.

Shotton, J., Johnson, M., and Cipolla, R. (2008). Semantic texton forests for image categorization and segmentation. In *Proceedings of IEEE International Conference on Computer Vision and Pattern Recognition (CVPR)*, 1–8. IEEE.

Shotton, J., Winn, J., Rother, C., and Criminisi, A. (2006). Textonboost: joint appearance, shape and context modeling for multi-class object recognition and segmentation. In *Proceedings of European Conference on Computer Vision (ECCV)*, 1–15. Springer.

Simonyan, K. and Zisserman, A. (2014). Very deep convolutional networks for large-scale image recognition. *arXiv preprint arXiv:1409.1556*.

Stutz, D., Hermans, A., and Leibe, B. (2017). Superpixels: an evaluation of the state-of-the-art. *Computer Vision and Image Understanding*.

Tang, M., Gorelick, L., Veksler, O., and Boykov, Y. (2013). Grabcut in one cut. In *Proceedings of IEEE International Conference on Computer Vision (ICCV)*, 1769–1776. IEEE.

Tang, W., Lu, Z., and Dhillon, I. S. (2009). Clustering with multiple graphs. In *Proceedings of IEEE The 9th International Conference on Data Mining (ICDM)*, 1016–1021. IEEE.

Torralba, A., Murphy, K. P., Freeman, W. T., Rubin, M. A., *et al.* (2003). Context-based vision system for place and object recognition. In *Proceedings of IEEE International Conference on Computer Vision (ICCV)*, Volume 3, 273–280. IEEE.

Tsai, Y.-H., Hamsici, O. C., and Yang, M.-H. (2015). Adaptive region pooling for object detection. In *Proceedings of the IEEE International Conference on Computer Vision and Pattern Recognition (CVPR)*, 731–739. IEEE.

Unnikrishnan, R., Pantofaru, C., and Hebert, M. (2007). Toward objective evaluation of image segmentation algorithms. *IEEE Transactions on Pattern Analysis and Machine Intelligence*, *29*(6), 929–944.

Van den Bergh, M., Boix, X., Roig, G., de Capitani, B., and Van Gool, L. (2012). SEEDS: superpixels extracted via energy-driven sampling. In *Proceedings of European Conference on Computer Vision (ECCV)*, 13–26. Springer.

Vedaldi, A. and Soatto, S. (2008). Quick shift and kernel methods for mode seeking. In *Proceedings of European Conference on Computer Vision (ECCV)*, 705–718. Springer.

Vega-Pons, S., Jiang, X., and Ruiz-Shulcloper, J. (2011). Segmentation ensemble via kernels. In *Proceedings of 1st Asian Conference on Pattern Recognition (ACPR)*, 686–690. IEEE.

Verbeek, J. and Triggs, B. (2007). Region classification with Markov field aspect models. In *Proceedings of IEEE International Conference on Computer Vision and Pattern Recognition (CVPR)*, 1–8. IEEE.

Vincent, L. and Soille, P. (1991). Watersheds in digital spaces: an efficient algorithm based on immersion simulations. *IEEE Transactions on Pattern Analysis and Machine Intelligence*, *13*(6), 583–598.

Von Luxburg, U. (2007). A tutorial on spectral clustering. *Statistics and Computing*, *17*(4), 395–416.

Wang, B., Hu, Y., Gao, J., Sun, Y., and Yin, B. (2015a). Kernelized low rank representation on Grassmann manifolds. *arXiv preprint arXiv:1504.01806*.

Wang, B., Hu, Y., Gao, J., Sun, Y., and Yin, B. (2015b). Low rank representation on Grassmann manifolds: an extrinsic perspective. *arXiv preprint arXiv:1504.01807*.

Wang, H., Zhang, Y., Nie, R., Yang, Y., Peng, B., and Li, T. (2014). Bayesian image segmentation fusion. *Knowledge-Based Systems*, *71*, 162–168.

Wang, M., Liu, X., Gao, Y., Ma, X., and Soomro, N. Q. (2017). Superpixel segmentation: a benchmark. *Signal Processing: Image Communication*, *56*, 28–39.

Wang, X., Du, J., Wu, S., Li, X., and Li, F. (2013). Cluster ensemble-based image segmentation. *International Journal of Advanced Robotic Systems*, *10*(7), 297.

Wang, X., Li, H., Bichot, C.-E., Masnou, S., and Chen, L. (2013). A graph-cut approach to image segmentation using an affinity graph based on ℓ_0-sparse representation of features. In *Proceedings of IEEE International Conference on Image Processing (ICIP)*, 4019–4023. IEEE.

Wang, X., Li, H., Masnou, S., and Chen, L. (2013). Sparse coding and mid-level superpixel-feature for ℓ_0-graph based unsupervised image segmentation. In *Proceedings of International Conference on Computer Analysis of Images and Patterns (ICCAIP)*, 160–168. Springer.

Wang, X., Tang, Y., Masnou, S., and Chen, L. (2015). A global/local affinity graph for image segmentation. *IEEE Transactions on Image Processing*, *24*(4), 1399–1411.

Wang, Y., Guan, L., and Venetsanopoulos, A. N. (2012). Kernel cross-modal factor analysis for information fusion with application to bimodal emotion recognition. *IEEE Transactions on Multimedia*, *14*(3), 597–607.

Wei, X., Yang, Q., Gong, Y., Yang, M.-H., and Ahuja, N. (2016). Superpixel hierarchy. *arXiv preprint arXiv:1605.06325v1*.

Wertheimer, M. (1938). Laws of organization in perceptual forms. In *A Source Book of Gestalt Psychology*, 71–88.

Wright, J., Ganesh, A., Rao, S., Peng, Y., and Ma, Y. (2009). Robust principal component analysis: exact recovery of corrupted low-rank matrices via convex optimization. In *Proceedings of Advances in Neural Information Processing Systems (NIPS)*, 2080–2088.

Wu, S., Wang, X., Ye, Q., and Dong, J. (2012). Region clustering with high level semantics for image segmentation. In *Proceedings of IEEE 2nd International Conference on Cloud Computing and Intelligence Systems (CCIS)*, Volume 2, 946–950. IEEE.

Yao, J., Fidler, S., and Urtasun, R. (2012). Describing the scene as a whole: joint object detection, scene classification and semantic segmentation. In *Proceedings of IEEE International Conference on Computer Vision and Pattern Recognition (CVPR)*, 702–709. IEEE.

Zhang, L., Zhang, Q., Zhang, L., Tao, D., Huang, X., and Du, B. (2015). Ensemble manifold regularized sparse low-rank approximation for multiview feature embedding. *Pattern Recognition*, *48*(10), 3102–3112.

Zheng, S., Jayasumana, S., Romera-Paredes, B., Vineet, V., Su, Z., Du, D., Huang, C., and Torr, P. H. (2015). Conditional random fields as recurrent neural networks. In *Proceedings of IEEE International Conference on Computer Vision (ICCV)*, 1529–1537. IEEE.

Zhou, D. and Burges, C. J. (2007). Spectral clustering and transductive learning with multiple views. In *Proceedings of the 24th International Conference on Machine learning (ICML)*, 1159–1166. ACM.

Zhou, P., Du, L., Wang, H., Shi, L., and Shen, Y.-D. (2015). Learning a robust consensus matrix for clustering ensemble via Kullback-Leibler divergence minimization. In *Proceedings of the 24th International Joint Conference on Artificial Intelligence (IJCAI)*, 4112–4118.

Zhou, Z.-H. (2012). *Ensemble methods: foundations and algorithms.* CRC press.

Zhu, H., Lu, S., Cai, J., and Lee, Q. (2015). Diagnosing state-of-the-art object proposal methods. *arXiv preprint arXiv:1507.04512*.

Zhu, H., Meng, F., Cai, J., and Lu, S. (2016). Beyond pixels: a comprehensive survey from bottom-up to semantic image segmentation and cosegmentation. *Journal of Visual Communication and Image Representation*, *34*, 12–27.